國立交通大學

機械工程學系

博 士 論 文

使用天然氣的微富氧燃燒之實驗研究

The Experimental Studies of Oxygen-Enriched Combustion
Using Natural Gas Fuel

研 究 生：陳遠達

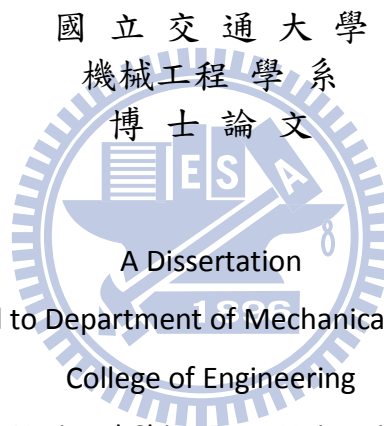指導教授：陳俊勳　教授

中 華 民 國 一百 年 一 月

使用天然氣的微富氧燃燒之實驗研究

The Experimental Studies of Oxygen-Enriched Combustion Using Natural Gas Fuel

研 究 生：陳遠達   Student：Yuan-Da Chen

指導教授：陳俊勳   Advisor：Prof. Chiun-Hsun Chen

國 立 交 通 大 學

機 械 工 程 學 系

博 士 論 文

A Dissertation

Submitted to Department of Mechanical Engineering

College of Engineering

National Chiao Tung University

in partial Fulfillment of the Requirements

for the Degree of

Doctor of Philosophy

In Mechanical Engineering

January 2011

Hsinchu, Taiwan, Republic of China

中 華 民 國 一 百 年 一 月

使用天然氣的微富氧燃燒之實驗研究

學生:陳遠達　　　　　　　　　　　　　指導教授:陳俊勳

國立交通大學機械工程學系研究所

摘要

本實驗研究目的是探討微富氧空氣的氧濃度變化對燃燒爐之加熱速度、煙氣、溫度分佈和燃料消耗量的影響。燃燒爐有實驗室與先導型二種尺度。每個尺度的燃燒爐都分別做加熱試驗和固定爐溫試驗，所使用的燃料是天然氣（CH_4:82%，C_2H_6:2.6%，C_3H_8:1.8% and CO_2:13.6%），實驗的氧濃度條件分別為 21%、24%、26%、28%以及 30%；而過剩空氣係數則控制在可以達到完全燃燒反應的範圍內。由實驗結果顯示，於實驗室與先導型尺度燃燒爐試驗都會因當氧濃度增加可以縮減加熱時間並且減少燃料消耗量而有節能的效果，這是由於減少富氧空氣中不參予反應的氮氣所致。而在實驗室尺度試驗中，氮氧化物的生成會隨著氧濃度的增加而急遽增加，同時也發現氮氧化物的生成在高氧濃度的狀態下對過剩氧是極為敏感的；但是在先導型尺度試驗中，氮氧化物的生成量則是幾乎相同的，這是由於其燃燒器無法將燃料與空氣混合很好所致。此外，在實驗研究中發現於實驗室與先導型尺度試驗，二氧化碳的濃度皆會隨著氧濃度的增加而呈線性提高。在實驗室尺度固定爐溫試驗中，在溫度分佈方面，氧濃度越高溫度分佈越不均勻，這是由於熱對流變弱所造成。另外在先導型尺度固定爐溫試驗中，發現輻射熱通量會隨著氧濃度增加而增加。因此由本論文實驗結果可確認富氧燃燒不僅能減少能源的花費，而且可提升生產效率和產品產量。

關鍵字: 富氧燃燒，實驗室燃燒爐，先導型燃燒爐，節能，氮氧化物，輻射熱通量。

The Experimental Studies of Oxygen-Enriched Combustion Using Natural Gas Fuel

Student: Yuan-Da Chen   Advisor: Chiun-Hsun Chen

Department of Mechanical Engineering

National Chiao Tung University

Abstract

The experimental investigations were aimed at studying the influence of oxygen-enriched air on the heating speed, emissions, temperature distributions and fuel consumption of the furnaces, which were Lab-Scale and Pilot-Scale, respectively. The experiments for each type of furnace were divided into two parts: the heating test and the fixed furnace-temperature test. The fuel used was the natural gas（CH_4:82%, C_2H_6:2.6%, C_3H_8:1.8% and CO_2:13.6%）, and there were five different oxygen concentrations, which are 21%, 24%, 26%, 28% and 30%. The excess air ratio was controlled such that it could achieve complete combustion in the experiment. Based on experimental results, the increase of oxygen concentration led to the faster heating speed and less fuel consumption in both Lab-Scale and Pilot-Scale tests because less energy was used to heat up the less amount of inert gas (N_2) in the oxygen-enriched air. The NO_x emission increases sharply as the oxygen concentration increases in the Lab-Scale experiments. Moreover, the NO_x emission was more sensitive to excess oxygen at higher oxygen concentration condition. However, the total amount of NO_x emissions was almost invariant as the oxygen concentration increased in the Pilot-Scale experiments. This is due to poor mixing of oxidant and fuel of burner. The CO_2 concentration increased linearly with the oxygen concentration in both

Lab-Scale and Pilot-Scale heating tests. The temperature distributions became more non-uniform as increasing oxygen concentration in the Lab-Scale fixing furnace-temperature test, because the convection heat transfer was weakened. The radiation heat flux increased with oxygen concentration in the Pilot-Scale fixing furnace-temperature test. Based on the experimental results of this study, the oxygen-enriched combustion can save energy, and elevate manufacture efficiency and product quality.

Keywords: Oxygen-enriched combustion, Lab-Scale furnace, Pilot-Scale furnace, Energy saving, Nitrogen oxides and Radiation heat flux.

ACKNOWLEDGEMENTS

Contents

List of Tables

List of Figures

Chapter 1
Introduction

Background

The energy usage is the basic consideration of national developments and economic activities. It is very important to national security and human's existence. Furthermore, the cost of energy production has shown a sharp increase and hence improving the energy efficiency becomes a very important issue. However, the energy resources that exist in the earth are depleted. The most of fossil fuels (ex: petroleum, coal, natural gas) can be turned into the energy that we need, which is under attack based on the concerns for the impact of carbon dioxide (CO_2) on global warming. Nevertheless, fossil fuel combustion is a major contributor to the greenhouse gas emissions, which are of increasing concern. As the fossil fuel is processed the transformation, it will lose the energy and cause the environmental degradation. In order to achieve the reduction goal in emissions of various global warming gases in 5% of 1990 levels by the year 2012 as declared Kyoto Protocol, it is indispensable to make every effort in reducing CO_2 and other anthropogenic pollutants, like NO_x. Fossil fuel, such as gas and oil, is well used in the various industrial processes and the energy savings on these will result in great effects on reducing of global warming gases. For example, 5.7 % primary energy demanded in EU is used in steel industry which accounts for 5 to 6% of anthropogenic emissions in the world. Therefore, the energy saving and environment protection technologies should be developed and applied as soon as possible in the practical fields.

The awareness of that the increases in greenhouse gas emissions and overall fuel consumption have resulted in the development of new

technologies with lower emissions and energy conservation. For this reason, oxygen-enriched combustion technology has been widely recognized as one of the most effective ways. Moreover, oxygen-enriched combustion is gradually gaining popularity in the industrial production of glass, aluminum, iron, and steel because of its inherent advantages. These include high combustion efficiency, low volume of exhaust gas, low fuel consumption, high melting capacity, and low NO_x emission. In addition, energy efficiency can be greatly enhanced because the unnecessary heating of nitrogen in air is eliminated.

All designed burner-based power systems have relied on oxygen in surrounding air as the oxidizer to date. Although air is easy to obtain and free, but nitrogen, a major component with a mole fraction of 79%, is an inert gas that does not contribute to the process of oxidizing fuel. It acts as an energy consumer and is responsible for unwanted pollutants (the nitrogen oxides (NO_x)). The nitrogen is a diluents medium that reduces the combustion temperature and increases energy losses. Pure oxygen substitution for air is an alternative to overcome these shortcomings. Reducing the amount of nitrogen in the reactant mixture is a topic of scientific and application importance. For example, when natural gas is burned in pure oxygen, the only significant products are water and carbon dioxide. The lower level of oxygen concentration in the range from 21 to 30% is interested by the high temperature industrial furnaces, which are used in the processing of metals, glass and ceramics. The low oxygen concentration of oxygen-enriched combustion is economical, and the corresponding furnace temperature, heating capability and combustion efficiency are performed better than those of atmospheric air with 21% of O_2. However, very few works have explored the characteristics of low-level oxygen-enrichment combustion. Therefore, this study was motivated to use the Lab-Scale and Pilot-Scale gas-fired burners to

2

investigate the effects of oxygen-enriched air from 21 to 30% on the related combustion features.

Literature survey

Baukal [1] proposed that flame temperatures and concentrations of H_2O and CO_2 are increased compared with hydrocarbon–air flames because the heat sink and diluents effects of N_2 are diminished in oxygen-enriched combustion. Baukhal et al. [2] demonstrates that oxygen-enriched combustion has proven to be economically viable, especially in the glass melting industry, where low operating costs, better glass quality, energy conservation, lower NO_x as well as particulate emission and production increase have been achieved. Dalton et al. [3] and Joshi et al. [4] adopted conventional air/fuel burners to carry out oxygen-enriched combustion. They found that air/fuel burners could be adapted to low-level oxygen enrichment (generally lower than 28% O_2) with no modifications. Qiu and Hayden [5] investigated oxygen-enriched combustion of natural gas in porous ceramic radiant burners, at oxygen concentrations varying between 21 and 28%. The experimental results indicated that the saving in natural gas was about 22% when oxygen concentration was increased to 28%.

Furthermore, oxygen enrichment of combustion air allows ignition with minimum amounts of premixed fuel, because it reduces the ignition delay and premixed combustion period, announced by Sekar et al. [6], Assanis et al. [7] and Iida et al. [8]. Moreover, Baukal et al. [2] experimentally studied total radiation measurements for oxygen-enhanced/natural gas diffusion flames. They found that a thermal radiation increase with an enriched oxygen level in the oxidizer as well as with an increased firing rate. And the result of study reveals the flame temperature up to nearly 3000K arise from oxygen concentration

enhancement. In the oxygen-enriched, NO_x formation is mainly controlled by thermal mechanisms. Because of this, many combustion applications that need high temperature environments use oxygen-enriched air or pure oxygen as oxidizer. Compared with fuel/air systems, oxygen enriched combustion can decrease pollutant emissions. Chen and Axelbaum [9] studied the variations of the extinction strain rate under oxygen-enriched conditions both numerically and experimentally. Oxygen-enriched combustion could yield extremely strong flames. They found that the extinction strain rate for a methane flame increased by more than two times as the oxygen concentration was increased to 100%. Bejarano and Levendis [10] observed the behavior of coal char in a drop-tube furnace in oxygen-enriched atmospheres. When the gas temperature was maintained within the range of 1300–1500 K, the average temperatures of the char surface increased from 1600–1800 K in air to ranges of 2100–2300 K and 2300–2400 K in 50% and 100% O_2, respectively. In addition, the combustion durations of chars were reduced from 25–45 ms in air to 8–17 ms and 6–13 ms in 50% and 100% O_2, respectively. Marphy and Shaddix [11] conducted a similar study showing that the ranges of oxygen concentration and gas temperature for the combustion of coal chars were 6–36% and 1320–1800 K, respectively. The experimental and numerical results were similar to those reported by Bejarano and Levendis [10] and showed that as the oxygen concentration increased, the char-combustion temperature was increased whereas the char burnout time was reduced.

Recently, oxygen combustion is the hot topic due to the CO_2 issue. However, almost studies are major on full oxygen combustion. Beltrame et al. [12] numerically and experimentally investigate NO and soot formations in oxygen-enriched counterflow diffusion flames. They find that oxygen variation significantly modified the diffusion flame structure and the flame temperature, resulting in a substantial increase of soot. High concentration

4

of soot in the flame leads to enhancement of radiant heat exchange and the reduction of temperature due to radiation is found to be between 10 and 50 K. Furthermore, Kang et al. [13] demonstrated that there is a dramatic effect on flame structure by changing the concentration of oxygen, and the soot formation caused by flame can keep a constant value. Ishizuka et al. [14], Puri et al. [15] and Chen et al. [16] have extensively developed a fundamental understanding of flame structure and extinction for oxygen combustion. Zhao et al. [17] numerically studies on flame structure and NO_x formation of oxygen-enriched air/methane counterflow diffusion flame. The simulation results show that high concentration of oxygen leads to high temperature, therefore, the NO_x emission increases promptly. In addition, increasing flame temperature reduces the soot formation, and enhances soot oxidation in the enriched oxygen environment. The soot formation and thermal radiation influences on flame structure, temperature, and pollutant emissions. In recent years, such as Beltrame et al. [18], Lee et al. [19], Naik et al. [20] and Naik et al. [21] studies revealed that the soot formation rate and the soot particle agglomeration rate progressively increase as the oxygen content of the oxidizer increases, in the soot formation process of an oxygen-enriched flame. Furthermore, Hedley et al. [22] measured detailed profiles for temperature and NO_x concentration, and they made a comparison of experimental data and numerical results. Other investigations, Ho et al. [23] experimentally investigated the oxygen-enriched/methane flame of combustion characteristics, flame structure and flame length in wide range of fuel nozzle diameters and oxidizer velocities. The experimental result reveals that the flame length decreases with increased fuel velocity or oxygen velocity due to greater turbulent mixing. They also found that the transitional flame characteristics of the oxygen/methane flame are not quite apparent. Another approach to reducing NO_x emissions and at the same time increasing furnace efficiency

or throughput, involves the use of oxygen-enriched air. Adding oxygen and reducing the air requirement for combustion results in less nitrogen entering the furnace (with air) making less nitrogen available to be converted to NO_x. As well, by reducing the amount of nitrogen passing through the furnace, less energy is lost out the stack by the unnecessary heating of that nitrogen. Significant fuel savings (up 50% reduction) are achievable. So it's significant for the application of oxygen-enriched combustion to study the formation characteristics and suppression methods of NO_x in high temperature oxygen-enriched combustion. In recent years, the scholars developed some methods for reducing NO_x emission during combustion. Narayanan et al. [24], Buhre et al. [25] and Czakiert et al. [26] demonstrates that the process involves burning fossil fuels in pure oxygen as opposed to air resulting in a more complete combustion. This result reveals that consists of almost pure CO_2 (typically 90%) and water vapour in an exhaust stream. The advantage of this technique is very low NO_x emissions because hot spots in the flame are minimized, which generally reduces NO_x. A potential disadvantage, besides the safety concern, is a reduction in heat transfer as both the temperature and effective emissivity of the flame may be reduced. Another method for oxygen-enriched staged combustion had been proposed by Neff et al. [27], El-Salmawy et al. [28] and Bool et al. [29]. Typically, the NO_x emissions are lower using O_2 lancing compared with premixing since this is a form of staging, which is a well-accepted technique for reducing NO_x. Depending on the injection location, the flame shape may be lengthened by staging the combustion reactions. The flame heat release is generally more evenly distributed than with premix O_2 enrichment. Under certain conditions, O_2 lancing between the flame and the load causes the flame to be pulled toward the material. This improves the heat transfer efficiency. Therefore, there is less likelihood of overheating the air/fuel burner, the burner block, and the

refractory in the combustion chamber. Another variant of this staging method involves lancing O_2 not into the flame but somewhere else in the combustion chamber. That technology for O_2 lancing is an inexpensive retrofit for existing processes. One potential disadvantage is the cost of adding another hole in the combustion chamber for the lance. This includes both the installation costs and the lost productivity. However, the hole is typically very small. Riley et al. [30], Nishimura et al. [31] and Poirier et al. [32] suggested that dilute oxygen combustion, is where fuel and oxygen are separately injected into the combustion chamber. In order to ensure ignition, the chamber temperature must be above the autoignition temperature of the fuel. Depending on the exact geometry, this can produce an almost invisible flame, sometimes referred to as flameless oxidation. The advantage of this technique is very low NO_x emissions because hot spots in the flame are minimized, which generally reduces NO_x. A potential disadvantage, besides the safety concern, is a reduction in heat transfer as both the temperature and effective emissivity of the flame may be reduced. There are three major mechanisms of NO_x formation: thermal, prompt and fuel NO_x mechanisms. So it's necessary to investigate the NO_x suppression issue according to its characteristics. The different methods are adopted for different NO_x formation mechanisms. Fuel savings are offset to some extent by the cost of the oxygen; however, O_2 production technologies are becoming more economical as time passes. Steel industries already use significant quantities of oxygen and so have the facilities to handle and supply oxygen to their processes. Kennedy et al. [33] investigated the effects of oxygen concentration on filtration-combustion waves. The equivalence ratios and oxygen concentrations studied were in the ranges 0.1–2 and 10–30%, respectively. They found that the peak combustion temperature decreased with increasing oxygen concentration, whereas the absolute flame-propagation rate increased. Furthermore, the CO emission

index decreased with increasing oxygen concentration, except for oxygen concentrations higher than 25% and an equivalence ratio near 1.0, when the reaction zone contracted to an area lower than the characteristic pore diameter. Molina and Shaddix [34] proved that ignition occurred faster at higher oxygen concentrations during both O_2/CO_2 and O_2/N_2 combustions applied for combustion of coal. For the same oxygen concentration, the ignition time for O_2/CO_2 combustion was longer than that for O_2/N_2 combustion. The experiment of Liu et al. [35] yielded the same results.

An important barrier to the use of oxygen-enhanced combustion in combustion systems, such as boilers, especially utility-combustion systems, is the current cost of oxygen production and retrofitting. The possible solution is using low-level oxygen-enrichment combustion. Huang et. al. [36] had analyzed economical feasibility of replacing traditional combustion into oxygen-enriched one for heating furnace, whose flue gas temperature is 920. The ROI (Return On Investment) is about 5.75 years when the oxygen source is generated by membrane method for 30% of O_2.

Scope of the present study

In the past, the majority of researches in oxygen-enriched combustion were focused on the fuel being burned in pure oxygen. However, there have been relatively few works conducted on the low level of oxygen concentration. Therefore, in this study, it explored the characters of oxygen-enriched combustion in the range of 21~30% oxygen concentrations in the heating process. The fuel used in the experiments was the natural gas（CH_4:82%, C_2H_6:2.6%, C_3H_8:1.8% and CO_2:13.6%）; there were five different oxygen concentrations, such as 21%, 24%, 26%, 28% and 30%, respectively. The furnaces used for testing were Lab-Scale and Pilot-Scale, respectively. The experiments for each type of furnace were

divided into two parts: the heating test and the fixing furnace-temperature test. The measured parameters include heating times, emissions, fuel consumption and temperature profiles etc... The experimental flow chart is show in Figure 1.1.

For both heating and fixing furnace-temperature tests, the total excess air ratio was maintained as a constant (Φ=1.05). In the heating tests, the fuel flow rates were fixed under various oxygen concentrations in a furnace. Heating was carried out from room temperature to 1200℃. In the fixing furnace-temperature tests, the furnace-temperature were fixed at 1220±10 ℃ under various fuel flow rates in a furnace. During the experimental periods of Lab-Scale and Pilot-Scale furnaces, the corresponding fuel flow rates were changed from 23 to 17 L/min and 383.4 ~ 300.0 L/min, respectively.
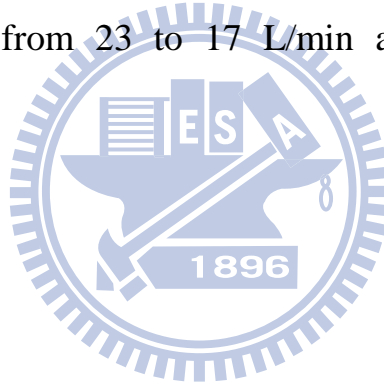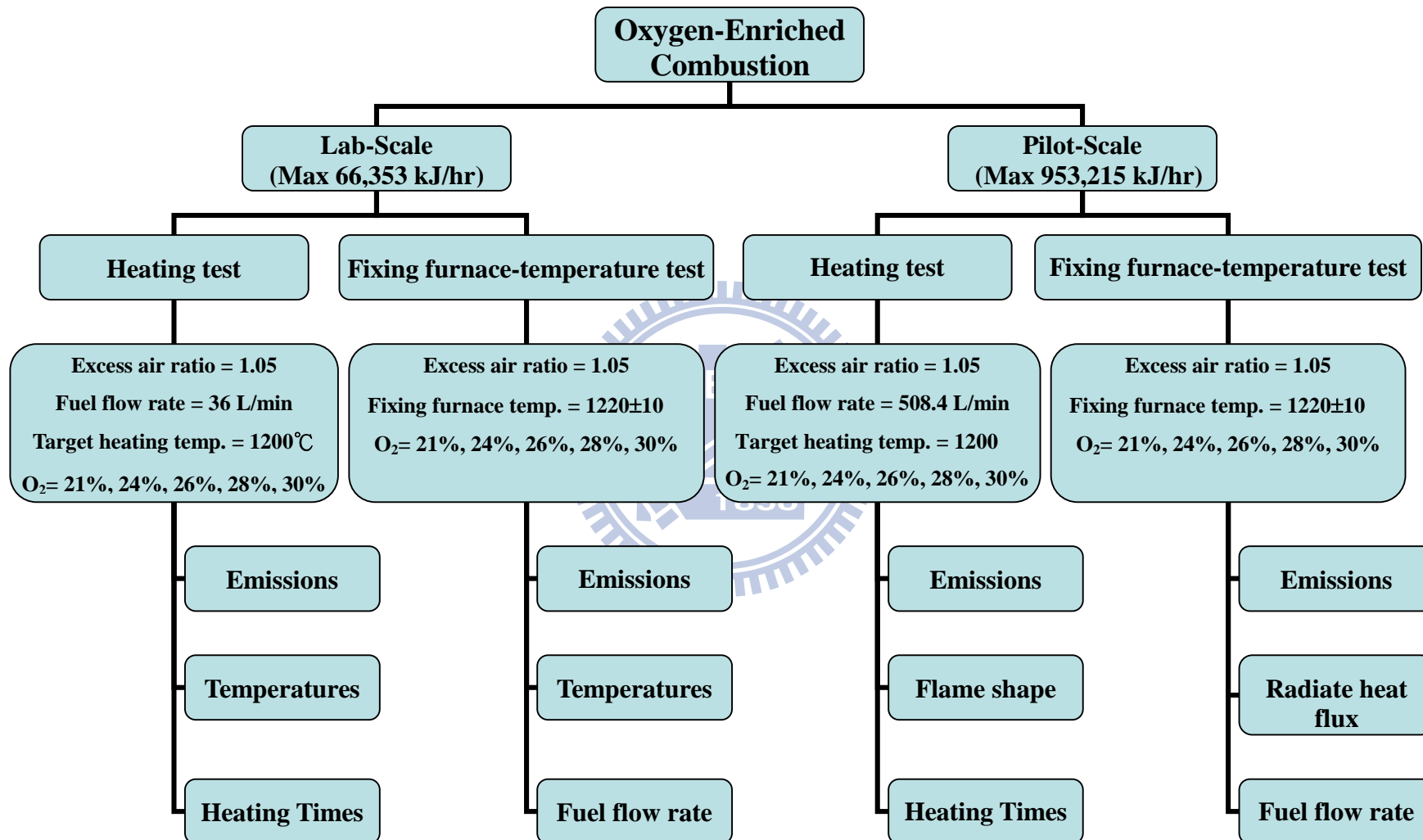
Figure 1.1 The experimental flow chart of Oxygen-enriched combustion.

Chapter 2
Experimental Apparatus

These experimental works were carried out in Energy and Environment Research Laboratories, Industrial Research and Technology Institute. All experimental device design and planning are by the author (ex: combustion chamber, pipeline control system, control system). The followings are the brief descriptions for the apparatus.

Lab-Scale Experimental Layout

A schematic diagram of the Lab-Scale experimental apparatus layout is shown in Fig. 2.1. The combustion chamber size is 30 cm × 30 cm ×100 cm and the natural gas is the fuel. The combustion chamber is rectangular and vertical. The actual combustion chamber size including flue at the top is 300mm wide, 300mm deep and 1,000mm high. The gas-fired burner was designed and built by North American (4423-0). The design capacity of the burner is 66,353 kJ / hr for heat input.

Furthermore, the experiment was parted into five kinds of different oxygen concentration (21%, 24%, 26%, 28% and 30%). Mixing air and pure oxygen in the gas mixer produces the different oxygen concentration, which is confirmed the desired value by an oxygen analyzer (Sensorbay Mini-25H) before the mixture enters the combustion chamber. The concentrations of flue gas compositions were analyzed by the gas analyzer (Testo 350XL), which can analyze O_2, CO, NO_x and CO_2. The excess air ratio was controlled at about 1.05 in order to achieve complete combustion in the experiments. The furnace temperatures were measured by thermocouples, whose outer diameter was 1.6 mm and the outer layer was covered by Inconel. The position of temperature measurement was in the

upper half furnace and the thermocouples were located at the center of perpendicular plane. The latitudinal distance of each measured point was 65mm and the longitudinal one was 60mm. Total measured points were 30. Each measured temperature was recorded by data acquisition system (Fluke 2680A) and the frequency was 1 point per second.

Combustion Test System

1.1.1.1 Burner

Furnace burner was used North American 4423-0 gas burner, as shown in Fig. 2.2. It can almost be used on any kind of industrial sector from low temperature air heaters to kilns and forge furnace that operate in 1093.3~1315.5℃ range. This burner characteristic has medium velocity flames with wide air/fuel ratio and turndown flexibility. The main body is made of cast iron, and air tubes are stainless steel. In the back of the gas connection, it has an observation port, and provision for pilot and flame detector. The flame supervision is done by a UV detector. When flame supervision is used, pilots must be interrupted. Pilot is automatically turned off within 10 seconds of main flame ignition so the detector monitors main flame only. For most reliable ignition and flame signals, operate pilot at no less than 10.16 cm H_2O mixture pressure.

1.1.1.2 Combustion Chamber

The dimension of combustion chamber is 30 cm $\times$ 30 cm $\times$100 cm, as shown in Fig. 2.3. This shell is encapsulated by iron material whose inside wall has insulating material (Glass Fiber) of 30-cm thickness to mitigate the heat loss.

1.1.1.3 Gas Mixer

The gas mixer system, shown in Fig. 2.4, consists of spiral mix tube, check valve, gas flow rotameter and pressure gauge. The schematic configuration of gas mixer is shown in Fig. 2.5. Air and oxygen are supplied from the blower and the gas cylinders, respectively, whose outlet pressures are controlled and fixed at 40 kg/cm² by using pressure regulator. These two gases separately pass through the inlet ports of mixer, equipped with the pressure gauge and gas flow rotameter. Then, air and oxygen with the desired volume flow rates controlled by gas flow rotameter enter the spiral tube to mix each other in the mixer. Finally the mixture gas passes through the oxygen analyzer and gas flow rotameter at the desired volume flow rate. The function of gas mixer is to well mix the air with oxygen in an assigned fraction. The interesting parameter is mass fraction rather than volume fraction. Therefore, the transformation between mass and volume fractions is described as follow.

$$X_{Air} = 1 - X_{O_2} \qquad M_{O_2} = 32, \qquad M_{N_2} = 28$$

$$M_{Air} = 0.21 \times M_{O_2} + 0.79 \times M_{N_2} = 0.21 \times 32 + 0.79 \times 28 = 28.84$$

$$Y_{O_2} = \frac{X_{O_2} \times M_{O_2} + 0.21(X_{Air} \times M_{Air})}{X_{O_2} \times M_{O_2} + X_{Air} \times M_{Air}} \tag{2.1}$$

$$= \frac{X_{O_2} \times M_{O_2} + 0.21\left[\left(1 - X_{O_2}\right) \times M_{Air}\right]}{X_{O_2} \times M_{O_2} + \left(1 - X_{O_2}\right) \times M_{Air}}$$

$$= \frac{X_{O_2} \times 32 + 0.21\left[\left(1 - X_{O_2}\right) \times 28.84\right]}{X_{O_2} \times 32 + \left(1 - X_{O_2}\right) \times 28.84}$$

$$= \frac{32X_{O_2} + 6.0564\left(1 - X_{O_2}\right)}{32X_{O_2} + 28.84\left(1 - X_{O_2}\right)}$$

$$= \frac{32X_{O_2} + 6.0564 - 6.0564X_{O_2}}{32X_{O_2} + 28.84 - 28.84X_{O_2}}$$

$$= \frac{6.0564 + 25.9436X_{O_2}}{28.84 + 3.16X_{O_2}}$$

$$Y_{O_2} = \frac{6.0564 + 25.9436X_{O_2}}{28.84 + 3.16X_{O_2}}$$
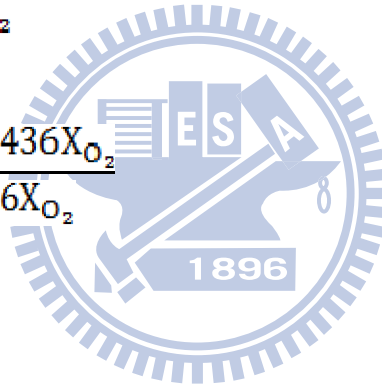
Therefore,

$$X_{O_2} = \frac{28.84Y_{O_2} - 6.0564}{25.9436 - 3.16Y_{O_2}} \tag{2.2}$$

where Y_{O_2} and X_{O_2} represent the mass fraction and volume fraction respectively.

Pilot-Scale of Experiment Layout

The combustion chamber size was 258 cm $\times$ 247 cm $\times$150 cm and the fuel was natural gas. Actual combustion chamber size including flue at the top is 258mm wide, 247mm deep and 150mm high. A schematic diagram

of the Pilot-Scale experimental apparatus is shown in Fig. 2.6. The gas-fired burner (4442-5) was designed and built by North American. The design capacity of the burner is 953,215 kJ/hr of heat input. Furthermore, the experiment was parted into five kinds of different oxygen concentration (21%, 24%, 26%, 28% and 30%). The blower was the primary air source of oxygen-enriched combustion system. The excess air ratio was controlled about 1.05 in order to achieve the complete combustion in the experiment as possible. The concentrations of flue gas compositions were analyzed by the gas analyzer (Testo 350XL), which can analyze O_2, CO, NO_X and CO_2. The flame shapes were visualized by digital camera (Sony TRV-950) with image sensor of 690,000 pixels video, and furnace temperature was measured by R-type thermocouples. The outer diameter of thermocouple was 17 mm with aluminum nitride insulation. The 25-cm-gap position for measured temperature was from the top of combustion chamber and its length was 160cm. The length of measuring points between burner and right side wall was 120 cm (see Fig. 2.7). The radiate heat flux was measured by radiometer (Vatell Corporation TG9000-2). There were four measured points, which are located on right side of wall and parallel to the center axis of burner, and spaced 85, 120, 175 and 210 cm from front wall to back wall of combustion chamber, respectively (see Fig. 2.7). The gap between bottom of chamber and center axis of burner is 75 cm. All data were collected by data acquisition system (Fluke 2680A) with 1-second frequency.

Combustion Test System

1.1.1.4 Burner

The furnace high velocity burner was made by North American TEMPEST 4442-5, as shown in Fig. 2.8. It has a very wide range of

applications with an operating temperature range from 315.5 to 1648.8 . This burner characteristic has high velocity flames with wide air/fuel ratio and turndown flexibility. It can apply to ceramic tunnel, heat treat furnaces, car bottom furnaces, scrap preheating, galvanizing tanks, crucible furnaces, air heating and drying. The main body is the cast iron, and the air tubes are stainless steel. In the back of the gas connection, have an observation port, and provision for pilot and flame detector. The flame supervision is used a UV detector. When flame supervision is used, pilots must be interrupted. Pilot is automatically turned off within 10 seconds of main flame ignition so detector monitors main flame only. For most reliable ignition and flame signals, operate pilot at no less than 10.16 cm H_2O mixture pressure.

1.1.1.5 Combustion Chamber

The dimension of combustion chamber is 258 cm $\times$ 247 cm $\times$150 cm, as shown in Fig. 2.9. This shell is encapsulated by iron material, whose inside wall has insulating material (Glass Fiber) of 30-cm thickness to mitigate the heat loss. The insulating material (Glass Fiber) can resist high temperature up to 1600 . The flame structure was observed by 18.5-cm-diameter of circular windows. A 30-cm-diameter chimney and manhole cover with area of 76 cm x 76 cm were installed on combustion chamber. The setup of chamber is shown in Fig. 2.9.

1.1.1.6 Pipeline Control System

Pipeline control system is divided into three categories, which are oxygen, natural gas and air pipelines. Figure 2.10 shows pipeline configuration image, and the whole of pipeline entity is shown in Fig. 2.11. Natural gas pipeline is 1.5-inch diameter of the tube. Because the experimental burner can produce a maximum calorific capacity of 953,215

kJ/hr, the emergency shut-off valve (Honeywell V4055A 1080) for natural gas pipeline is installed in the upstream of pressure regulating valve. Its role is to ensure safety on the system operation if the combustion system produces an anomalous situation, then it can shut off the supply source of natural gas. The orifice plate (Hauck) installed in the downstream of pressure regulating valve helps to measure flow by the pressure difference between the upstream and downstream of a partially obstructed pipe. The plate provides a precisely measured obstruction that narrows the pipe and forces the flowing substance to constrict. A differential pressure transmitter (Yokogawa Dpharp transmitter EJA 110A) allows the comparison of the pressures between the upstream (unobstructed) and the downstream (constricted). Based on the magnitude of pressure drop, flow rate can be calculated. The Pressure switch (Kromschroder DG.B) installed in the upstream of orifice plate. It is a form of switch that makes electrical contact when a certain set pressure has been reached on its input. This is used to provide on/off switching from a pneumatic or hydraulic source. The switch may be designed to make contact either on pressure rise or on pressure fall. Thus, it can turn off the test system to ensure that operational safety when the pressure of pipeline is out of control. Servo motor (Honeywell M7284C1000) and butterfly valve (Hauck) are installed in the downstream of pressure switches. Besides, the solenoid valve is installed in the downstream of butterfly valve that turns on the switch for natural gas according to combustion progress. The component entities of natural gas pipeline are shown in Fig. 2.12.

The oxygen pipeline mainly provides both air and oxygen to flow into the gas mixer and the oxygen concentration is adjusted by a flowmeter in the combustion chamber. It is a 1.5-inch diameter of the tube. The experimental oxygen was supplied from the liquid oxygen through the evaporator gasification. Then, oxygen and air are mixed to provide the

desired oxygen concentration of oxygen-enriched air. A pressure switch (Kromschroder DG.B), installed in the upstream of evaporator, can turn off the test system to ensure that operational safety when the pressure of pipeline is higher than an assigned allowable value. The orifice plate (Hauck) installed in the downstream of pressure regulating valve is used measure flow. A differential pressure transmitter (Yokogawa Dpharp transmitter EJA 110A) allows the comparison of the pressure on the upstream (unobstructed) and the downstream (constricted). Based on the magnitude of pressure drop, the oxygen of flow rate can be calculated. The solenoid valve was installed in the downstream of orifice plate that can turn on the switch of oxygen. Servo motor (Honeywell M7284C1000) and butterfly valve (Hauck) are installed in the downstream of pressure switch that can control the oxygen flow. It can mix the different concentrations of oxygen to obtain the desired combustion air to meet the required experimental conditions. The component entities of oxygen pipeline are shown in Fig. 2.13.

Air pipeline uses 6-inch diameter of the tube. The supply of air source for oxygen-enriched combustion system is carried out by a direct drive blower (HTB-100-505), shown in Fig. 2.14. Its specifications are as follows: Power is of 5 hp (3.7 kW), Rated voltage of 220 V, Current of 13 A, Maximum pressure of 1100 mmAq, and Maximum air flow of 16.5 m3/min. A low pressure sensor is installed in the downstream of blower that it can turn off the test system to ensure that operational safety when the blower cannot work properly. An orifice plate (Hauck) installed in the downstream of low pressure sensor is used to measures flow. The differential pressure transmitter (Yokogawa Dpharp transmitter EJA 110A) allows the comparison of the pressure on the upstream (unobstructed) and the downstream (constricted). The air flow rate can be calculated based on the magnitude of pressure drop. Servo motor (Honeywell M7284C1000)

and butterfly valve (Hauck) are installed in the downstream of orifice plate to control the air flow. The component entities of air pipeline are shown in Fig. 2.15.

Measurement Instrumentations

Temperature Measurement
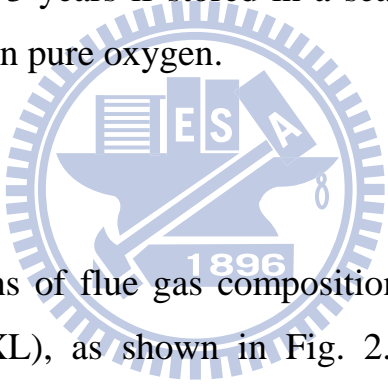
Temperature distributions in the combustion chamber at various O_2 concentrations were measured by thermocouples with 1.6 mm wire diameter, and the outer layer is covered by inconel, as shown in Fig. 2.16. The type of thermocouples is K. Type K (chromel–alumel) is the most commonly used general purpose thermocouple. It is inexpensive and, owing to its popularity, available in a wide variety of probes. They are available in the −200 °C to +1350 °C range. The measured plane located at vertical-upper-central half plane. There were ten measured points in the x-axis and three measured points in the y-axis. The measured points were thirty totally and each point space of x-axis and y-axis were 6 cm vertically and 6.5 cm horizontally, as shown in Fig. 2.17. Each measured temperature data is obtained by data acquisition system (Fluke 2680A) and the frequency is 1 point per second.

Oxygen Analyzer

In order to confirm that well mix the air with oxygen in an assigned fraction. Therefore, the mixture gas passes through the oxygen analyzer (Sensorbay Mini-25H) to measure the oxygen concentration, as shown in Fig. 2.18. This oxygen sensor has a wide measuring range of oxygen concentration from 0% to 100% (Response time: T90 ≦ 10s), and the

accuracy is 0.1% O_2. It uses chemical reaction occurs in the fuel cell when the potassium hydroxide in the cell comes into contact with oxygen. This creates an electric current between the lead anode and the gold-plated cathode through a load resistance. The voltage produced is proportional to the concentration of oxygen present. The sensor has a limited lifetime which is reduced by exposure to high concentration of oxygen. The reaction between oxygen and lead at the anode consumes lead, which eventually results in the cell to fail to sense high concentrations of oxygen. Even when installed in an instrument which is never turned on, oxygen sensors which are exposed to atmosphere which contains oxygen are generating current, and being used up. Typically, the oxygen sensor will function correctly for 3 years if stored in a sealed bag of air but only for four months if stored in pure oxygen.

Gas Analyzer

The concentrations of flue gas compositions are analyzed by the gas analyzer (Testo 350XL), as shown in Fig. 2.19. The gas analyzer can analyze O_2, CO, NO_x, CO_2 and SO_2. The measurement principles of gas analyzer uses electrochemical measuring cells for the O_2, CO, NO, NO_2 and SO_2 parameters. Besides, an NDIR sensor is used for CO_2. The detailed data of sensors are shown in Table 2.1. The gas analyzer system consists of sampling probe, condensate trap, filter, pump P, capillary, antechamber and sensors. The schematic configuration of gas analyzer is shown in Fig. 2.20. The flue gas is drawn through the sampling probe by the pump P and sent to the condensate trap. The condensate trap and integral filter dry the flue gas. The gas sample passes through the pump P and is forced through a capillary (narrowing the gas path) into an antechamber which damps the hammer effect produced by the diaphragm pump. On leaving the

antechamber, the gas to be measured flows into the measuring cells, which depending on the design measure the O_2, CO_2, CO, NO, NO_2 and SO_2 concentrations. The concentrations of species were dry volume base. For fair comparison, CO, CO_2, NO_x and SO_2 were corrected to 6% O_2 base based on the following equation:

$$[S]_c = [S]_m \times \frac{[O_2]_a - 6}{[O_2]_a - [O_2]_m} \tag{2.3}$$

Where $[S]_c$ is the corrected CO, CO_2, SO_2 or NO_x concentration at 6% O_2 base, $[S]_m$ is the measured CO, CO_2, SO_2 or NO_x concentration, $[O_2]_a$ is the O_2 concentration of supply combustion air, and $[O_2]_m$ is the measured O_2 concentration in the flue gas.

Radiation Measurement

The radiate heat flux is measured used radiometer (Vatell Corporation TG9000-2), as shown in Fig. 2.21. It is water cooled purged radiometer. When constructed as a radiometer, convective heat flux is blocked from reaching the sensor by a window. This allows only radiation to be measured. The window is placed directly on the water-cooled copper surface to minimize its heating. The radiation sensor is designed to provide an approx output signal of 10 mV when exposed to the specified heat flux range. The sensor can be exposed to approx 50% higher heat flux and still provide a good output signal. The measuring points which are located in the center axis of burner (Distance from the bottom 75 cm combustion chamber) on the right side of wall which distance from the burner 85 cm, 120cm and 175 cm, as shown in Fig. 2.7.

Flame Shape Analysis

The appearance of the flame is to use a digital video camera (Sony TRV-950) to record, as shown in Fig. 2.22. The flame shape analysis is to use National Instruments LabVIEW to do image processing.

Data Acquisition System

Each measured temperature data is obtained by data acquisition system (Fluke 2680A Series) and the frequency is 1 point per second. The picture of the data logger is shown in Fig. 2.23.

Experiment Test Conditions

In this study, there were two kinds of experimental tests, one was heating test and the other one was fixing furnace temperature test. For the heating test, the target heating temperature was 1200℃. Natural gas with heating value of 42 MJ/m^3, which is supplied by Chinese Petroleum Corporation (CPC), is the fuel. When the furnace temperature reached 1200 ℃, the experiment was stopped and we recorded the elapsed time. For the fixing furnace temperature test, we changed the natural gas flow rate to control furnace temperature at 1220±10 ℃ at different oxygen concentration. The experimental time was 90 minutes that started from the furnace temperature was stable. In spite of heating and fixing furnace temperature tests, we firstly adjusted the oxygen and air flow rates to mix to desired oxygen concentration and then starting the experiments. In this study, we selected five oxygen concentrations to perform the experiments. These five selected oxygen concentrations were 21%, 24%, 26%, 28%, and 30%, respectively.

Experimental Procedures

Procedure of the Lab Scale Experimental Operation

Ignition program

1. Open the room windows fully.

2. Press the start button of control panel (System ON).

3. Press the start button of combustion air fan to let it continues to operate for three minutes.

4. Press the start button of natural gas switch (MAIN VALVE ON).

5. Open the natural gas valve at the cylinder.

6. Press the ignition button (IGNITION).

7. Confirm the flame being ignited.

Oxygen-enriched combustion experiment program

1. Open the oxygen valve after the flame ignition.

2. Adjust the air, oxygen and natural gas flow rates, respectively, to the assigned values.

3. Measure and record the experimental data.

Shutdown procedure

1. Press the shutdown button of control panel.

2. Turn off the natural gas valve.

3. Turn off the oxygen valve.

4. Press the shutdown button of combustion air fan after the fan continues to operate at least three minutes.

5. Press the shutdown button of control panel (System OFF).

6. Turn off the exhaust fan.

7. Shut off the room windows.

Procedure of the pilot Scale Experimental Operation

Ignition program

1. Open the room windows fully.

2. Turn on the exhaust fan.

3. Press the start button of control panel (System ON).

4. Adjust burning mode to oxygen-enriched combustion.

5. Adjust control mode to panel rotary control.

6. Adjust combustion air fan mode to bypass (5HP FDF BYPASS).

7. Press the start button of 5HP combustion air fan (5HP FDF ON) and let it continues to operate for three minutes.

8. Press the start button of natural gas switch (MAIN VALVE ON).

9. Turn on the natural gas valve.

10. Press the ignition button (IGNITION).

11. Confirm the flame being ignited.

Oxygen-enriched combustion experiment program

1. Open the valve and solenoid valve of oxygen tube after the flame ignition (oxygen, VALVE ON).

2. Adjust air, oxygen and natural gas flow rates to the assigned values.

3. Measure and record the experimental data.

Shutdown procedure

1. Press the shutdown button of control panel.

2. Turn off the natural gas valve.

3. Turn off the oxygen valve.

4. Press the shutdown button of 5HP combustion air fan (5HP FDF OFF) after the fan continues to operate at least three minutes.

5. Press the shutdown button of control panel (System OFF).

6. Turn off the exhaust fan.

7. Shut off the room windows.

Table 2.1 The detailed data of gas analyzer sensor

	O_2	CO	NO	NO_2	SO_2	CO_2
Meas. Range	0 to 25% Vol.	0 to +10000 ppm H_2 comp.	0 to +3000 ppm	0 to 500 ppm	0 to 5000 ppm	0 to 50% Vol.
Accuracy	±08% of fsv (0 to +25 Vol. %)	±5% of mv (+200 to +2000 ppm CO) ±10% of mv (+2001 to +10000 ppm CO) ±10 ppm CO (0 to +199 ppm CO)	±5% of mv (+100 to +1999.9 ppm NO) ±10% of mv (+2000 to +3000 ppm NO) ±5 ppm NO (0 to +3000 ppm NO)	±5% of mv (+100 to +500 ppm NO_2) ±5 ppm NO_2 (0 to +99.9 ppm NO_2)	±5% of mv (+100 to +2000 ppm SO_2) ±10% of mv (+2001 to +5000 ppm SO_2) ±5ppm SO_2 (0 to +99 ppm SO_2)	±0.3% vol. CO_2 +1% of m.v. (0 to 25% vol. CO_2) ±0.5% vol. CO_2 +1.5% of m.v (>25 to 50% vol. CO_2)
Resolution	0.01 Vol. % O_2 (0 to +25 Vol. % O_2)	1 ppm CO (0 to +1000 ppm CO)	1 ppm NO (0 to +30000 ppm NO)	0.1 ppm NO_2 (0 to +500 ppm NO_2)	1 ppm SO_2 (0 to +5000 ppm SO_2)	0.01% vol. CO_2 (0 to 25% vol. CO_2) 0.01% vol. CO_2 (>25% vol. CO_2)
Resp. Time	20s (t95)	40s (t90)	30s (t90)	40s (t90)	30s (t90)	<10s (t90)
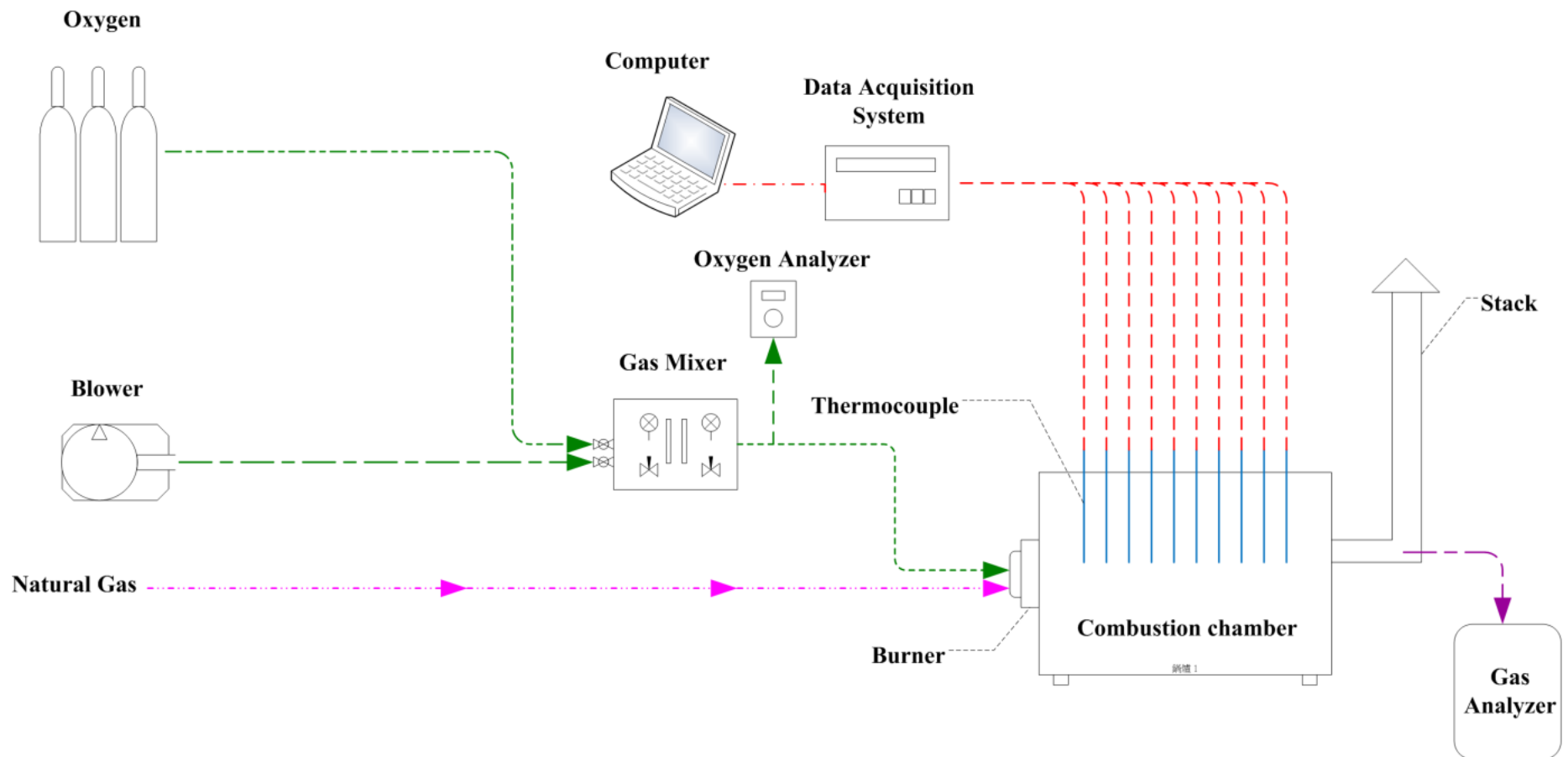
Figure 2.1 Schematic diagram of the Lab-Scale experimental apparatus

(a)

DIMENSIONS in inches

⁵/₈ slots for ¹/₂ studs or bolts

¹/₈ fpt air pressure tap

³/₄ fpt hole at 45° to all Ȼ's
for pilot or manual lighting

³/₄ fpt hole for flame supervision

9 sq.

gas tube nozzle
used on
-0 size only

steel shell
(4423- -L & 4424- -L only)

refractory face
(4424 only)

B–fpt
Gas

A–fpt Air

Section C-C

weight: 47 lb
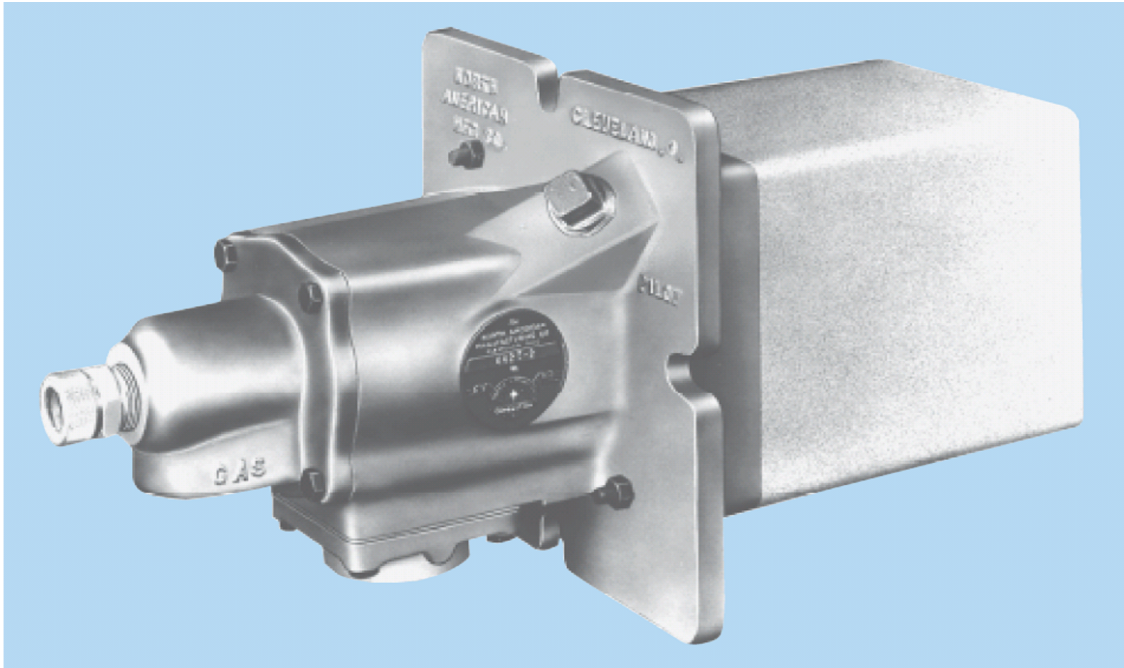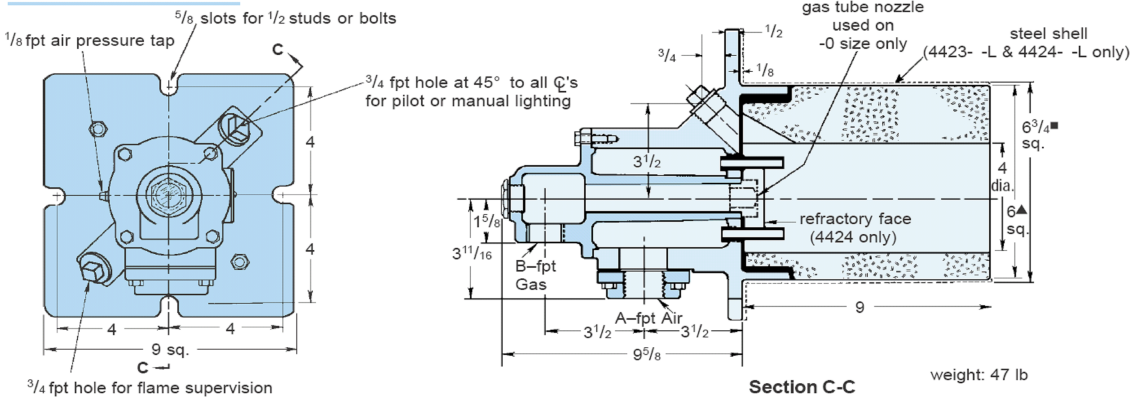
(b)

Figure 2.2 Burner of the furnace (North the American 4423-0)

(a) The picture and (b) The schematic configuration

Figure 2.3 The Picture of combustion chamber (Lab-Scale)
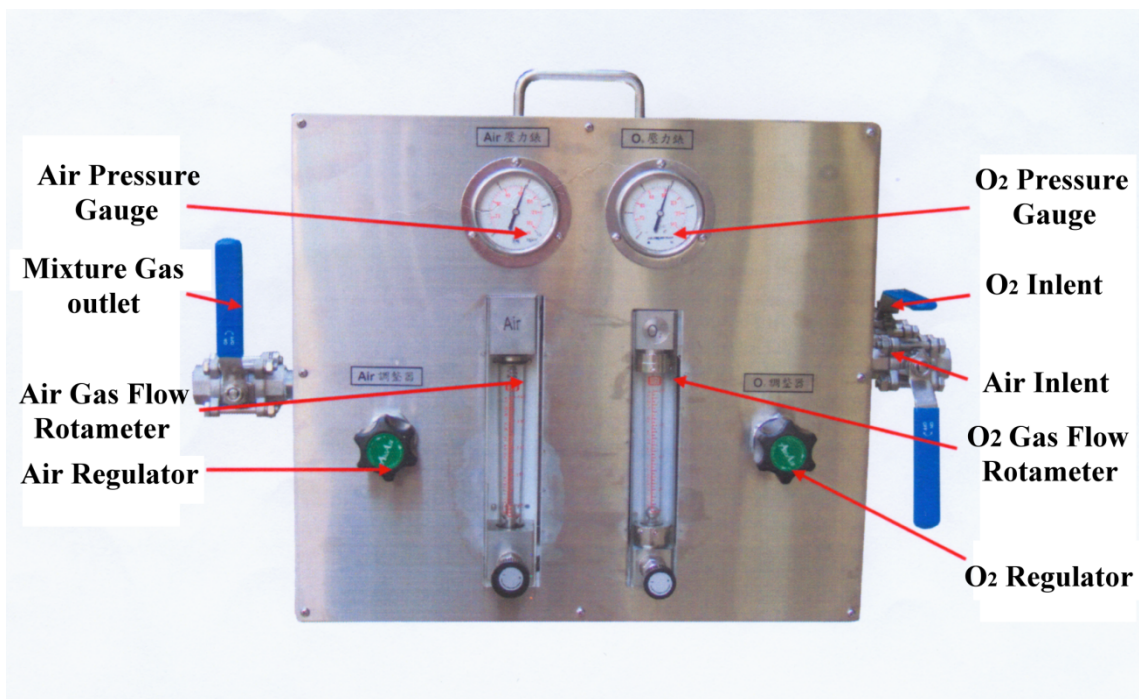
Figure 2.4 The picture of gas mixer system consists
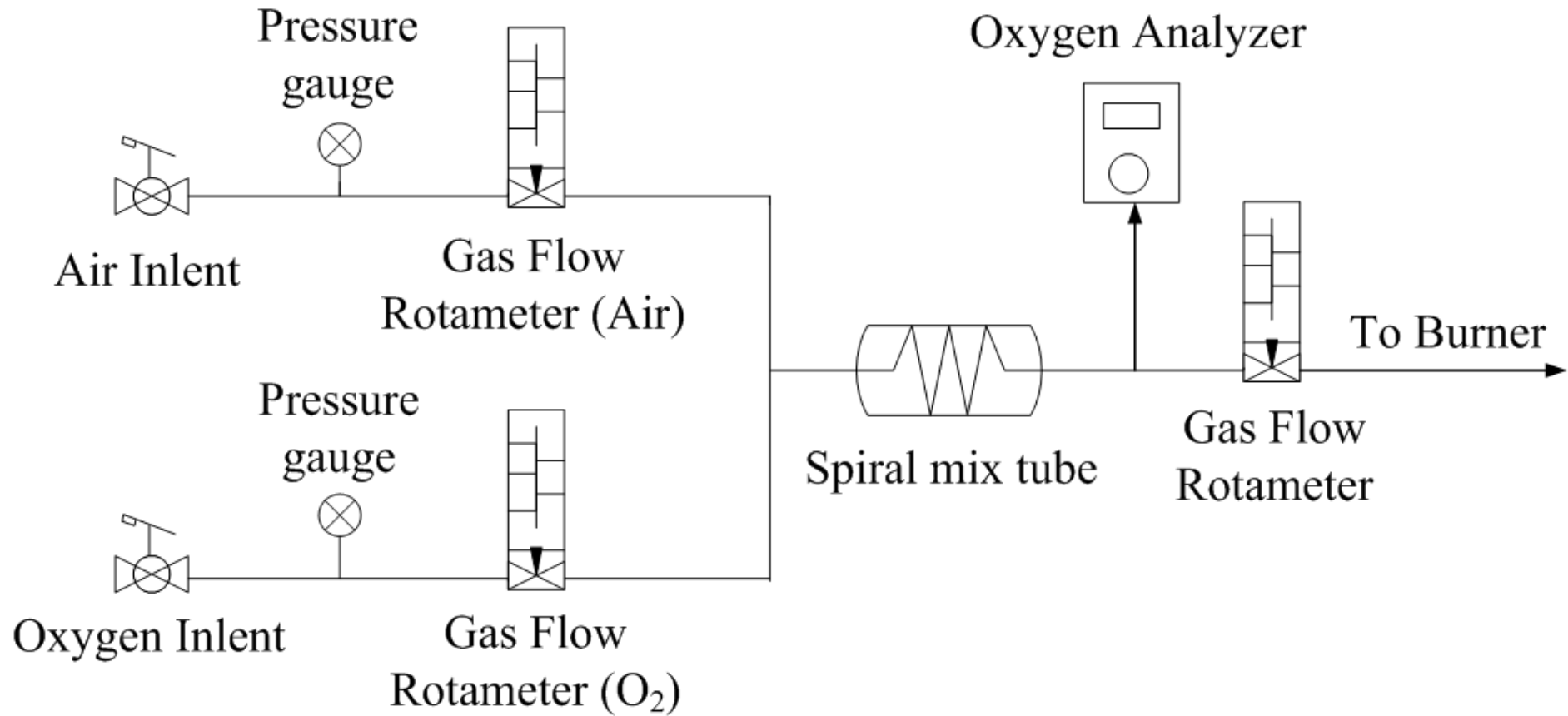
Figure 2.5 The schematic configuration of gas mixer
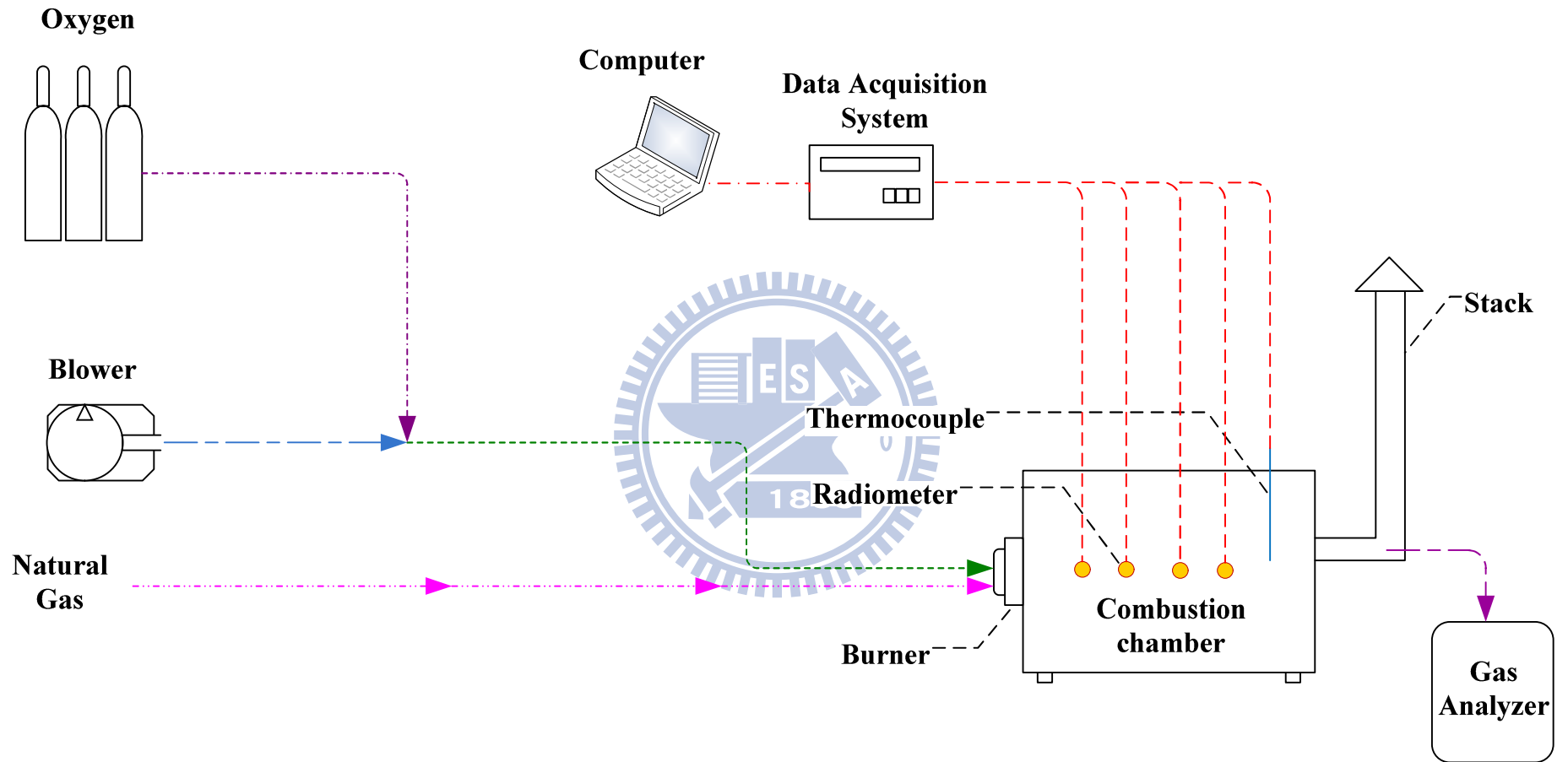
Figure 2.6 Schematic diagram of the Pilot-Scale experimental apparatus

258
247
160
120
25
Furnace temperature
150
Radiate heat flux
75
Burner
85
120 175
210
Unit :(cm)
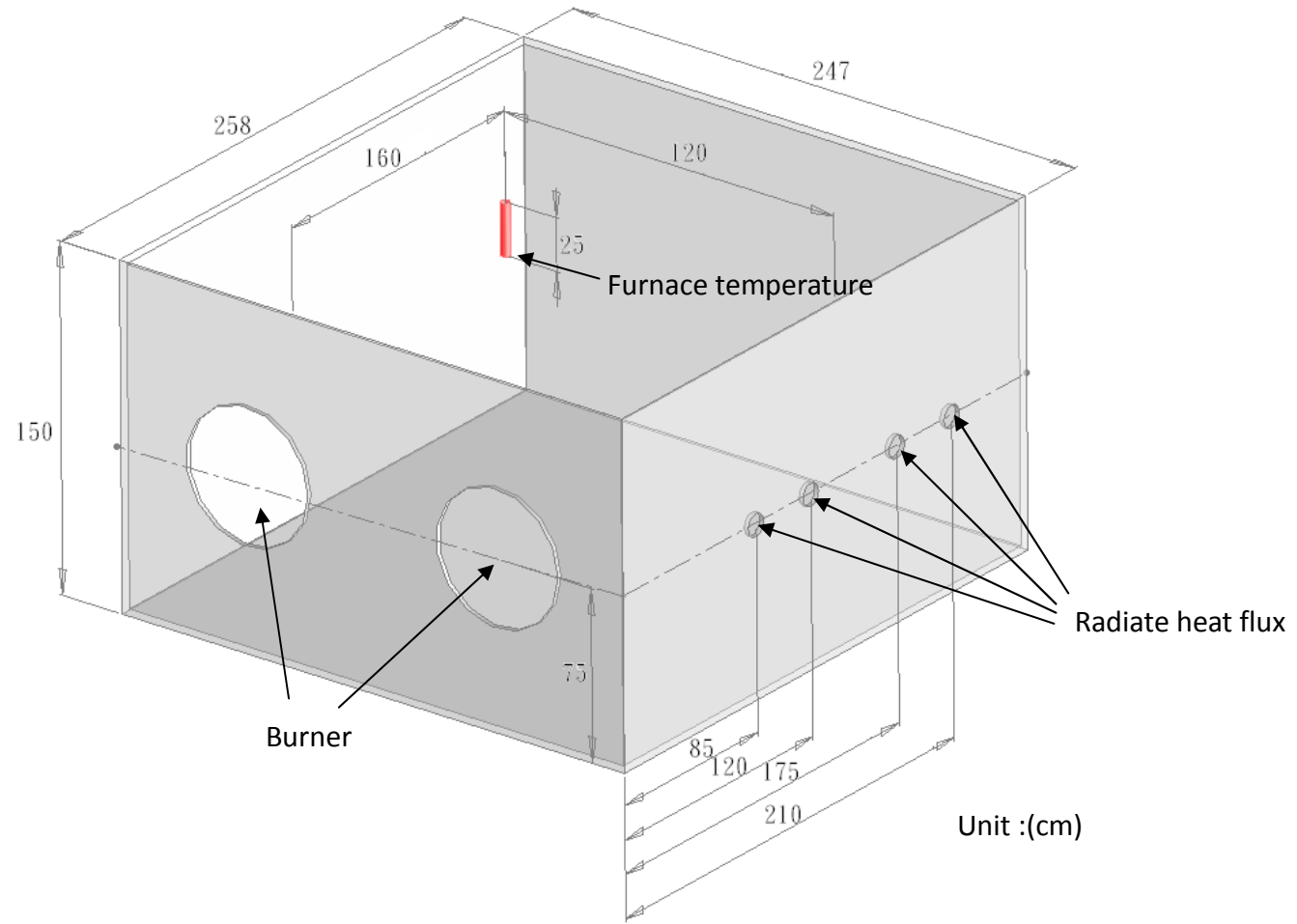
Figure 2.7 Schematic configuration of the Pilot-Scale experimental sensors

33

(a)

45°   **A**– NPT
      Air Inlet

D sq.

C
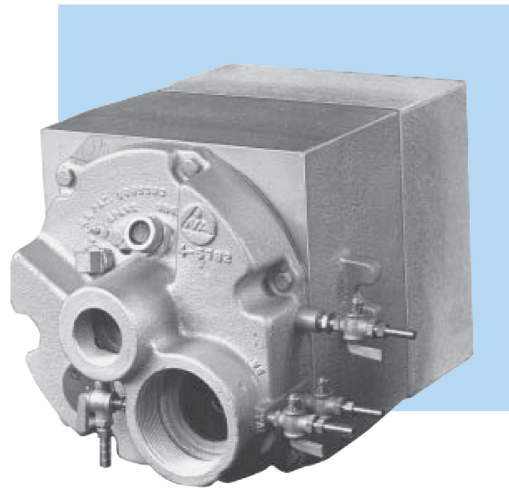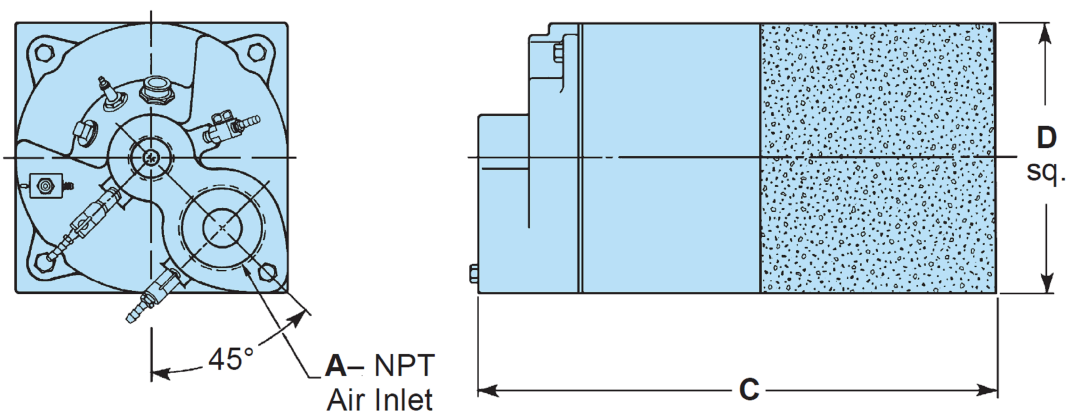
(b)

Figure 2.8 Burner of the furnace (North the American TEMPEST

4442-5) (a) The picture and (b) The schematic configuration

(a) The position of the burner   (b) Chimney

(c) Manhole cover   (d) Observation window

Figure 2.9 The Picture of combustion chamber (Pilot-Scale)
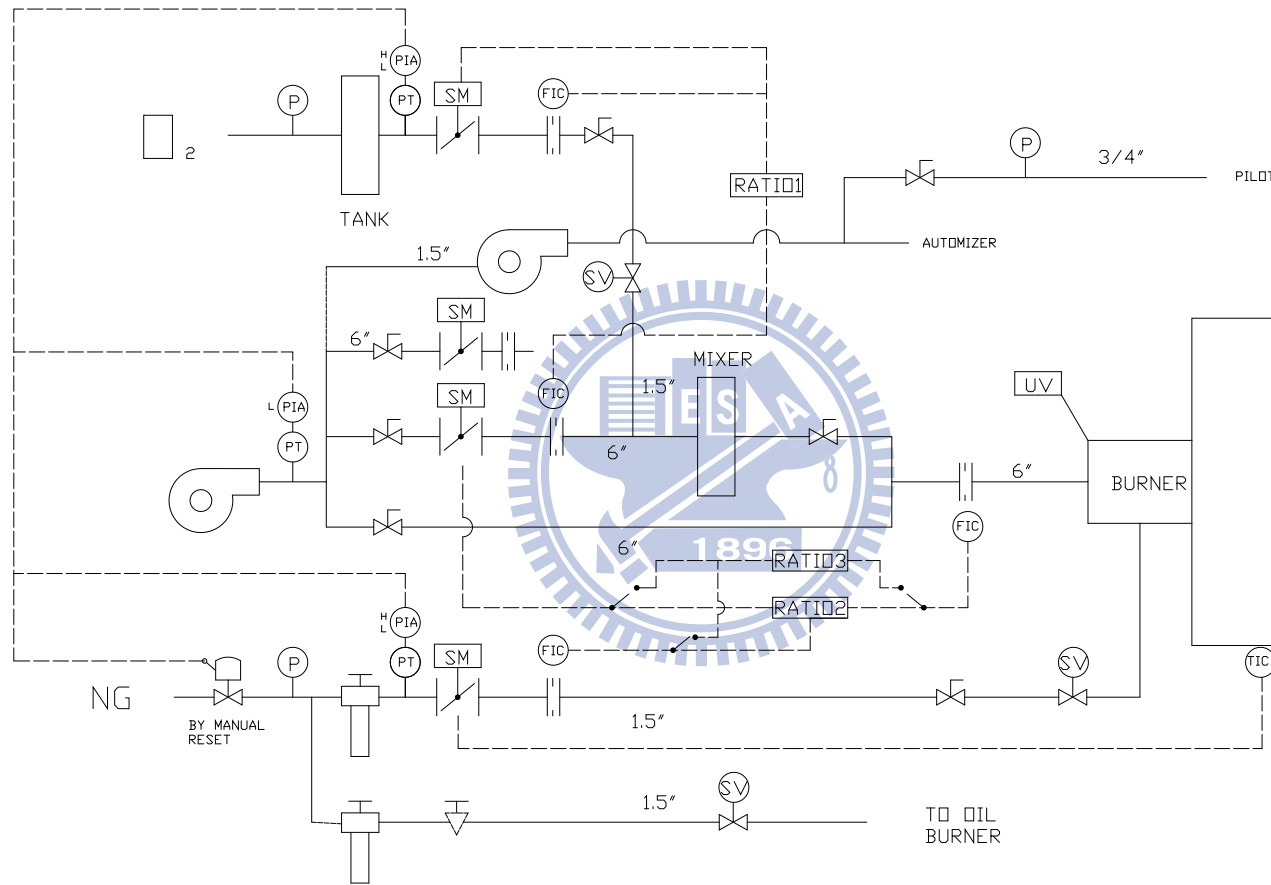
Figure 2.10 The schematic configuration of pipeline control system (Pilot-Scale)

Figure 2.11 The Picture of pipeline control system (Pilot-Scale)

(a) Emergency shut-off valve (b) Pressure regulating valve
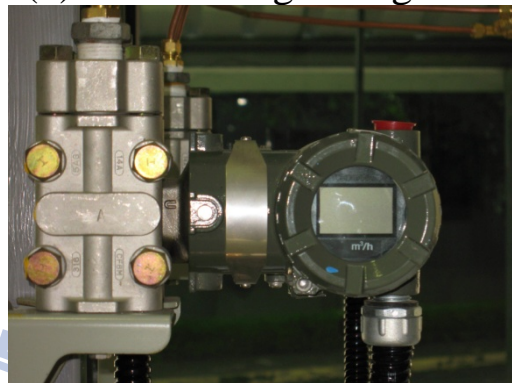
(c) Orifice plate (d) Differential pressure transmitter

(e) Pressure switch (f) Servo motor

(g) Butterfly valve

Figure 2.12 The Picture of natural pipeline components (Pilot-Scale)

(a) Servo motor

(b) Pressure switch

(c) Differential pressure transmitter

(e) Liquid oxygen

(f) Orifice plate

(g) Butterfly valve

Figure 2.13 The Picture of oxygen pipeline components

(Pilot-Scale)

(a)
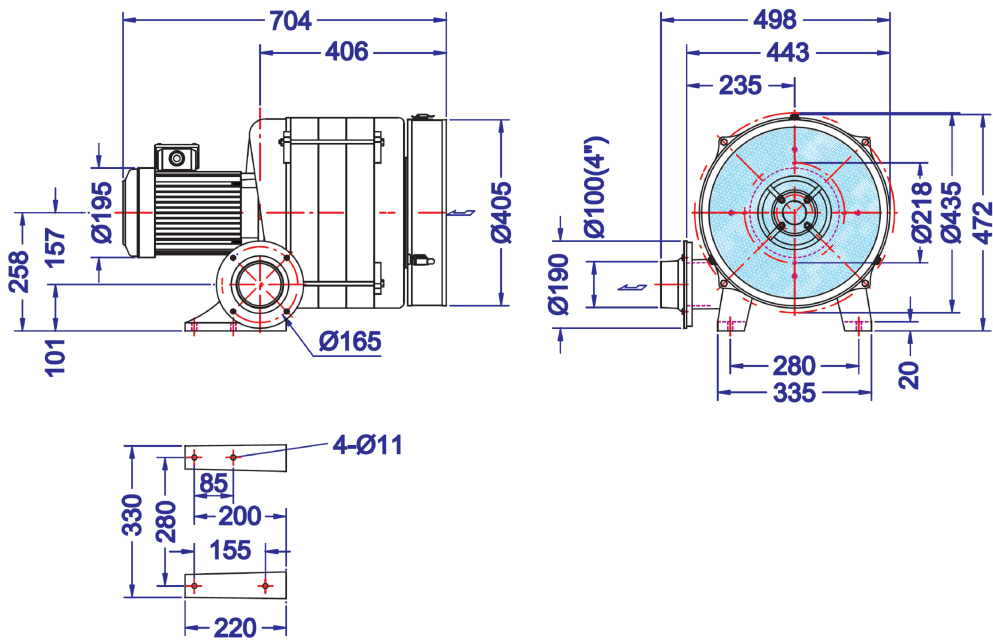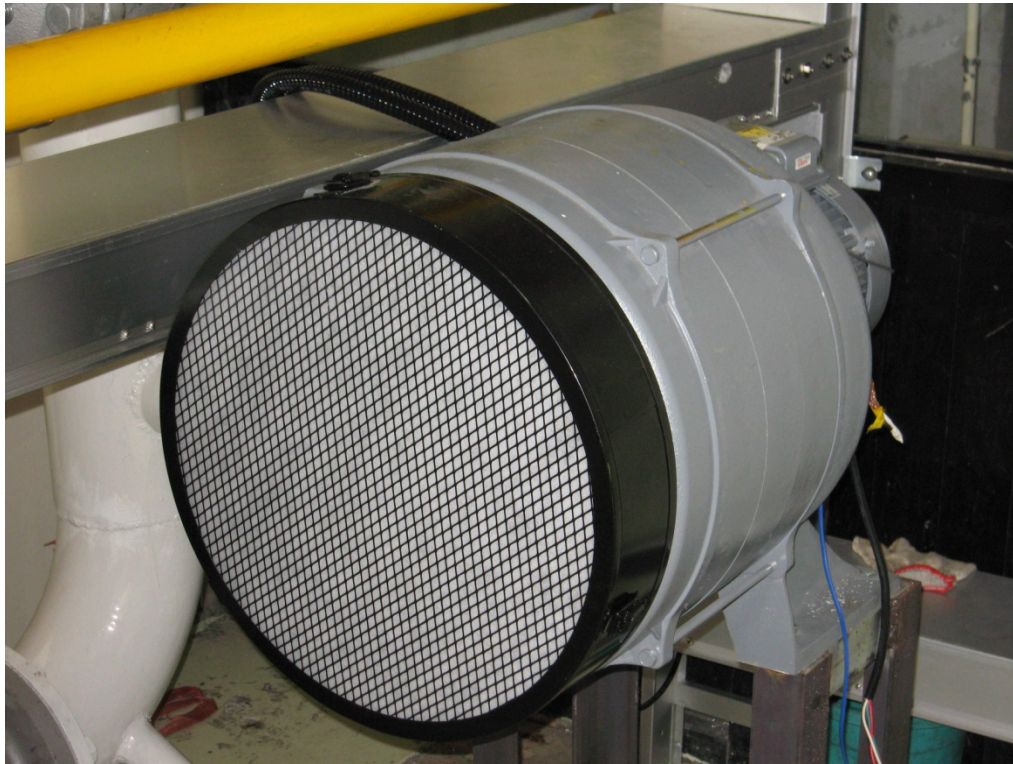
(b)

Figure 2.14 Direct drive blower (HTB-100-505) (a) The picture

and (b) The schematic configuration (Pilot-Scale)

(a) Orifice plate
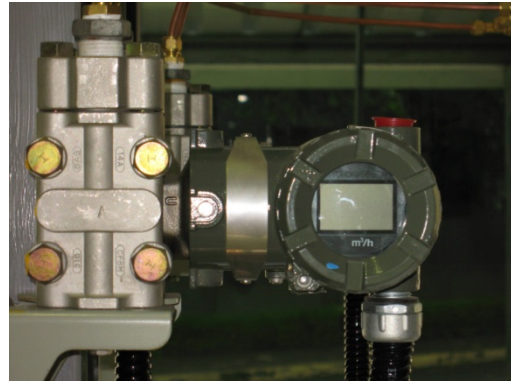
(b) Differential pressure transmitter

(c) Pressure switch

(d) Servo motor

Figure 2.15 The Picture of air pipeline components (Pilot-Scale)

Figure 2.16 The picture of K-type thermocouple
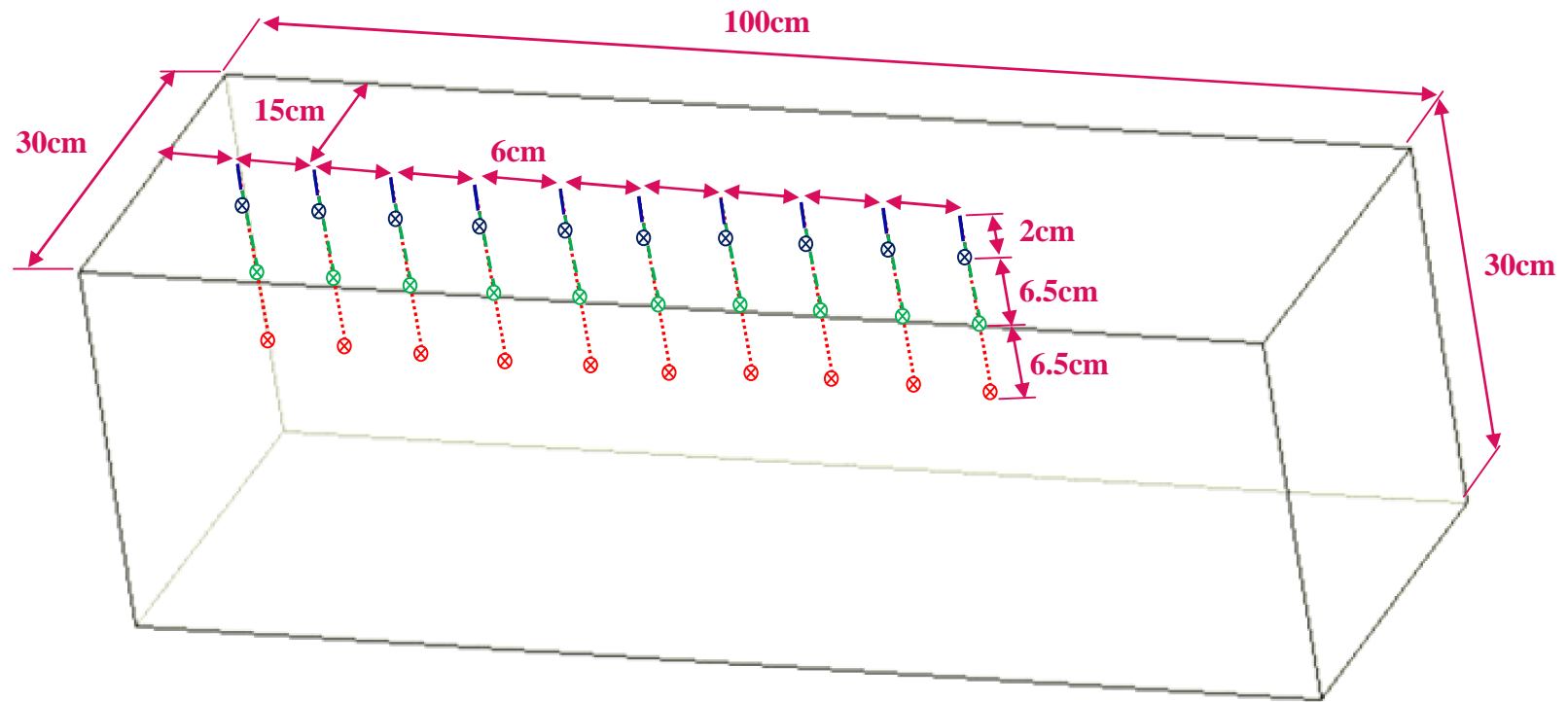
Figure 2.17 The measuring position of thermocouple (Lab-Scale)

Figure 2.18 The picture of oxygen analyzer (Sensorbay Mini-25H)

(a)   (b)

Figure 2.19 The picture of gas analyzer (Testo 350XL)

(a) Front view and (b) Back view
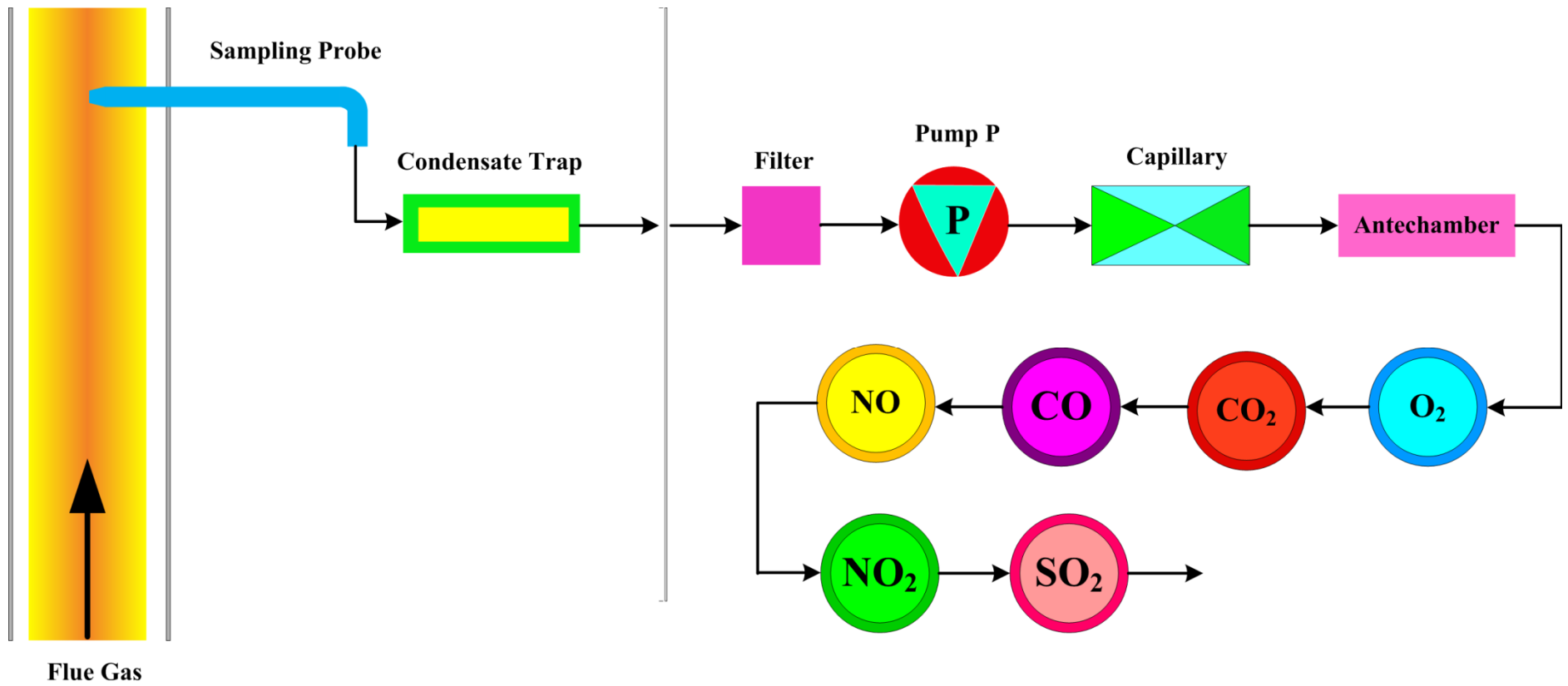
Figure 2.20 The schematic configuration of gas analyze
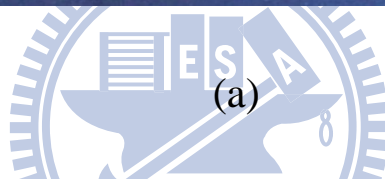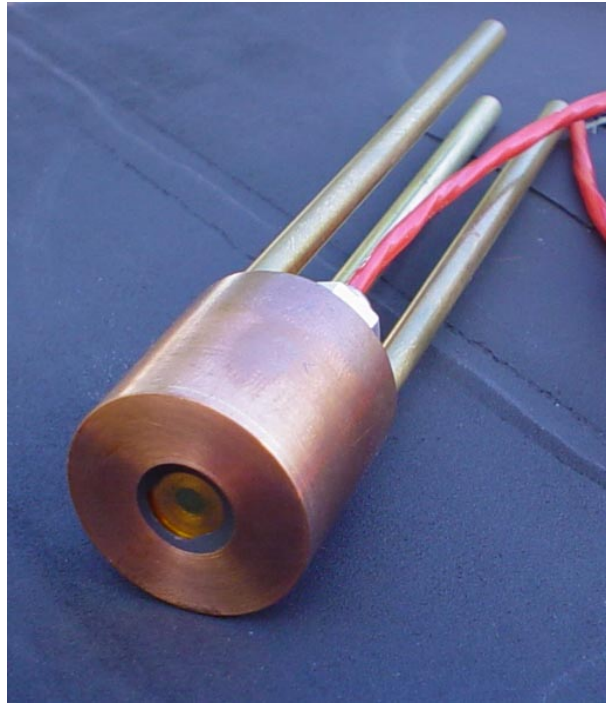
(a)
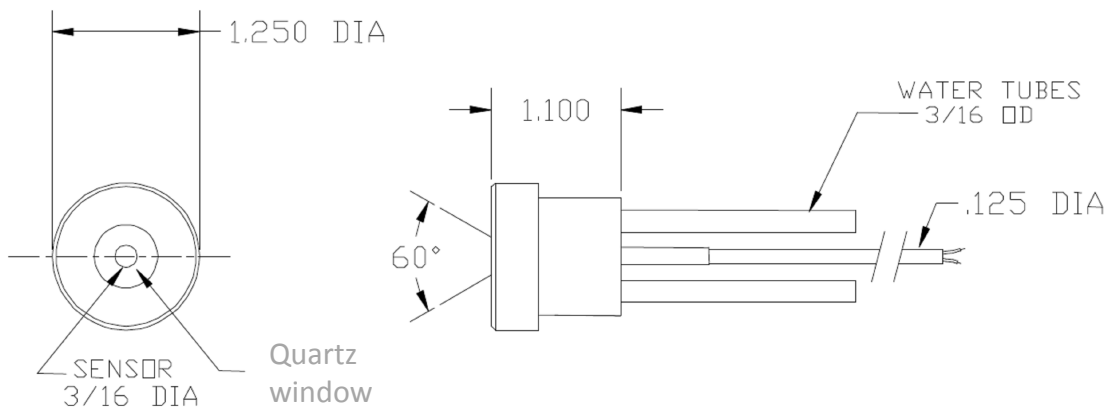
(b)

Figure 2.21 Radiometer (Vatell Corporation TG9000-2)

(a) The picture and (b) The schematic configuration

Figure 2.22 The picture of digital video camera (Sony TRV-950)

(a)

Figure 2.23 The picture of data acquisition system

(Fluke 2680A Series) (a) Front view and (b) Back view

Chapter 3

Uncertainty Analysis

All of the data from experimental results may not be equally good to adopt. Their accuracy should be confirmed before the analyses of experimental results are carried out. Uncertainty analysis (or error analysis) is a procedure used to quantify data validity and accuracy [37]. Errors are always presented in experimental measurements.　Experimental errors can be categorized into the fixed (systematic) error and random (non-repeatability) error, respectively [37]. Fixed error is the same for each reading and can be removed by proper calibration and correction. Random error is different for every reading and hence cannot be removed. The objective of uncertainty analysis is to estimate the probable random error in experimental results.

From the viewpoint of reliable estimation, it can be categorized into single-sample and multi-sample experiments. If experiments could be repeated enough times by enough observers and diverse instruments, then the reliability of the results could be assured by the use of statistics [38]. Like such, repetitive experiments would be called multi-sample ones. Experiments of the type, in which uncertainties are not found by repetition because of time and costs, would be called single-sample experiments.

Analyses of the Propagation of Uncertainty in Calculations

Uncertainty analysis is carried out here to estimate the uncertainty levels in the experiment. Formulas for evaluating the uncertainty levels in the experiment can be found in many papers [38,39] and textbooks [37,40,41]. They are presented as follows:

Suppose that there are n independent variables, x_1, x_2,…, x_n, of

experimental measurements, and the relative uncertainty of each independently measured quantity is estimated as ui. The measurements are used to calculate some experimental result, R, which is a function of independent variables, $x_1, x_2, \ldots, x_n$; $R = R(x_1, \ x_2 \ ,..., \ x_n)$.

An individual xi, which affects error of R, can be estimated by the deviation of a function. A variation, δx_i, in x_i would cause R to vary according to

$$\delta R_i = \frac{\partial R}{\partial x_i} \delta x_i .$$
(3.1)

Normalize above equation by dividing R to obtain

$$\frac{\delta R_i}{R} = \frac{1}{R} \frac{\partial R}{\partial x_i} \delta x_i = \frac{x_i}{R} \frac{\partial R}{\partial x_i} \frac{\delta x_i}{x_i}$$
(3.2)

Eq. (3.2) can be used to estimate the uncertainty interval in the result due to the variation in xi. Substitute the uncertainty interval for xi,

$$u_{R_i} = \frac{x_i}{R} \frac{\partial R}{\partial x_i} u_{x_i}$$
(3.3)

To estimate the uncertainty in R due to the combined effects of uncertainty intervals in all the xi's, it can be shown that the best representation for the uncertainty interval of the result is [39]

$$u_R = \pm \left[\left(\frac{x_1}{R} \frac{\partial R}{\partial x_1} u_1 \right)^2 + \left(\frac{x_2}{R} \frac{\partial R}{\partial x_2} u_2 \right)^2 + ... + \left(\frac{x_n}{R} \frac{\partial R}{\partial x_n} u_n \right)^2 \right]^{\frac{1}{2}}$$
(3.4)

Uncertainty Level Analysis in the Experiment

All uncertainty analyses according to the calculations of above formula. Several parameters are selected to demonstrate the process of uncertainty level analyses as follows.

The surface area of the laboratory-scale burner, A_{Lab_burner}, is

$$A_{Lab\_burnwe} = \frac{\pi}{4} \times a^2, \quad a = 101.6 \pm 0.5 mm$$

$$A_{Lab\_burner} = A(a)$$

$$u_A = \pm \left[\left(\frac{a}{A} \frac{\partial A}{\partial a} u_a \right)^2 \right]^{1/2} = \pm \left[(u_a)^2 \right]^{1/2} = \pm 0.0049$$

Where ($u_a = \frac{0.5}{101.6} = 0.0049$)

The uncertainty of airflow velocity, $u_{V_{air}}$, is

$$U_{in} = \frac{Q_{Air}}{A_{Lab\_burner}}, \quad U_{in} : \text{Airflow velocity}, \quad Q_{Air} : \text{Flux of air}$$

$$U_{in} = U_{in}(Q_{Air}, A_{Lab\_burner})$$

$$u_{U_{in}} = \pm \left[(u_{Q_{Air}})^2 + (-u_{A_{Lab\_burner}})^2 \right]^{1/2}$$

The uncertainty of fuel velocity, $u_{V_{fuel}}$, is

$$V_w = \frac{Q_{fuel}}{A_{Lab\_burner}}, \quad V_w : \text{Fuel velocity}, \quad Q_{fuel} : \text{Flux of fuel}$$

$$V_w = V_w(Q_{fuel}, A_{Lab\_burner})$$

$$u_{V_w} = \pm \left[(u_{Q_{fuel}})^2 + (-u_{A_{Lab\_burner}})^2 \right]^{1/2}$$

The uncertainties of the properties are

$$u_{\rho(T)} = \pm \frac{\delta \rho}{\rho} = \frac{1}{\rho} \frac{d\rho}{dT} (\pm \delta T)$$

$$u_{v(T)} = \pm \frac{\delta v}{v} = \frac{1}{v} \frac{dv}{dT} (\pm \delta T)$$

The uncertainty of P_{sat} is

$$ln(P_{sat}(T_0)) = 23.2 - \frac{3816}{(-46+T_0)}$$

$$P_{sat} = e^{23.2 - \frac{3816}{(-46+T_0)}}$$

$$u_{P_{sat}} = \frac{T}{P_{sat}} \frac{\partial P_{sat}}{\partial T} \frac{\partial T}{T}$$

The uncertainty of Φ is

$$\Phi = \frac{X_{O_2}^{A^0} - X_{O_2}^{A}}{(1 - X_{O_2}^{A}) X_{O_2}^{A^0}}$$

$$\Phi = \Phi\left(X_{O_2}^{A^0}, X_{O_2}^{A}\right)$$

$$u_{\Phi} = \pm\left[\left(u_{X_{O_2}^{A^0}}\right)^2 + \left(u_{X_{O_2}^{A}}\right)^2\right]^{\frac{1}{2}}$$

The Asymmetric Uncertainties of Thermocouple

The temperatures were measured by thermocouples with 1.6 mm wire diameter, and the outer layer is covered by inconel, as shown in Fig. 2.16. The accuracy of the thermocouple itself without coating is ±0.2%. Due to the effects of conduction, convection, and radiation heat flux, it is worthwhile to check the correctness of gas temperature measured by such K-typed thermocouple. Via an application of energy balance, i.e.,

Energy in = Energy out, or

Convection to the junction of thermocouple = Radiation from the junction of thermocouple + Conduction loss from the probe

Because of the fine thermocouple (1.6mm), the conduction term can be neglected. Then, the steady-state energy equation can be rewritten as follows.

$$A_w h(T_g - T_t) - A_w \sigma(\varepsilon T_t^4 - \alpha T_w^4) = 0 \tag{3.5}$$

In practice, the flame temperature is much higher than the wall temperature of thermocouple, so the absorption term, αT_w^4, from the relatively low wall temperature of thermocouple can be removed from Eq. (3.5). According to Eq. (3.5), the expression of correlation is given as:

$$T_g = T_t + \frac{\varepsilon \sigma T_t^4}{h} \qquad (3.6)$$

where T_g =   the true gas temperature

              T_t =   the temperature measured by thermocouple probe

              ε =   emissivity of the thermocouple

              σ =   Stefan Boltzmann constant

              h =   convection heat transfer coefficient at wire surface

Now, the analysis method of uncertainty can be utilized to obtain the uncertainty in the flame temperature from the correlation associated with h, T_t, and ε. The relationship between temperature and error is shown in Fig. 3.1.

The Uncertainties of Radiometer

The radiometer (Vatell Corporation TG9000-2) is provided with the certified calibrations. These calibrations were performed using instruments, whose accuracy is traceable to the National Institute of Standards and Technology (NIST) and following procedures set in the Vatell quality assurance manual, as shown in Fig. 3.2. The uncertainty of its performance is 3%, indicated by the report.

The Uncertainties of Gas Analyzer

The Gas Analyzer (Testo 350XL) is provided with the certified calibrations, compiled with ISO/IEC 17025. Calibrations are corrected by the National Measurement Laboratory (NML) R.O.C., and Physikalisch-Technische Bundesanstalt (PTB) B.R.D through temperature

standards and electrical standards. The uncertainties of O_2, CO, CO_2, NO_X, and SO_2 are given in Fig. 3.3 of the NML report, respectively.

The Experimental Repeatability

Because the flame length under a specific condition is impossible fixed, in order to confirm the accuracy and coincidence of experimental data, it is obtained by taking 350 pieces of images to make the average. The flame length is defined by the constant gray-scale value. The averaged value and the coefficient of variation are listed in Table 3.1.The coefficient of variation (C.V.) is defined as the ratio of the standard deviations to the mean $\overline{X}$, where the standard deviation s is calculated as:

$$s = \sqrt{\frac{1}{N} \sum_{i=1}^{N} (X_i - \overline{X})^2}$$

(3.7)

The coefficient of variation is a dimensionless number that allows comparison of the variation of data points in a data series around the mean. Figure 3.14 graphically shows the presentation of Table 3.1. It can be seen that in general the coefficients of variation are within the acceptable range since the maximum is below 8%, consequently, the experimental is quite good.

Table 3.1 Experimental repeatability

O_2(%)	Excess Air Ratio	Flame Length (cm)	
		Average	C.V.
21%	1.02	66.34	7.7%
	1.05	64.46	7.9%
	1.10	60.47	7.1%
	1.15	55.92	6.4%
24%	1.02	73.30	6.9%
	1.05	72.61	7.0%
	1.10	68.90	7.2%
	1.15	64.81	7.7%
26%	1.02	76.08	5.8%
	1.05	74.38	5.6%
	1.10	70.16	5.6%
	1.15	66.41	4.4%
28%	1.02	78.95	5.7%
	1.05	76.36	5.3%
	1.10	72.62	5.9%
	1.15	68.28	6.2%
30%	1.02	82.79	6.4%
	1.05	81.22	5.49%
	1.10	76.45	5.57%
	1.15	73.12	5.99%
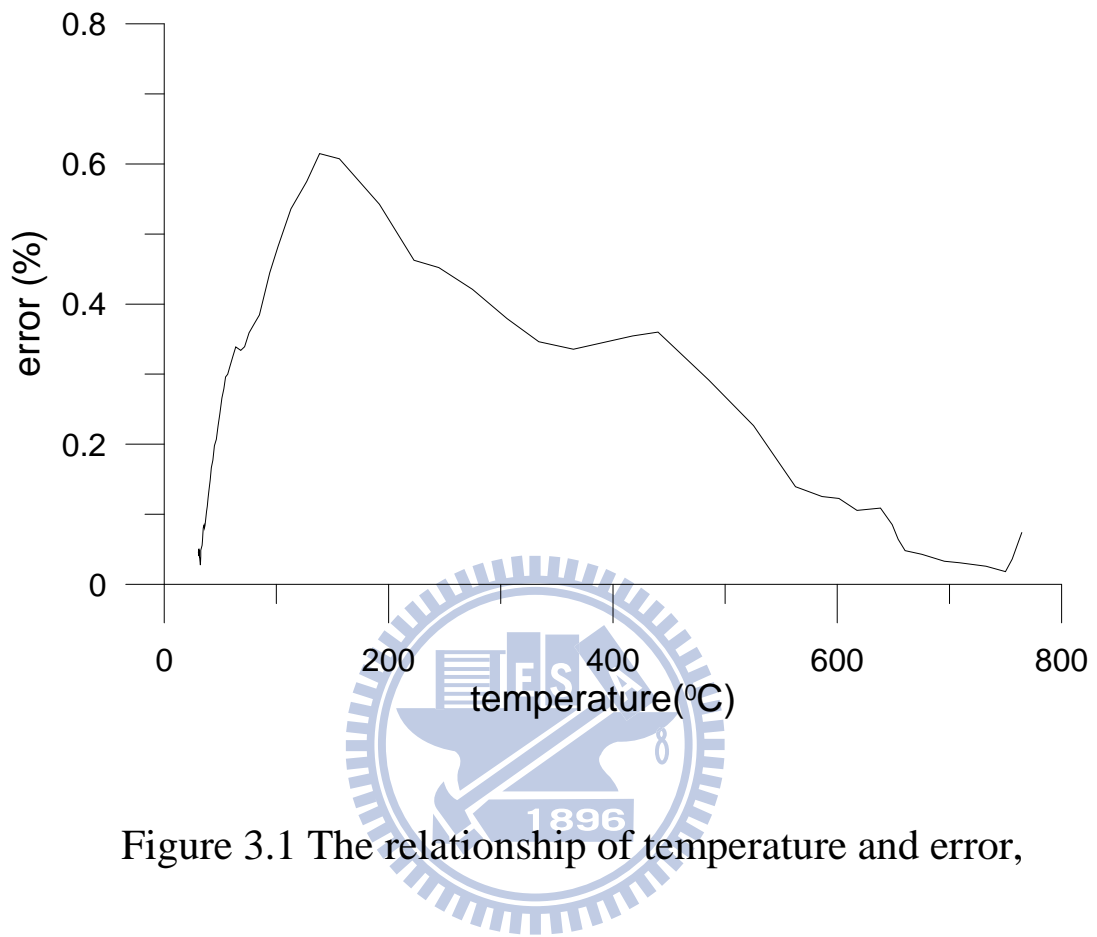
Figure 3.1 The relationship of temperature and error,

reproduced from Ref. [42]

VATELL CORPORATION

Certificate of Calibration

Customer:	Industrial Technology Research
Model Number:	TG9000-2
Serial Number:	8608
Date Calibrated:	05-20-2008
Recalibration Due Date:	05-20-2009

Thermogage Circular Foil Radiometer

Sensor Scale Factor*:	84.331 W / cm^2 / mV
Sensor Sensitivity*:	0.012 mV / W / cm^2
Heat Flux Sensor Calibrated At:	0 - 1265 W / cm^2
Sensor Coating:	Colloidal Graphite
Window Material:	Quartz
Bezel Angle:	120°

* Scale factor and sensitivity are for incident heat flux. Sensor emissivity is 0.82. The scale factor is the reciprocal of the sensitivity; both are provided here for convenience.

These calibrations were performed using instruments whose accuracy is traceable to the National Institute of Standards and Technology (NIST) and following procedures set in the Vatell Quality Assurance Manual.

Calibrated by:

COMMONWEALTH OF VIRGINIA
LAWRENCE W. LANGLEY
No. 16702
5-20-08
PROFESSIONAL ENGINEER

Figure 3.2 The certificate of calibration of the radiometer
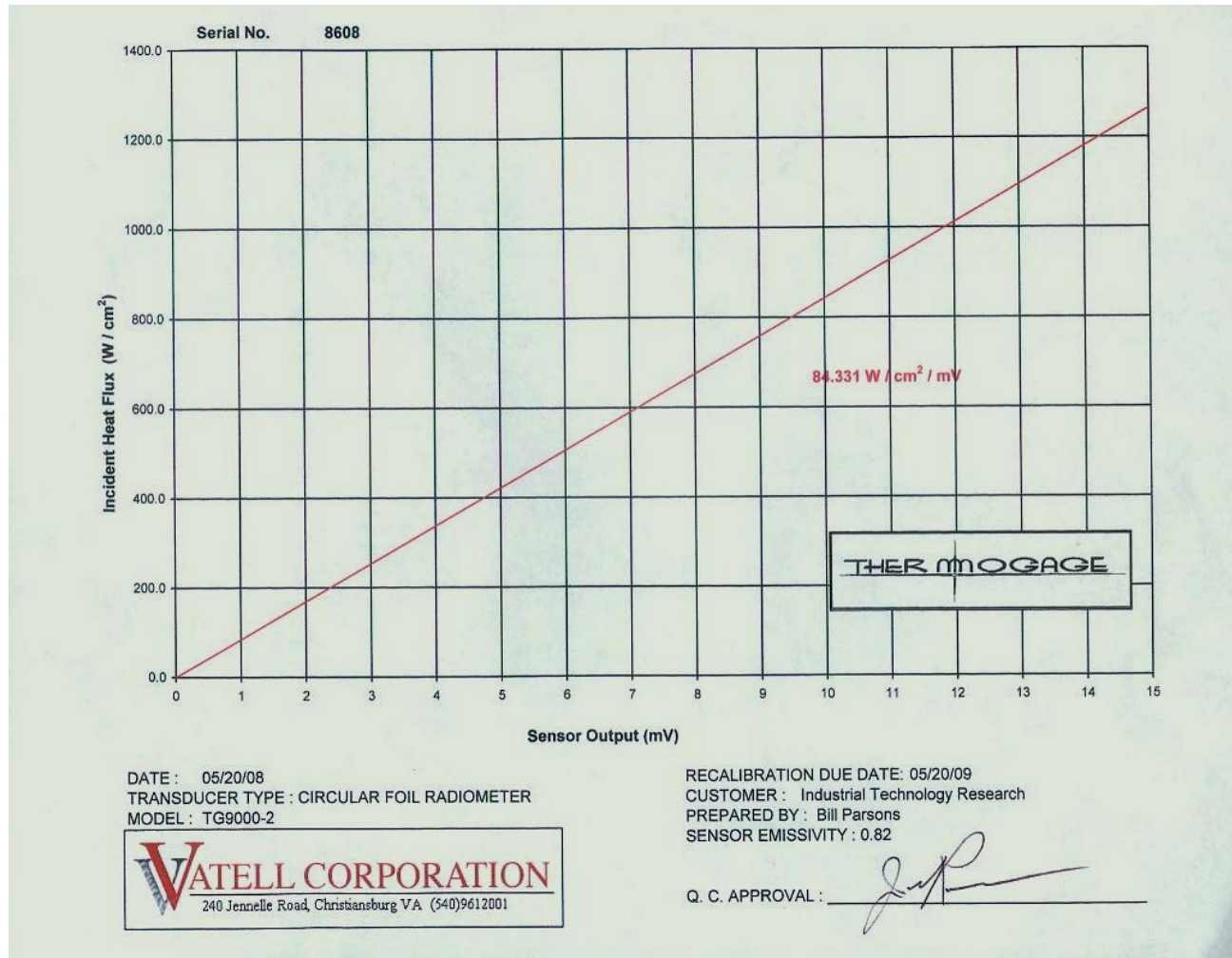
Figure 3.2 (continue) The certificate of calibration of the radiometer

校正號碼：HOTCAL-972821
儀器型號：testo 350-XL　燃燒效率分析儀
儀器序號：01065352
送校單位：財團法人工業技術研究院-能資所
單位地址：新竹縣竹東鎮中興路四段 195 號 62 館 202 室

在此聲明本實驗室之測量系統是依據 **DIN EN ISO 9001:2000** 下的品質認證系統來評鑑；校正測量
裝置是完成國家標準(NML 中華民國國家標準實驗室及 PTB 德國聯邦物理技術學院)之追溯；實驗室
之管理及運作符合 ISO/IEC 17025 之需求。
本實驗室以獨立慎重的態度來執行校正工作，本報告僅對該校正件有效，報告內容需完整使用，單
獨或部份使用皆不具效力。

校正裝置

說明	追溯號碼	有效期限
氣體追溯系統	TK3350	12-Aug-2009
氣體追溯系統	TK3501	12-Aug-2008
標準氣體鋼瓶	HOT-G-1012	30-Aug-2008
標準氣體鋼瓶	HOT-G-1013	30-Aug-2008
標準氣體鋼瓶	HOT-G-1015	30-Aug-2008
標準氣體鋼瓶	HOT-G-1016	30-Aug-2008
標準氣體鋼瓶	HOT-G-1017	30-Aug-2008

環境參數

溫度	23 ℃	±5 ℃
相對溼度	60 %RH	±20 %RH
大氣壓力	1013 hPa	±20 hPa

測量程序

本報告校正過程是依據本實驗室各校正系統之校正
程序，將追溯標準與被校件同時置於相同環境內，
以比較法進行校正，本報告之擴充不確定度信賴水
準在 95 %(k=2)。

校正日期　　下次校正日期　　　　　　　　　　　報告簽署人
26-Jun-2008　(原廠建議一年)　　　　　　　　　證書號碼：9603011

德斯特儀器有限公司 / 台北縣中和市中山路二段 351 號 3 樓之 6 / 電話 (02) 2228-9556 / 傳真 (02) 2228-9559

Figure 3.3 The certificate of calibration of the gas analyzer

校正結果

説明	標準值	實際值	誤差值	允差值(原廠建議)
O_2	0.60 Vol. %	**0.59 Vol. %**	- 0.01 Vol. %	± 0.2 Vol. %
	16.70 Vol. %	**16.65 Vol. %**	- 0.05 Vol. %	± 0.2 Vol. %
CO	57 ppm	**60 ppm**	+ 3 ppm	± 10 ppm
	927 ppm	**956 ppm**	+29 ppm	± 46 ppm
CO_2	0.60 Vol. %	**0.65 Vol. %**	+ 0.05 Vol. %	±0.3 Vol. %
	12.70 Vol. %	**12.79 Vol. %**	+ 0.09 Vol. %	±0.3 Vol. %
NO	195 ppm	**198 ppm**	+3 ppm	± 10 ppm
NO_2	239 ppm	**240 ppm**	+1 ppm	± 12 ppm
SO_2	319 ppm	**330 ppm**	+11 ppm	± 16 ppm

説明
- 本實驗室以獨立慎重的態度來執行校正工作，服務內容不包含儀器調整與修正
- 本報告之校正結果為在本實驗室內，依照自訂之校正程序與環境參數下執行校正之結果
- 標準值為標準件之讀值
- 器示值為送校件之讀值
- 器差值為標準件與送校件讀值之差異 (器差值 = 送校件之讀值 - 標準件之讀值)
- 送校件之精確度維持，將依儀器使用之環境、方式與頻率而異
- 為確保儀器之可靠度，請依使用單位自訂之校正週期按時送校
- 本報告僅對該校正件有效，報告內容需完整使用，單獨或部份使用皆不具效力

Figure 3.3 (continue) The certificate of calibration of the gas

analyzer

Chapter 4
Results and Discussion

This experimental investigation was explored the characters of oxygen-enriched combustion under 21-30% oxygen concentrations in the heating process and fixing furnace temperature tests, respectively. The fuel used to the experiments was the natural gas; there were five kinds of different oxygen concentration in both tests, they are 21%, 24%, 26%, 28% and 30%. The excess air ratio is controlled to achieve complete combustion in the experiments. The results of Lab-Scale and Pilot-Scale tests are discussed as follows:

Lab-Scale Experiments

In this section, the effect of oxygen concentration on the combustion characteristics, including heating speed, temperature distributions, emissions and fuel consumption, were examined herein. In the experiments, the furnace temperature was defined as the one of the farthest measurement point, where was located at the center of burner.

The excess air ratio (Φ) is defined as the ratio of the actual air-fuel (or oxygen enriched air-fuel) (AF) to the theoretical air-fuel (or oxygen enriched air-fuel) ratio (AF$_s$) :

$$\Phi = \frac{AF}{AF_s} \tag{4.1}$$

According to this definition, the excess air ratio can be maintained constant as long as the air-fuel ratio is fixed.

The excess air ratio was adjusted in order to achieve the best combustion efficiency. The test began with a fixed natural gas flow of 36

L/min, then, continued to adjust the excess air ratio from 1.20 approximately toward a lower ratio.

The adjustments of excess air ratio can be referred in Table 4.1. It can be seen that the concentration of carbon monoxide suddenly skyrocketed after a critical value of excess air ratio $\Phi = 1.05$ around for all cases. As a consequence, this study selected $\Phi = 1.05$ to be the assigned excess air ratio under the fixed fuel supply rate of 36 L/min to achieve the complete combustion. At the same time, the CO_2 concentration almost did not vary with excess air ratio as Φ 1.05. Similar to that of CO, the CO_2 concentration skyrocketed as $\Phi < 1.05$.

Table 4.1 The test results under different excess air ratios (Lab-Scale)

21% O_2			
O_2 (%)	CO (ppm)	excess air ratio	CO at 6% O_2 (ppm)
3.46	0	1.20	0
2.43	0	1.13	0
0.93	0	1.05	0
0.5	1172	1.02	858
24% O_2			
O_2 (%)	CO (ppm)	excess air ratio	CO at 6% O_2 (ppm)
4.13	0	1.21	0
2.63	0	1.12	0
1.02	4	1.04	3
0.12	1296	1.01	977
26% O_2			
O_2 (%)	CO (ppm)	excess air ratio	CO at 6% O_2 (ppm)
4.26	0	1.20	0
2.76	0	1.12	0
1.42	1	1.06	1
0.16	1267	1.01	981

28% O_2			
O_2 (%)	CO (ppm)	excess air ratio	CO at 6% O_2 (ppm)
4.59	0	1.22	0
3.08	0	1.12	0
1.38	0	1.05	0
0.45	993	1.02	791
30% O_2			
O_2 (%)	CO (ppm)	excess air ratio	CO at 6% O_2 (ppm)
5.32	0	1.21	0
2.98	0	1.11	0
1.75	0	1.06	0
0.65	1183	1.02	967

The effects of oxygen concentration for the heating test

Figure 4.1 shows the heating time at different oxygen concentrations. The heating time was defined as the elapsed time of heating furnace from ambient temperature to 1200℃. As shown in Fig. 4.1, the heating time was shorter when oxygen concentration increased. The reason was that nitrogen is an inert gas, does not contribute in the process of oxidizing the fuel and is reduced while the oxygen concentration increased. It acts as an energy consumer and is responsible for unwanted pollutants. Due to this, the combustion heat could be more efficient to raise the furnace temperature. Moreover, the magnitude of decrease of elapsed time was more obvious in higher oxygen concentration. The heating times for different oxygen concentrations were 4212 s (21%), 3507 s (24%), 3143 s (26%), 2716 s (28%) and 1954 s (30%), respectively. Compared with 21% O_2, the elapsed time of heating to 1200℃ was only needed 46.4% for 30% O_2. On other words, the fuel saved approximately 53.6%. Moreover, the difference of heating times for all cases is unobvious when the furnace temperature is lower than 700℃. It meant that the advantage of heating speed for

oxygen-enriched combustion is apparent for the high furnace temperature situation. Therefore, using the oxygen-enriched combustion technology could save energy in the situation that needs to fast heat-up to reach high temperatures.

For emissions, the CO and NO_x concentrations of the flue gas corrected to 6% O_2 base were shown in Fig. 4.2. The NO_x emission was defined as the sum of NO and NO_2 emissions in this study. Based on experimental results, the CO concentration maintained low level (<30 ppm) for all O_2 concentrations. The combustion efficiency (C. E.) is defined as follows:

$$C.E. = \frac{[CO_2]}{[CO_2]+[CO]} \times 100\% \tag{4.2}$$

where $[CO_2]$ is the volume concentration (dry) of CO_2 and [CO] the volume concentration (dry) of CO. Based on equation (4.2), the combustion efficiencies could achieve above 99.9% in this study. This indicated that excellent combustion efficiency was achieved. However, the NO_x emission increased sharply from 86 ppm to 545 ppm as the O_2 concentration increased from 21 to 30% O_2, as shown in Fig. 4.2. However, the maximum furnace temperature increased to about 50°C with an increase in O_2 concentration from 21 to 30%, as shown in Fig. 4.4. The variation in temperature was relatively minor, but NO_x variations reached levels greater by more than 6.34 times. Generally, the maximum proportion of NO_x produced during combustion was thermal NO_x. The production of thermal NO_x was directly associated with the temperature and the oxygen concentration. Moreover, the thermal NO_x showed exponential growth with temperature. Due to this, even a minor variation in temperature caused a huge increase in NO_x emission. In addition, it was found that the NO_x emission was more sensitive to the excess oxygen prevalent at higher oxygen concentrations during the experimental process. Increase in excess

oxygen by even a small amount caused a sharp increase in NO_x emission. Because of the effects of temperature and excess oxygen, NO_x emission increased obviously with the oxygen concentration.

Figure 4.3 displays the variations of NOx emissions per million joules at different oxygen concentrations. The results show the NO_x emission increased sharply from 30.95 to 137.29 mg/MJ as the O_2 concentration increased from 21% to 30% O_2.

Figure 4.4 compares the trends of CO_2 concentration (corrected to 6% O_2) and the maximum furnace temperature (T_{max}) at different O_2 concentrations. As shown in the figure, the CO_2 concentration increased almost linearly with the oxygen concentration. However, the measured values of CO concentration are very low in all cases, indicating that the complete combustion is reached for all cases. So the CO_2 formations are nearly the same for all cases. Because the N_2 concentration in the combustion air was decreased as the O_2 concentration was increased, the N_2 concentration was lowered in the flue gas also, causing the CO_2 concentration in the flue gas to increase although the magnitude of CO_2 emission remained the same. This phenomenon can reduce the post-processing cost and improve CO_2 capture efficiency. In terms of the maximum furnace temperature, the higher the oxygen concentration, the higher was the maximum furnace temperature. For example, the maximum furnace temperature was 1285°C at 21% O_2, and it increased to 1337°C at 30% O_2.

Figure 4.5 displays the variations of CO_2 emissions per million joules at different oxygen concentrations. The results show almost the same amount of CO_2 emissions per million joules (49.08 g / MJ to 49.95 g / MJ) at different oxygen concentrations.

Temperature distributions for different O_2 concentrations during the

process of heating the sample to 1200°C are displayed in Fig. 4.6. It is evident from the figure that temperature distributions were uniform at points away from the burner. However, the temperature rose gradually near the burner region as the oxygen concentration increased. For example, the temperature was about 1260　for 21% of O_2 (Fig. 4.6a), whereas for 30% of O_2, it rose to about 1300　(Fig. 4.6e). Moreover, the temperature variations became greater near the region of the burner, with the temperature gradient becoming progressively greater (higher contour density) as the oxygen concentration increased.

On the basis of the results of the heating test, it can be summarized that the heating rate, the maximum furnace temperature, and the NO_x emission and CO_2 concentration were increased with oxygen concentration.

The effects of oxygen concentration for the fixed furnace temperature test

Figure 4.7 illustrated the variations of CO_2 emission and fuel flow rate (i.e. fuel consumption) at different oxygen concentration in the fixed furnace temperature test. The trend of CO_2 emission the same as one in the heating test, namely that CO_2 concentration was increased linearly with oxygen concentration. Additionally, increasing oxygen concentration could save energy apparently as shown in Fig. 4.7. The fuel consumption decreased from 23 L/min at 21% O_2 to 17 L/min at 30% O_2 as the furnace temperature was maintained at 1220±10℃. This meant that we could save 26.1% fuel when oxygen concentration was increased to 30%. Excluding less N_2 contained, the radiation heat transfer was enhanced due to higher CO_2 and H_2O concentrations when increasing O_2 concentration. Because CO_2 and H_2O were good radiation emitters, the total gas emissivity was increased when upgrading oxygen enrichment level. That caused the

radiation intensity became stronger. In sum, increasing oxygen concentration could upgrade the energy availability. Additionally, the fuel consumption decreased near linearly with increasing O_2 enrichment level as maintained furnace temperature. This trend was the same as the experimental results of Poirier et al [32].

Figure 4.8 displays the variations of CO_2 emissions per million joules at different oxygen concentrations. The results show almost the same amount of CO_2 emissions per million joules (47.10 g / MJ to 49.08 g / MJ) at different oxygen concentrations.

Figure 4.9 shows the variations of CO concentration and NO_x emission, corrected to 6% O_2, at different oxygen concentrations in the fixing furnace-temperature test. From this figure, the CO concentration can be observed to be lower than 6 ppm for all O_2 concentrations. This indicated that incomplete combustion did not occur. The trend of NO_x emission was also assessed. In the heating test, the NO_x emission increased dramatically as the oxygen concentration was enhanced. Similarly, NO_x emission in the furnace-temperature fixing test showed an increasing trend; i.e., NO_x concentration increased with oxygen concentration, but the NO_x concentration was much less than that in the heating test at the same oxygen concentration. For example, at 30% O_2, the NO_x concentrations were 545 and 95 ppm in the heating test and the furnace–temperature fixing test, respectively. Moreover, the NO_x concentration increased 6.33 times (from 86 to 545 ppm) as the oxygen concentration was increased from 21 to 30% in the heating test, but it only increased 2.11 times (from 45 to 95 ppm) in the furnace-temperature fixing test. As mentioned in section 4.1.1, the production of thermal NO_x was affected severely by temperature.

Figure 4.10 displays the variations of NO_x emissions per million joules at different oxygen concentrations. The results show the NO_x emission

increased sharply from 11.54 to 23.93 mg/MJ as the O_2 concentration increased from 21% to 30% O_2.

The maximum furnace temperatures in the furnace-temperature fixing test, as shown in Figure 4.11, were lower than those in the heating test (Fig. 4.4) for all oxygen concentrations. At 30% O_2, the maximum furnace temperature in the furnace-temperature fixed test was 1291°C, whereas it was 1337°C in the heating test. Furthermore, the increases of maximum furnace temperatures in the heating and the furnace-temperature fixed tests with an increase from 21% to 30% O_2 were 52 and 26°C, respectively. The reason is that the energy input in the heating test is greater than that in the furnace-temperature fixed test. Consequently, the increases in the concentration of NO_x were relatively higher for the heating test. Although the NO_x concentration increased with oxygen concentration, the total NO_x emission did not show an increase similar to that of the concentration because the magnitude of flue gas also decreased when the oxygen concentration increased. Because the total NO_x emission is a product of the volume concentration of NO_x and the flue gas volume flow rate, these two effects—increase in NO_x concentration and decrease in amounts of flue gas—competed with each other. In addition, there was a peculiar value of NO_x emission for 24% O_2; i.e., the NO_x emission was lower than 21% O_2. The possible reason was that the emission of thermal NO_x was affected not only by temperature, but also by excess oxygen. The maximum furnace temperature at 24% O_2 was higher than that at 21% O_2 (1265°C for 21% O_2 and 1268°C for 24% O_2); however, the excess oxygen was lower at 24% O_2 (1.85% for 21% O_2 and 1.30% for 24% O_2). Increasing the furnace temperature caused an increase in the NO_x emission, but reducing the excess oxygen caused NO_x emission to decrease. Although the effect of the furnace temperature was greater than that of excess oxygen (the effect of

temperature was exponential), as long as the hot spots (the zones with a concurrent occurrence of relatively high temperature and oxygen concentration) were less in number, the quantity of NO_x emission was reduced. Thus, the NO_x emission under 24% O_2 was less than that at 21% O_2.

The temperature distributions at different oxygen concentrations in the fixing furnace temperature test were shown in Fig.4.12. From the figure, the higher temperature zones concentrated near the burner region and their area increased with the oxygen concentration. Moreover, when the oxygen concentration was up, the uniformity of temperature field seemed worse. The reason was that the convection heat transfer was changed. The convection heat transfer associated with fluid velocity and flow pattern. The combustion needed less combustion air when the oxygen concentration was increased so that the fluid velocity and flow pattern were changed obviously. For example, the combustion only needed 70% combustion air for 30% O_2 compared with 21% O_2. Because of this, the temperature distribution became non-uniform as increasing the oxygen concentration.

Summarily, based on experimental results of fixing furnace temperature test, the fuel consumption decreased and the NO_x concentration increased with oxygen concentration, moreover, the temperature distribution was non-uniform as increasing the oxygen concentration. Besides, the NO_x concentration could be controlled at low level by reducing excess oxygen and furnace temperature.

Pilot-Scale Experiments

In this section, the effect of oxygen concentration on the combustion characteristics, including heating rate, radiation heat flux, flame shape, emissions, and fuel consumption, are discussed. In these experiments, the

furnace temperature is the value measured by the furthest thermocouple.

The adjustment procedures of excess air ratio were completes the same as the last section, and could not repeated hear. The corresponding results can be referred in Table 4.2. According to this table, this study also selected $\Phi = 1.05$ to be the assigned excess air ratio under the fixed fuel supply rate of 508.4 L/min to achieve the complete combustion in the Pilot-Scale test.

Table 4.2 The test results under different excess air ratios (Pilot-Scale)

21% O_2			
O_2 (%)	CO (ppm)	excess air ratio	CO at 6% O_2 (ppm)
3.46	0	1.20	0
2.28	0	1.12	0
1.28	0	1.06	0
0.3	60	1.01	43
24% O_2			
O_2 (%)	CO (ppm)	excess air ratio	CO at 6% O_2 (ppm)
4.28	0	1.22	0
2.66	0	1.12	0
0.82	4	1.04	3
0.10	1324	1.00	997
26% O_2			
O_2 (%)	CO (ppm)	excess air ratio	CO at 6% O_2 (ppm)
5.15	0	1.25	0
2.60	0	1.11	0
1.24	0	1.05	0
0.16	1260	1.01	975
28% O_2			
O_2 (%)	CO (ppm)	excess air ratio	CO at 6% O_2 (ppm)
5.36	0	1.24	0
3.22	0	1.13	0
1.64	0	1.06	0
0.45	990	1.02	791

30% O$_2$			
O$_2$ (%)	CO (ppm)	excess air ratio	CO at 6% O$_2$ (ppm)
4.74	0	1.19	0
3.11	0	1.12	0
1.58	0	1.06	0
0.49	20	1.02	16

The effects of oxygen concentration for the heating test

The flame length is defined by the constant gray-scale value. Because the flame length under a specific condition is impossible fixed, it is obtained by taking 350 pieces of images to make the average.

Figures 4.13 to 4.17 show the flame shapes under different excess air ratio at the respective oxygen concentration of 21%, 24%, 26%, 28% and 30%. From these figures, it can be seen that the brightness of the flame is increased with the oxygen concentrations. On the other hand, the flame length decreases with an increase of the excess air ratio at constant (fixed) oxygen concentration. However, the flame length expands with the oxygen concentration at constant excess air ratio.

Figure 4.18 displays the variations of flame length at different oxygen concentrations and excess air ratio. Actually, it is a summation of Figs. 4.13 to 4.17. The results show that flame length is shortened almost linearly with the excess air ratio under a fixed oxygen concentration. Furthermore, the flame length increases almost linearly with the oxygen concentration at constant excess air ratio. This is because the high-speed burner is an impinging type that both air and fuel flows are impinged together in front of the burner mouth to mix, and then ignited. Air supply was decreased substantially at constant natural gas flow when using oxygen-enriched combustion. As a consequence, the natural gas and air were not mixed well;

in the meantime, the resultant mixture flow rate was decreased. Therefore, the flame lengths increased.

Figure 4.19 displays the time elapsed for heating the natural gas fuel to 1200°C at different oxygen concentrations. The fuel supply rate was 30.5m^3/hr. The elapsed time was decreased as the oxygen concentration increased. This was due to the reduction in the inert gas, nitrogen, as the oxygen concentration increased. Hence, the energy availability is raised. The definition of energy availability (η) is as follows:

$$\eta = \frac{E_{in} - E_{loss}}{E_{in}} \qquad (4.3)$$

where E_{in} is the energy input and E_{loss} the energy loss. The major energy loss is from flue gas. Diluting N$_2$ concentration can reduce energy loss by flue gas apparently so that the energy availability can be raised, i.e. saving energy. Because of this, the combustion heat was more efficient in increasing the furnace temperature. Moreover, the magnitude of decrease in the elapsed time was more obvious at higher oxygen concentrations. For example, the elapsed time for 24% O$_2$ was 80.8% of the time recorded at 21% O$_2$ (11396 s for 21% O$_2$ and 9209 s for 24% O$_2$); however, for 30% O$_2$, the elapsed time was only 64.3% of that at 21% O$_2$ (7330 s for 30% O$_2$). In other words, using combustion air containing 30% O$_2$ in the heating test could save 35.7% of the fuel compared to using combustion air with 21% O$_2$. This shortening of the heating time implies savings in terms of fuel. Furthermore, the heating rate was comparable for all O$_2$ concentrations when the furnace temperature was lower than 700°C. This phenomenon indicates that the advantage of oxygen-enriched combustion is apparent only in the high-temperature environment during the heating process.

The effects of oxygen concentration for the fixing furnace temperature test

In this section, the effect of oxygen concentration on the combustion characteristics, radiation heat flux, emissions, and fuel consumption, are discussed. In the experiments, the furnace temperature was the value measured by the furthest thermocouple. For the fixing furnace temperature test, the natural gas flow rate was changed to control furnace temperature at $1220\pm10℃$ at different oxygen concentration. The experimental time was 90 minutes as soon as the furnace temperature was stable.

Figure 4.20 illustrates the variations of CO_2 and CO concentrations, corrected to 6% of O_2, at different oxygen concentrations in the fixed furnace-temperature test. From this figure, the CO concentration can be observed lower than 10 ppm for all O_2 concentrations, implying that incomplete combustion did not occur for all cases. The CO_2 concentration increases almost linearly with the oxygen concentration. As just mentioned, no incomplete combustion occurs at all, the CO_2 formations are nearly the same for all cases. Because the N_2 concentration in the combustion air decreased as the O_2 concentration increased, the N_2 concentration was lowered in the flue gas also, causing the CO_2 concentration in the flue gas to increase although the magnitude of CO_2 emission remained the same. This phenomenon could reduce the post-processing cost and improve CO_2 capture efficiency.

Figure 4.21 displays the variations of CO_2 emissions per million joules at different oxygen concentrations. The results show almost the same amount of CO_2 emissions per million joules (48.76 g / MJ to 50.06 g / MJ) at different oxygen concentrations.

The rates of fuel flow at different oxygen concentrations in the fixed

furnace-temperature test are shown in Fig. 4.22. The fuel flow rate actually represents the fuel consumption rate in such experiment. The results show that increasing the oxygen concentration could in fact save energy. The fuel consumption rate decreased from 383.4 L/min at 21% O_2 to 300.0 L/min at 30% O_2 at a constant furnace temperature of 1220±10°C. This implies that 21.74% of fuel could be saved when the oxygen concentration increased from 21% to 30%. Excluding the lower levels of N_2 contained within the combustion air, the radiation heat transfer was enhanced due to higher concentrations of CO_2 and H_2O while O_2 concentration increased. Because CO_2 and H_2O are good radiation emitters, the total gas emissivity is increased when the oxygen-enrichment level is upgraded; in turn, causes the radiation intensity to become stronger. In summary, increasing the oxygen concentration could upgrade the availability of energy. In addition, the fuel consumption decreases almost linearly with increasing O_2-enrichment level at constant furnace temperature. This trend is the same as the experimental results of Poirier et al. [32].

Figure 4.23 shows the variations of NO_x emission, corrected to 6% O_2, at different oxygen concentrations in the fixed furnace-temperature test. The NO_x emission is defined in this study as the sum of NO and NO_2 emissions. The NO_x emission increases as the oxygen concentration is enhanced. For example, the NO_x concentration increases 1.26 times (from 38 to 48 ppm) as the oxygen concentration is increased from 21 to 26%. Generally, the maximum proportion of NO_x produced during combustion was thermal NO_x, whose production is directly associated with the temperature and the oxygen concentration. Moreover, the thermal NO_x shows exponential growth with temperature. Owing to this, even a minor variation in temperature can cause a huge increase in NO_x emission. In addition, it can be found that the NO_x emission is more sensitive to the

excess oxygen prevalent at higher oxygen concentrations during the experimental process. Increase in excess oxygen by even a small amount causes a sharp increase in NO_x emission. Because of the effects of temperature and excess oxygen, NO_x emission increases obviously with the oxygen concentration. Although the NO_x concentration increases with oxygen concentration, the total NO_x emission does not show an increase similar to that of the concentration because the magnitude of flue gas also decreases when the oxygen concentration increases. Because the total NO_x emission is a product of the volume concentration of NO_x and the flue gas volume flow rate, these two effects- increase in NO_x concentration and decrease in amounts of flue gas- competed with each other.

Figure 4.24 illustrates the variations of total NO_x emissions per hour at different oxygen concentrations. From this figure, the total NO_x emissions reduces as the oxygen concentration is enhanced. Although the NO_x concentration increases 1.26 times (from 38 to 48 ppm) as the oxygen concentration is increased from 21 to 26%; nevertheless, the total NO_x emissions decreases 0.13 times (from 11.70 to 10.22 g/hr) as the oxygen concentration is increased from 21 to 26%. However, the total NO_x emissions decreases 0.29 times (from 11.70 to 8.27 g/hr) as the oxygen concentration is increased from 21 to 30%. The results demonstrate that the oxygen-enriched combustion is favorable in not only energy conservation but also Environmental protection at proper air-fuel ratio control.

Figure 4.25 displays the variations of NO_x emissions per million joules at different oxygen concentrations. The results show almost the same amount of NO_x emissions per million joules (12.34 mg / MJ to 13.95 mg / MJ) at different oxygen concentrations.

Figure 4.26 shows the radiation heat flux distributions at different oxygen concentrations in the fixing furnace-temperature test. The

maximum radiation heat flux occurs at a distance of 120cm from the burner. The measuring point is located in the posterior region of flame, where the area possesses higher temperature. The radiation intensity is proportional to the four power of temperature; consequently, the radiation heat flux is increased. The second highest radiation heat flux is at 210 cm distance from the burner. Because the radiation heat flux is obtained not only from the combustion gases but also from the posterior region of burner. However, the upper limit of oxygen concentration in these experiments was 30% such that the concentrations of CO_2 and H_2O produced were also limited. Therefore, the radiation heat flux increases with oxygen concentration. The reason is mainly attributed to dilution of N_2 concentration due to an increase of oxygen concentration under the fixed air/fuel ratio. Furthermore, the CO_2 and H_2O are good radiation emitters, the total gas emissivity are increased when the oxygen-enrichment level is upgraded; in turn, causes the radiation intensity to become stronger.

Comparison between Lab-Scale and Pilot-Scale Experiments

Remind that the geometries of Lab-Scale and Pilot-Scale furnaces were not similar, although both were rectangular. The former one is symmetric, whereas the latter one is not.

The results show that the elapsed time is decreased as the oxygen concentration increases in the Lab-Scale and Pilot-Scale heating tests. Furthermore, the fuel consumption decreases with increasing oxygen concentration in the Lab-Scale and Pilot-Scale fixing furnace-temperature test. This is because the reduction in the inert gas, nitrogen, as the oxygen concentration increases. Diluting N_2 concentration can apparently reduce energy loss in flue gas so that the energy availability can be raised, i.e. saving energy.

The NO_x emission increases sharply as the oxygen concentration increases in the Lab-Scale experiments. However, the total amount of NO_x emissions is almost invariant as the oxygen concentration increases in the Pilot-Scale experiments. The reason for the former one is due to the thermal NO_x, whereas the one for latter is due to poor mixing of oxidant and fuel. The complete reasons have been given in the related discussions.
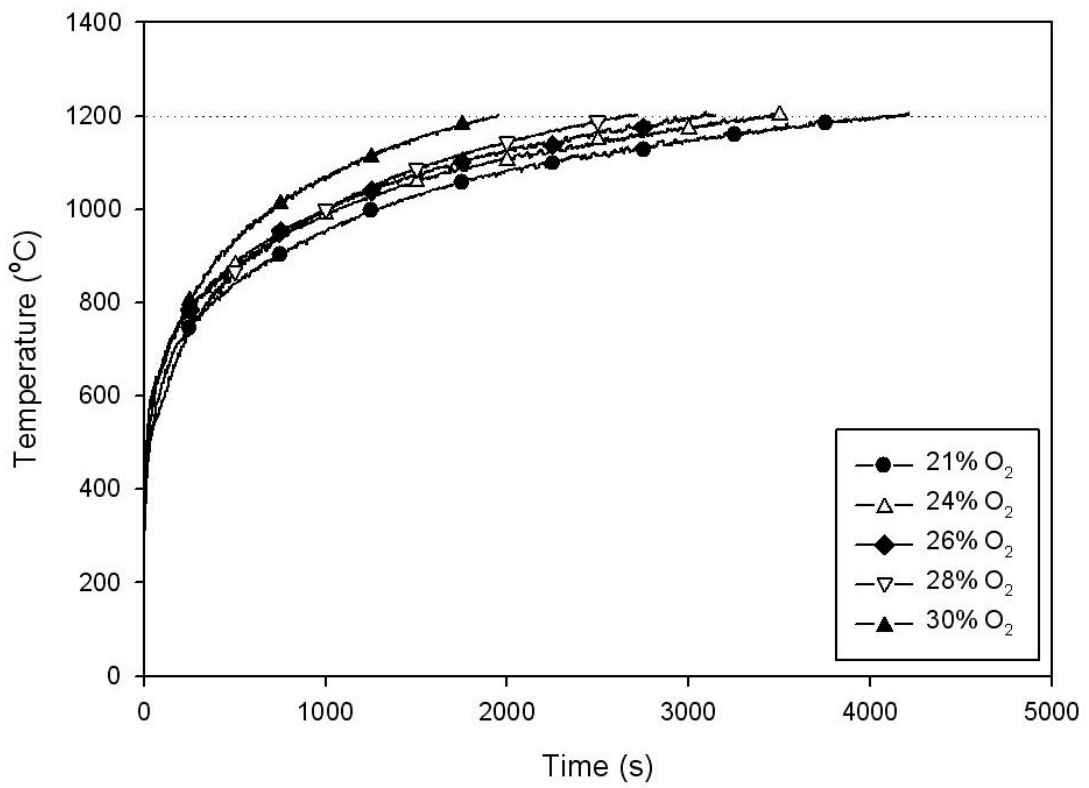
Figure 4.1 Heating times for different oxygen concentrations

(Lab-Scale)
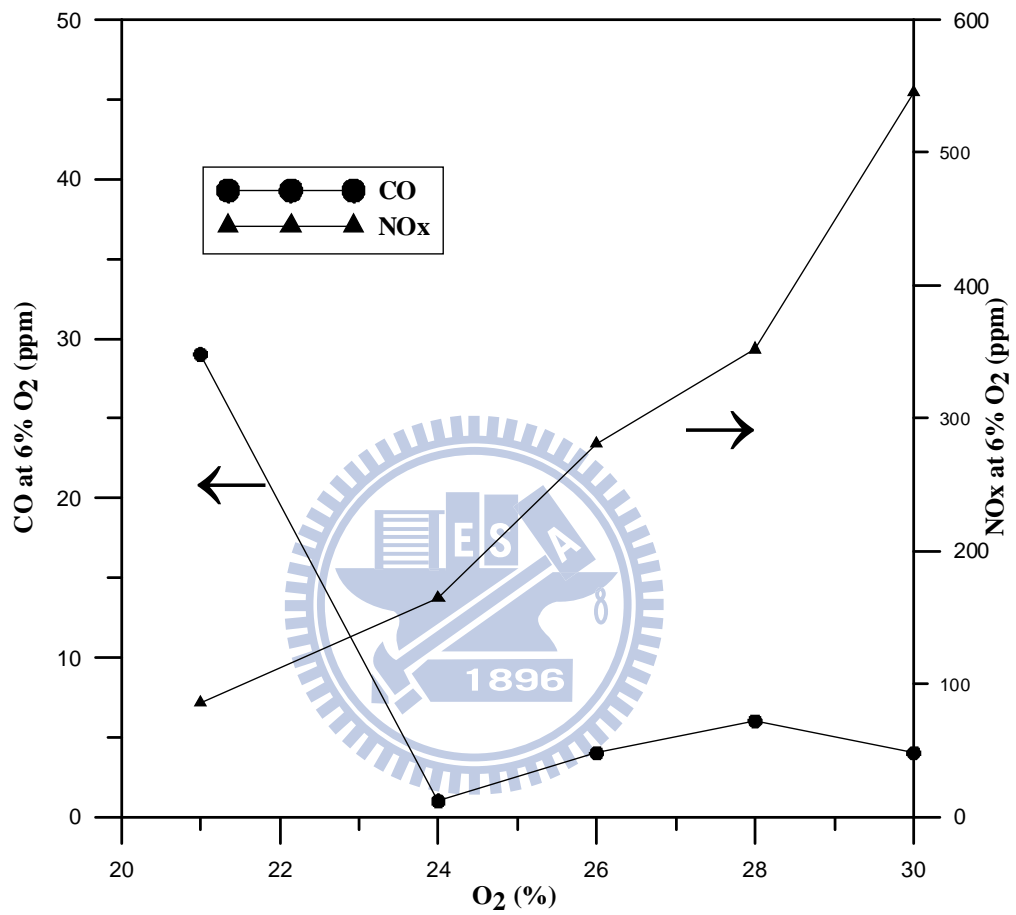
Figure 4.2 Variation of CO and NO$_x$ emission at different oxygen

concentration in the heating test (Lab-Scale)
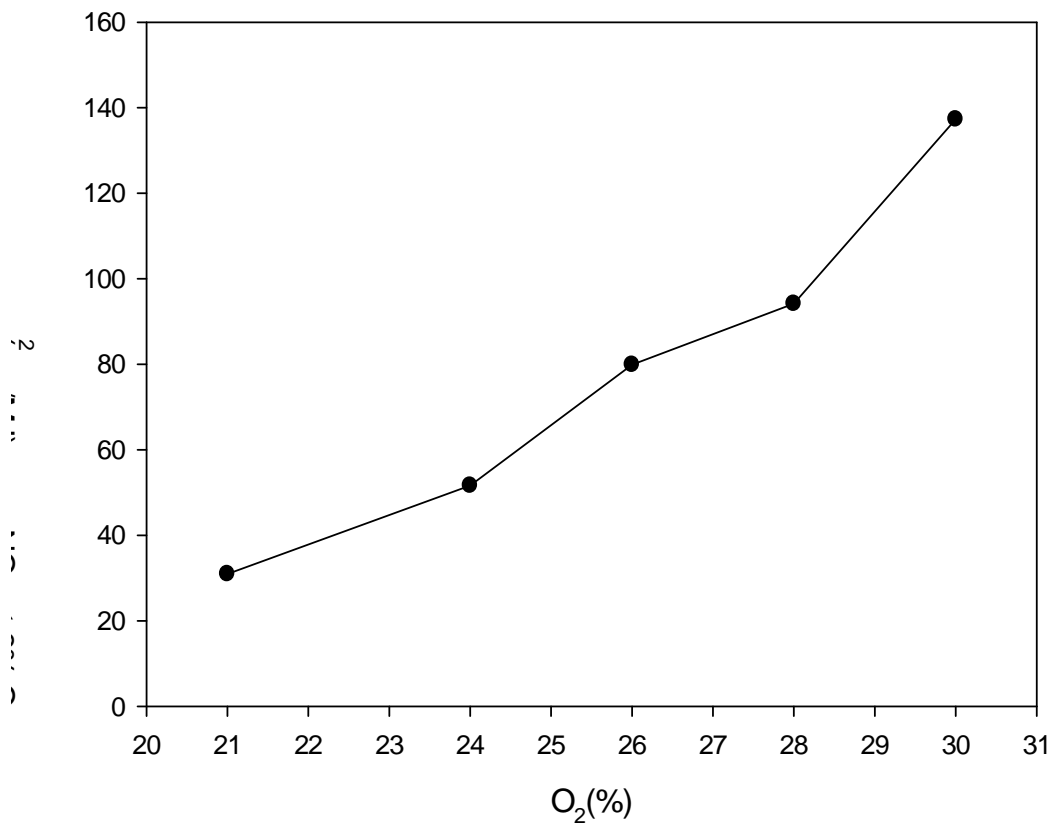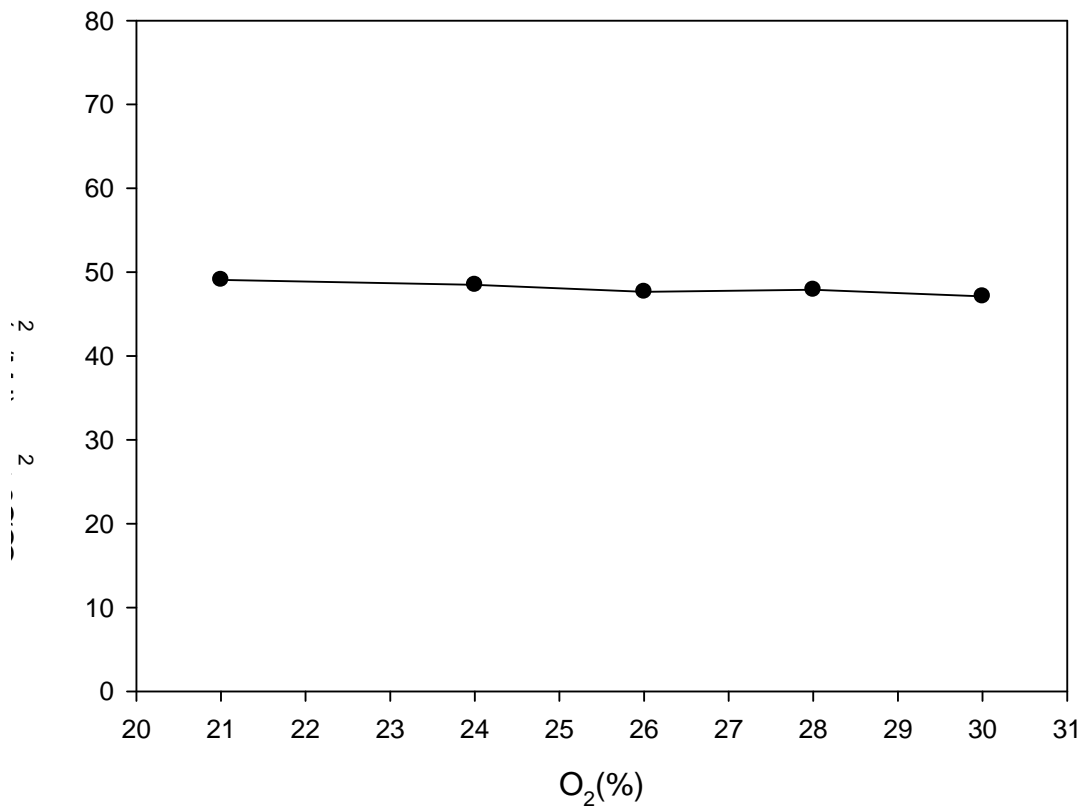
Figure 4.3 Variations of NOx emission per million joules at

different oxygen concentration in the heating test (Lab-Scale)
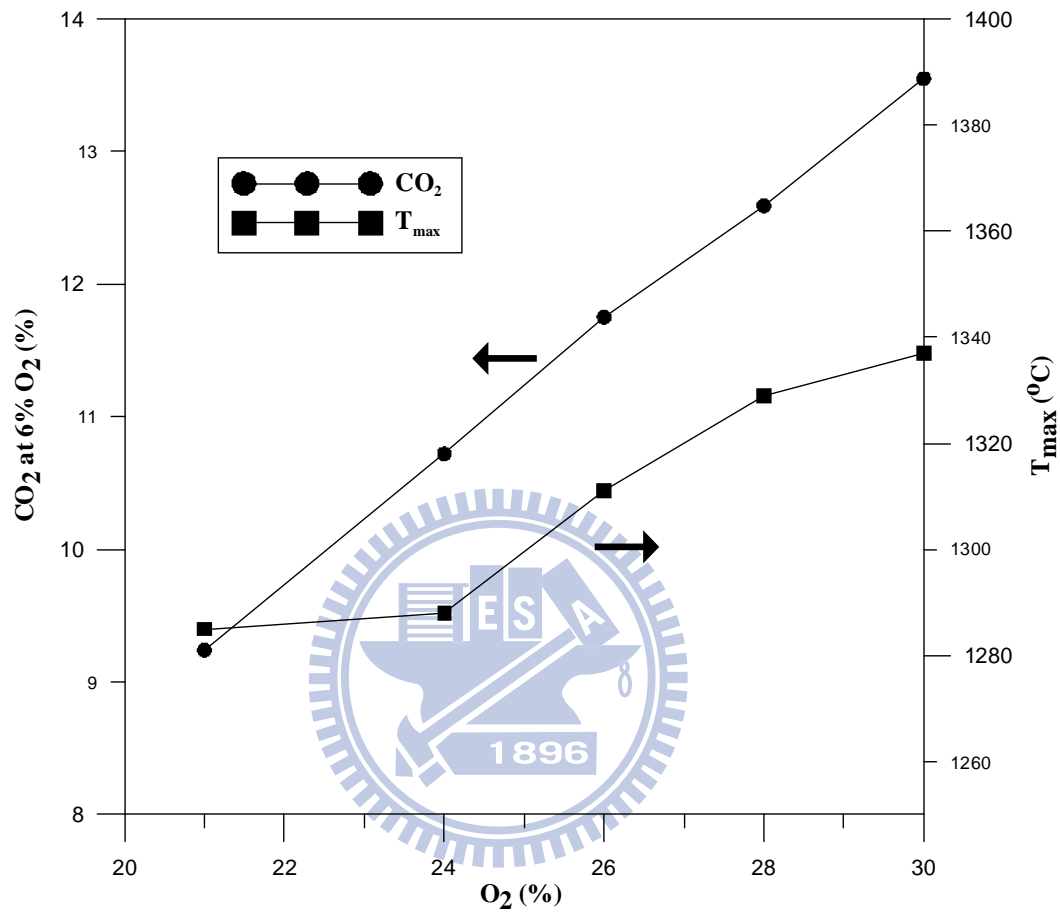
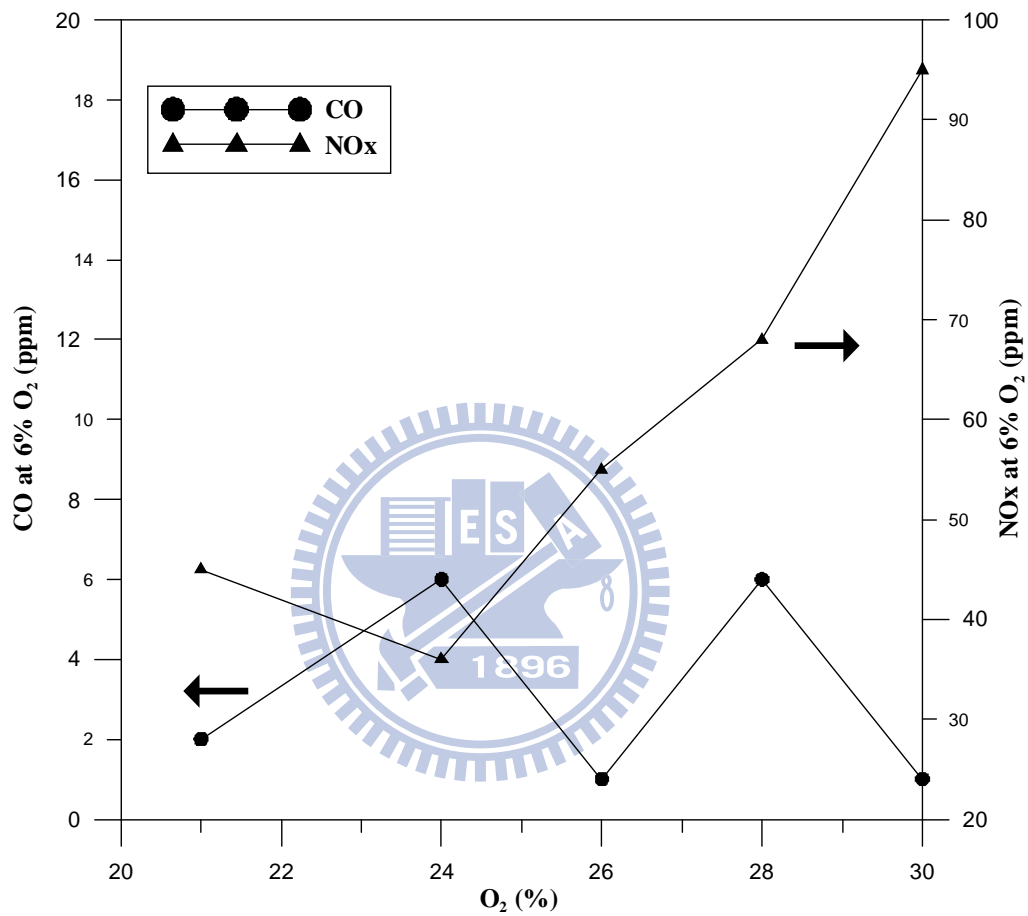Figure 4.4 Variation of CO_2 emission and maximum furnace

temperature at different oxygen concentration in the heating test
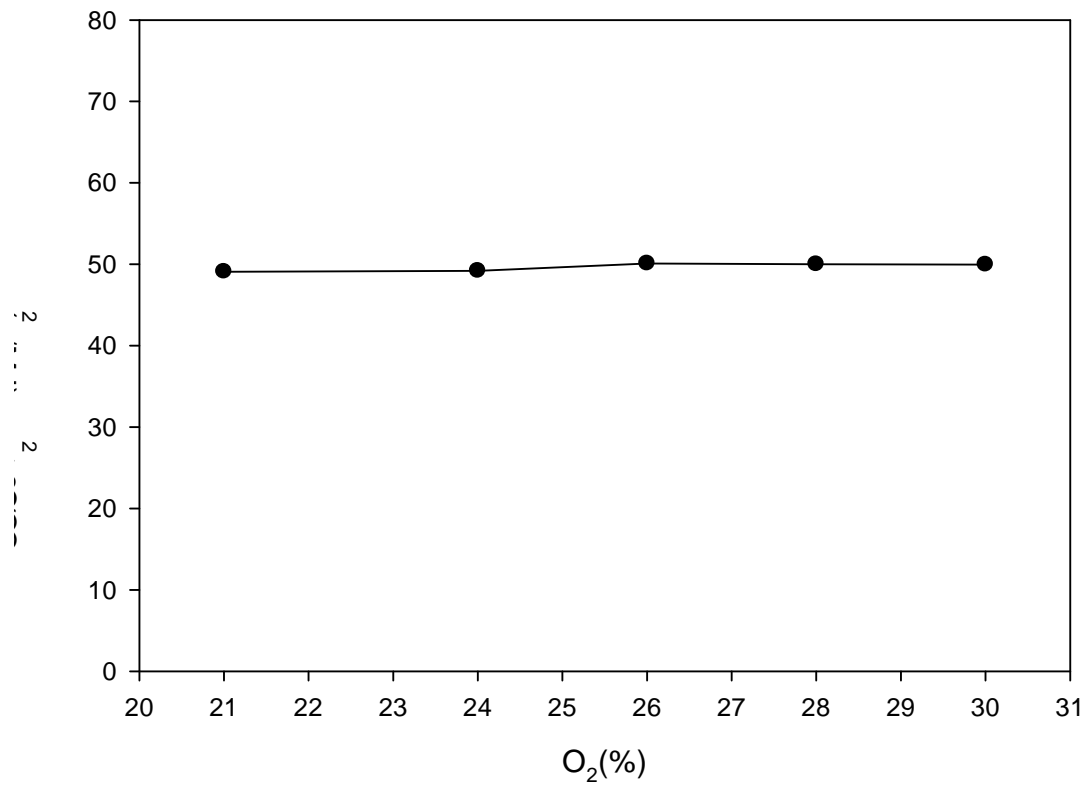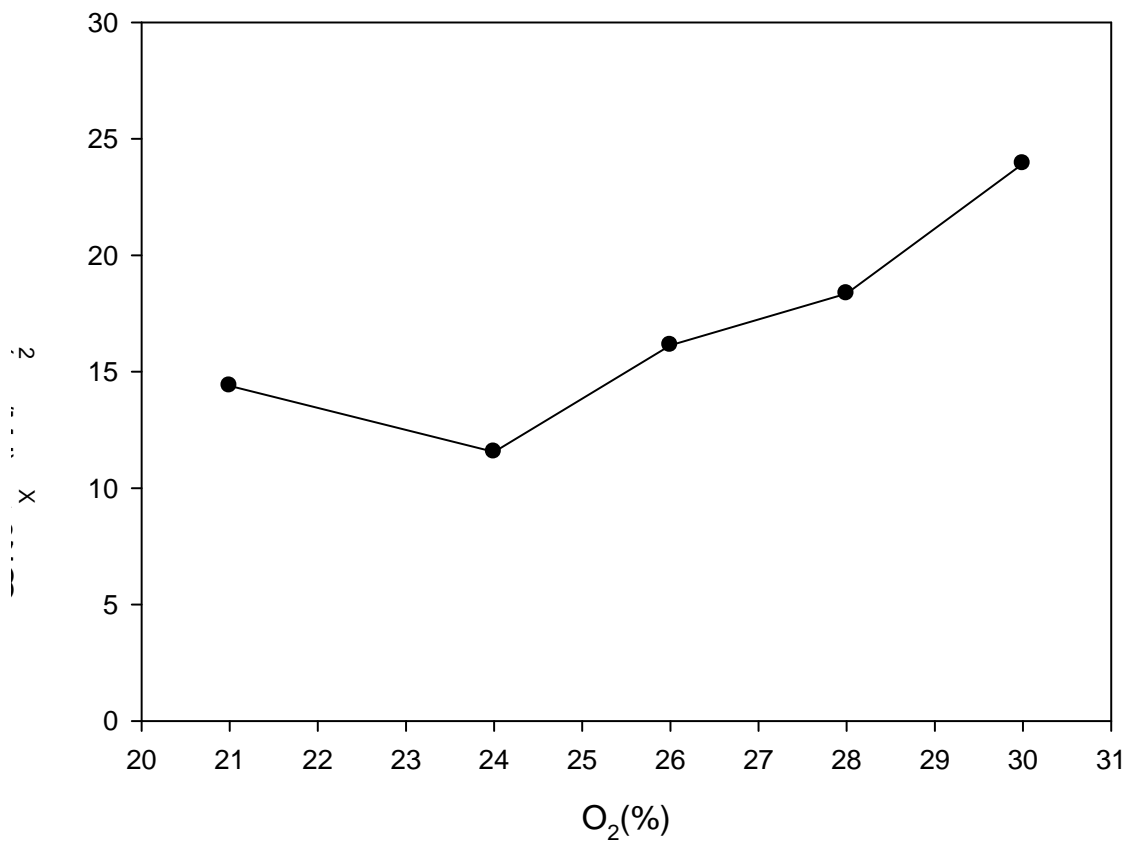
(Lab-Scale)

Figure 4.5 Variations of CO_2 emission per million joules at

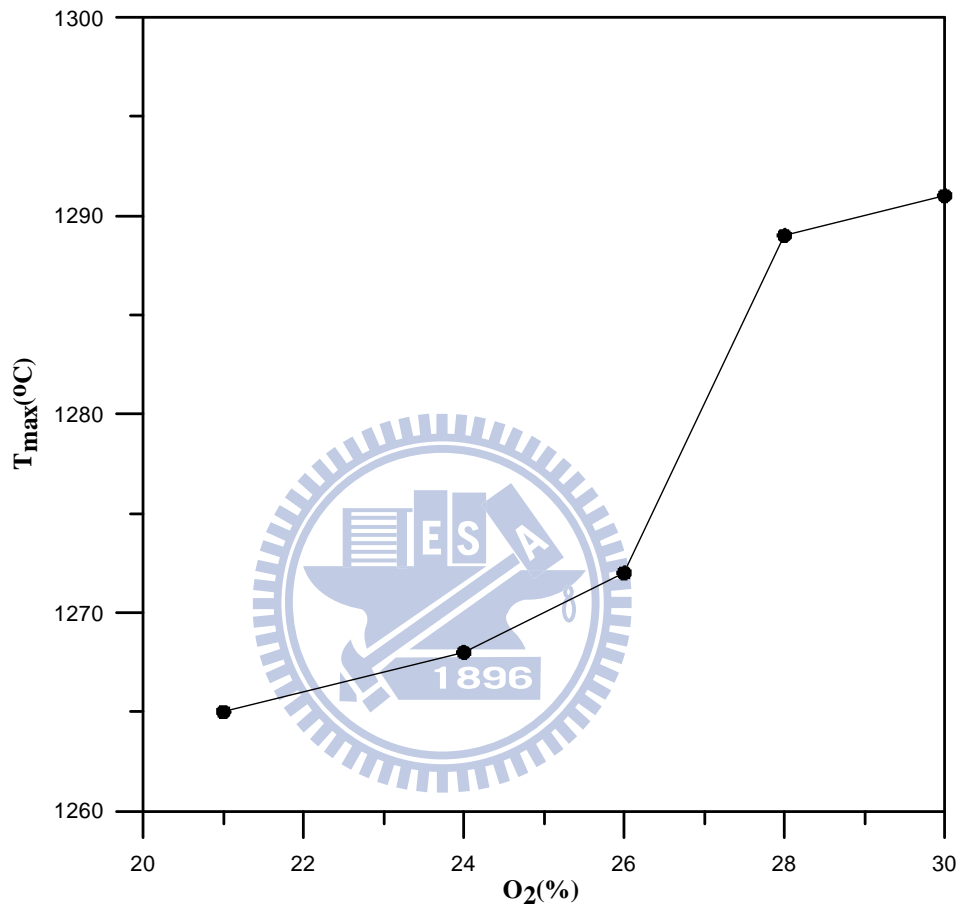different oxygen concentration in the heating test (Lab-Scale)
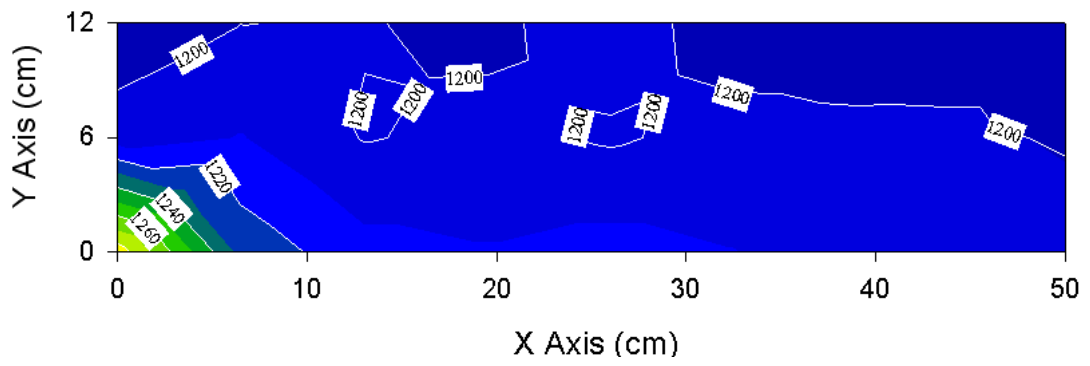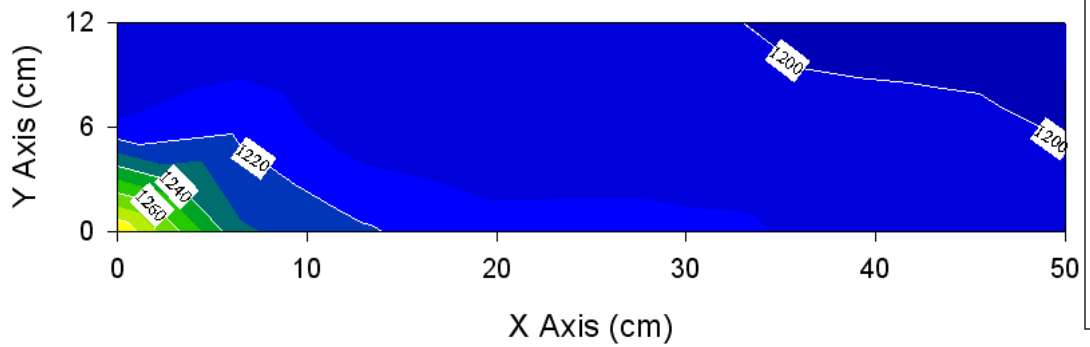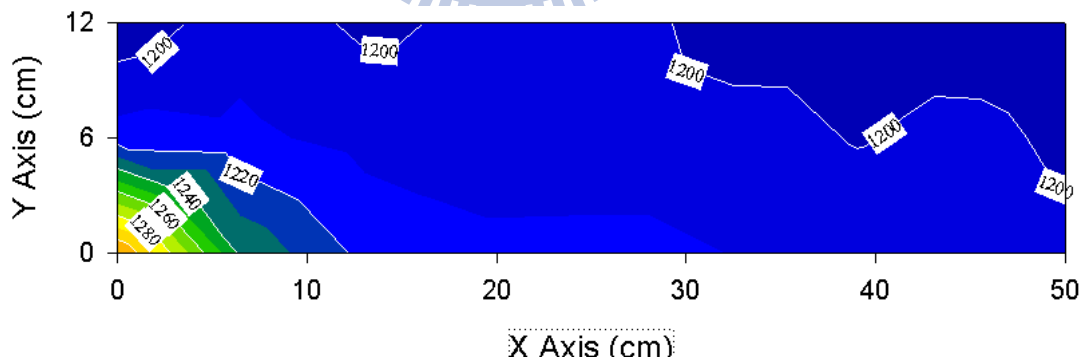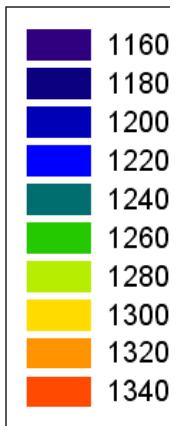
Figure 4.6 Temperature distributions of heating to 1200℃ for (a)

21% O_2, (b) 24% O_2 and (c) 26% O_2 in the heating test (Lab-Scale)

(d)

(e)
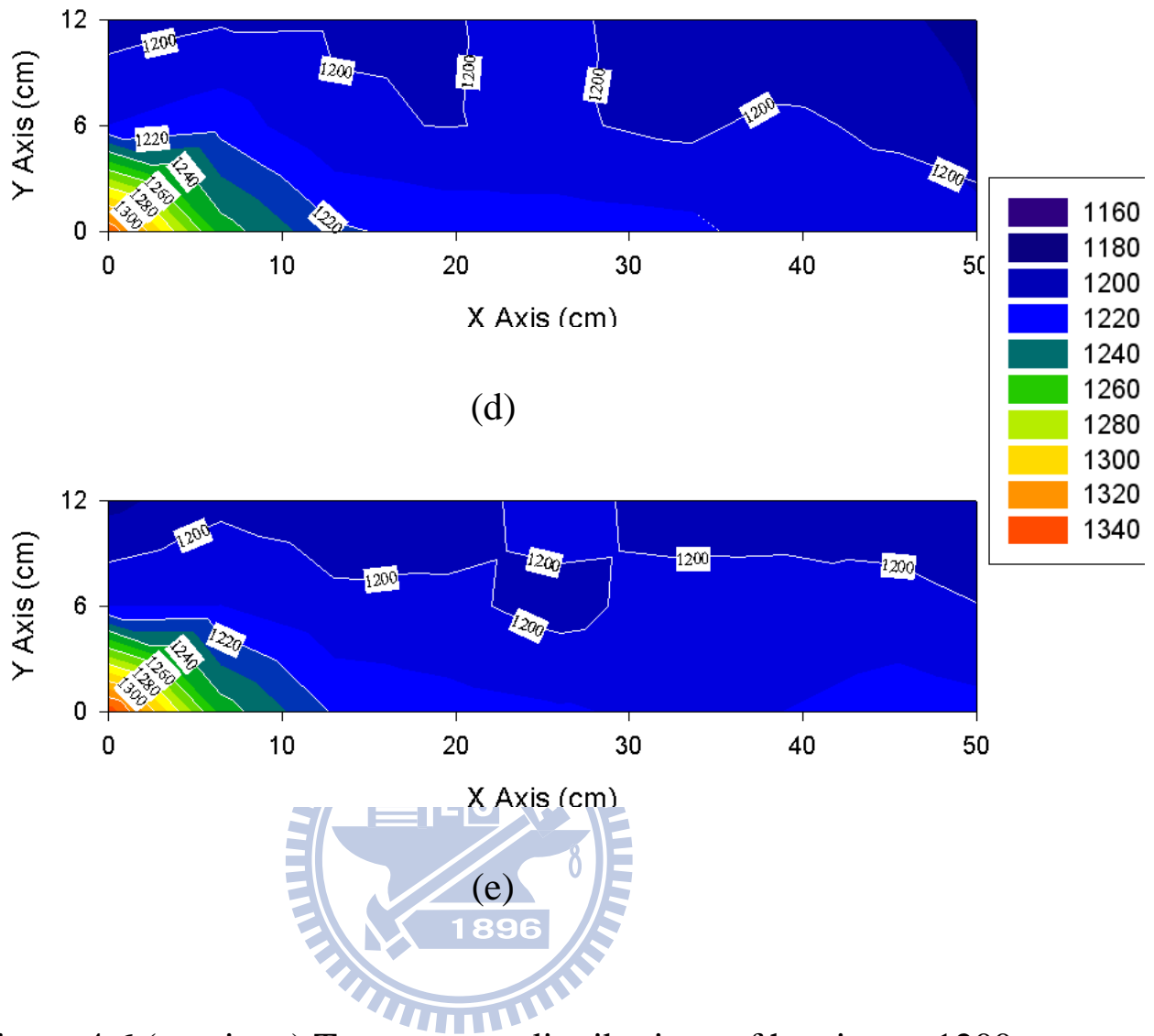
Figure 4.6 (continue) Temperature distributions of heating to 1200

℃ for (d) 28% O_2 and (e) 30% O_2 in the heating test (Lab-Scale)
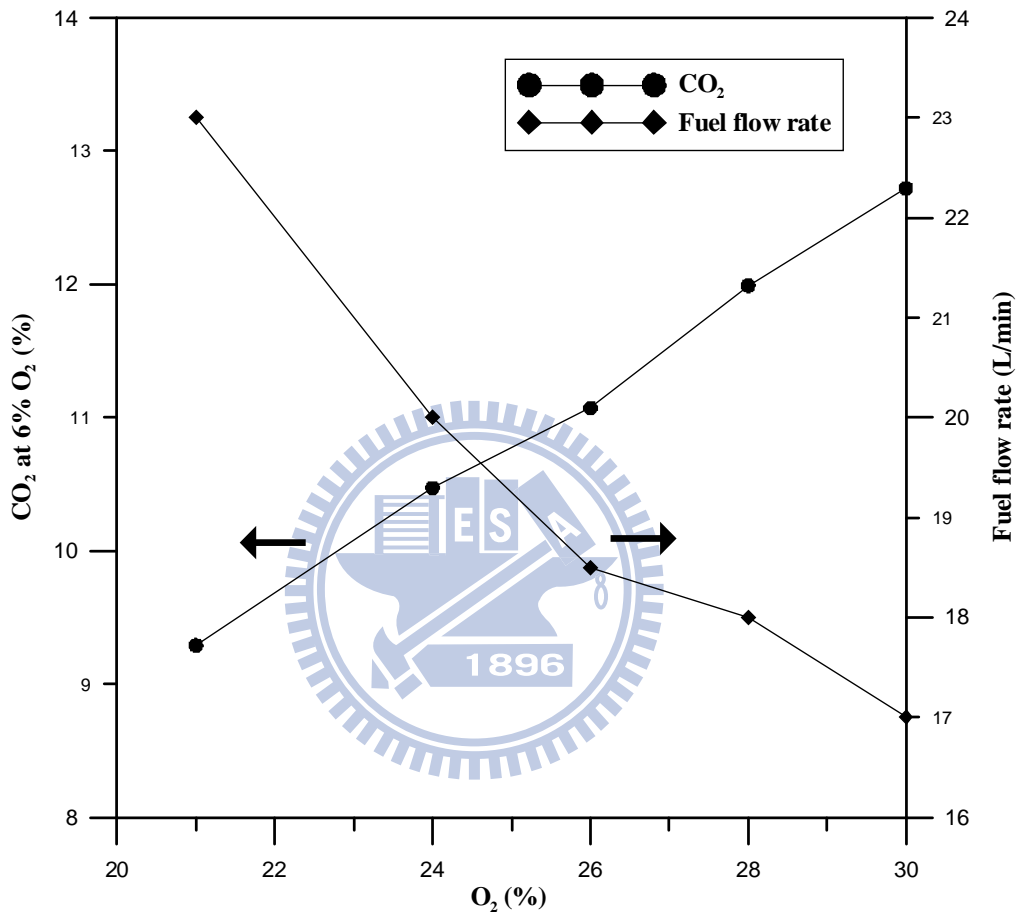
Figure 4.7 Variations of CO_2 emission and fuel flow rate at

different oxygen concentration in the fixed furnace

temperature test (Lab-Scale)

Figure 4.8 Variations of CO_2 emission per million joules at

different oxygen concentration in the fixed furnace

temperature test (Lab-Scale)

Figure 4.9 Variations of CO and NO$_x$ emission at different oxygen

concentration in the fixed furnace temperature test (Lab-Scale)

Figure 4.10 Variations of NOx emission per million joules at

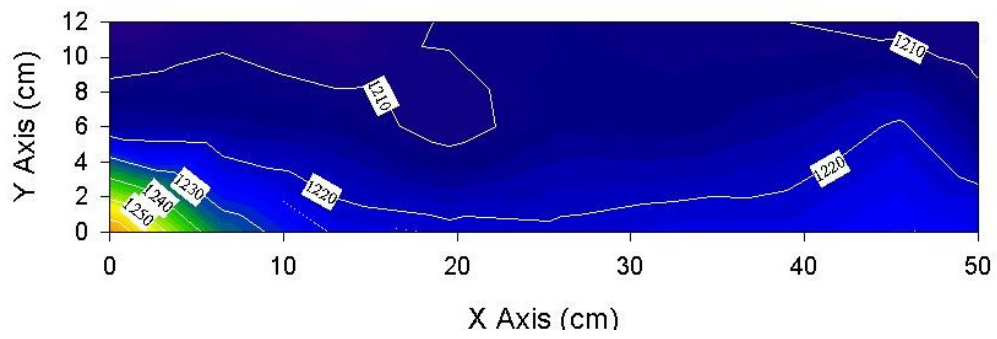different oxygen concentration in the heating test (Lab-Scale)
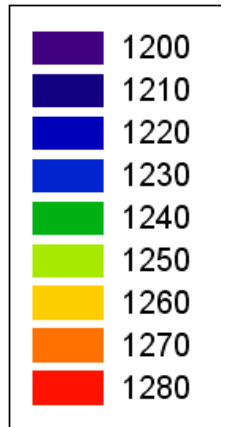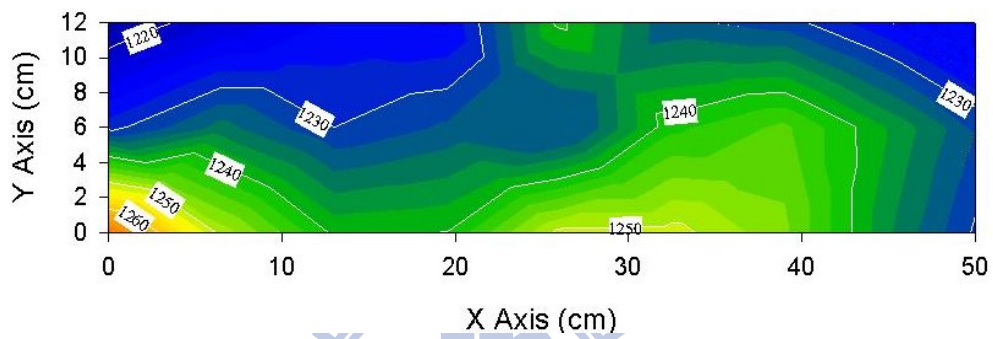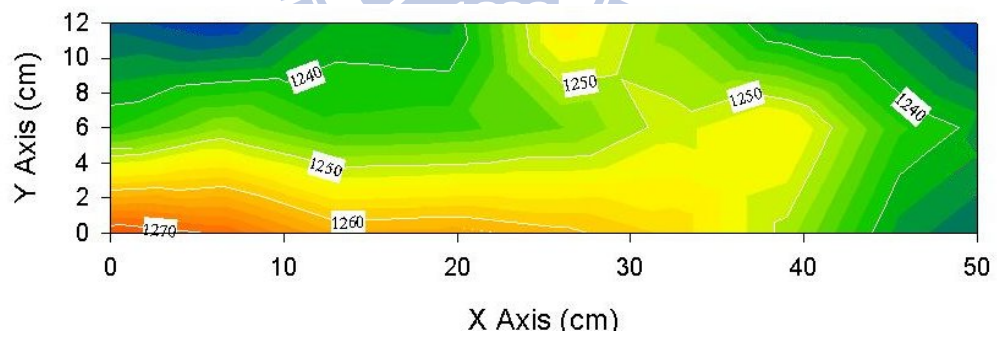
Figure 4.11 Variation of maximum furnace temperature at different

oxygen concentration in the fixed furnace temperature test

(Lab-Scale)

(a)

(b)

(c)

Figure 4.12 Temperature distributions for (a) 21% O_2, (b) 24% O_2

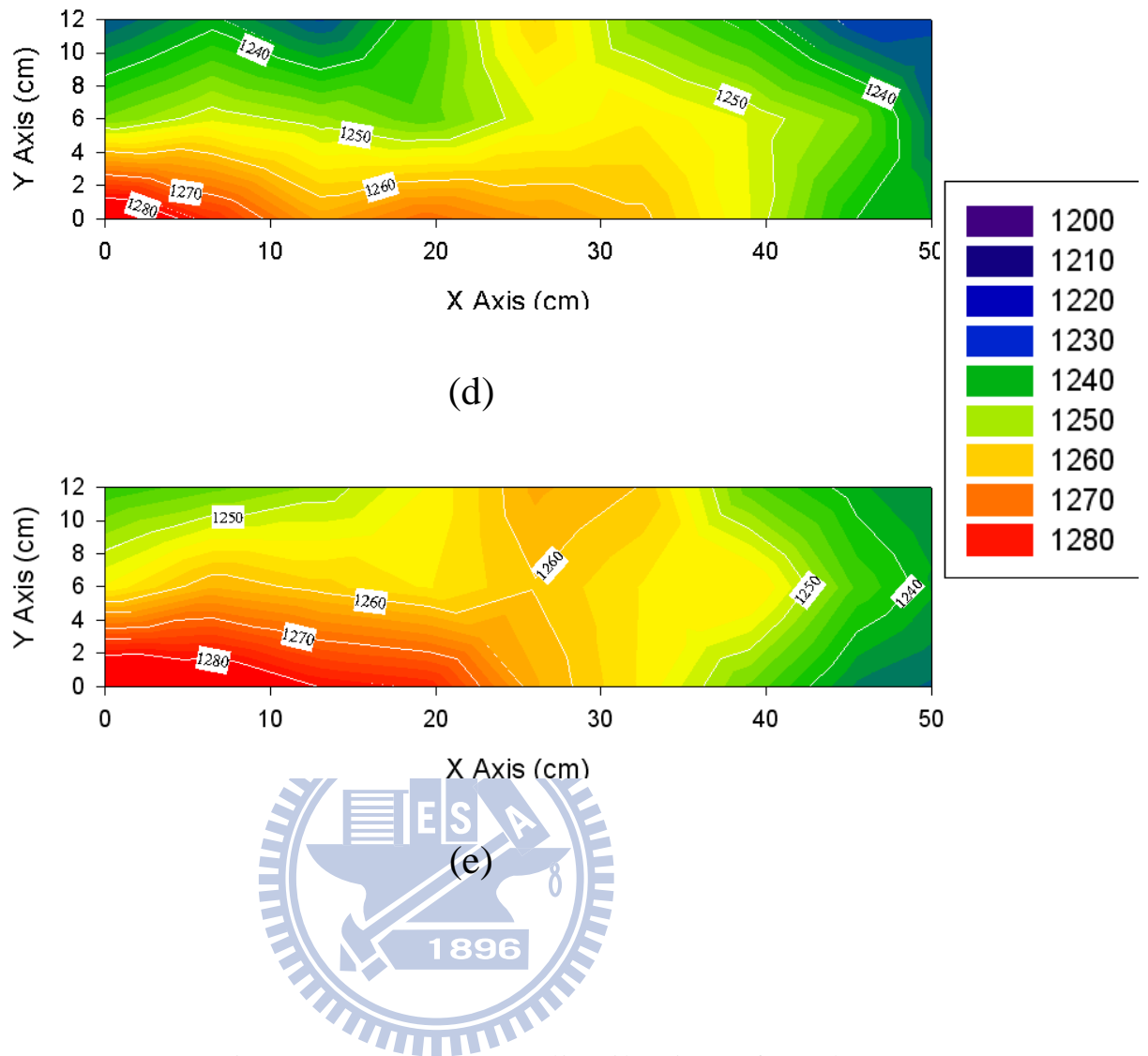and (c) 26% O_2 in the fixed furnace temperature test (Lab-Scale)

(d)

(e)

Figure 4.12 (continue) Temperature distributions for (d) 28% O_2

and (e) 30% O_2 in the fixed furnace temperature test (Lab-Scale)

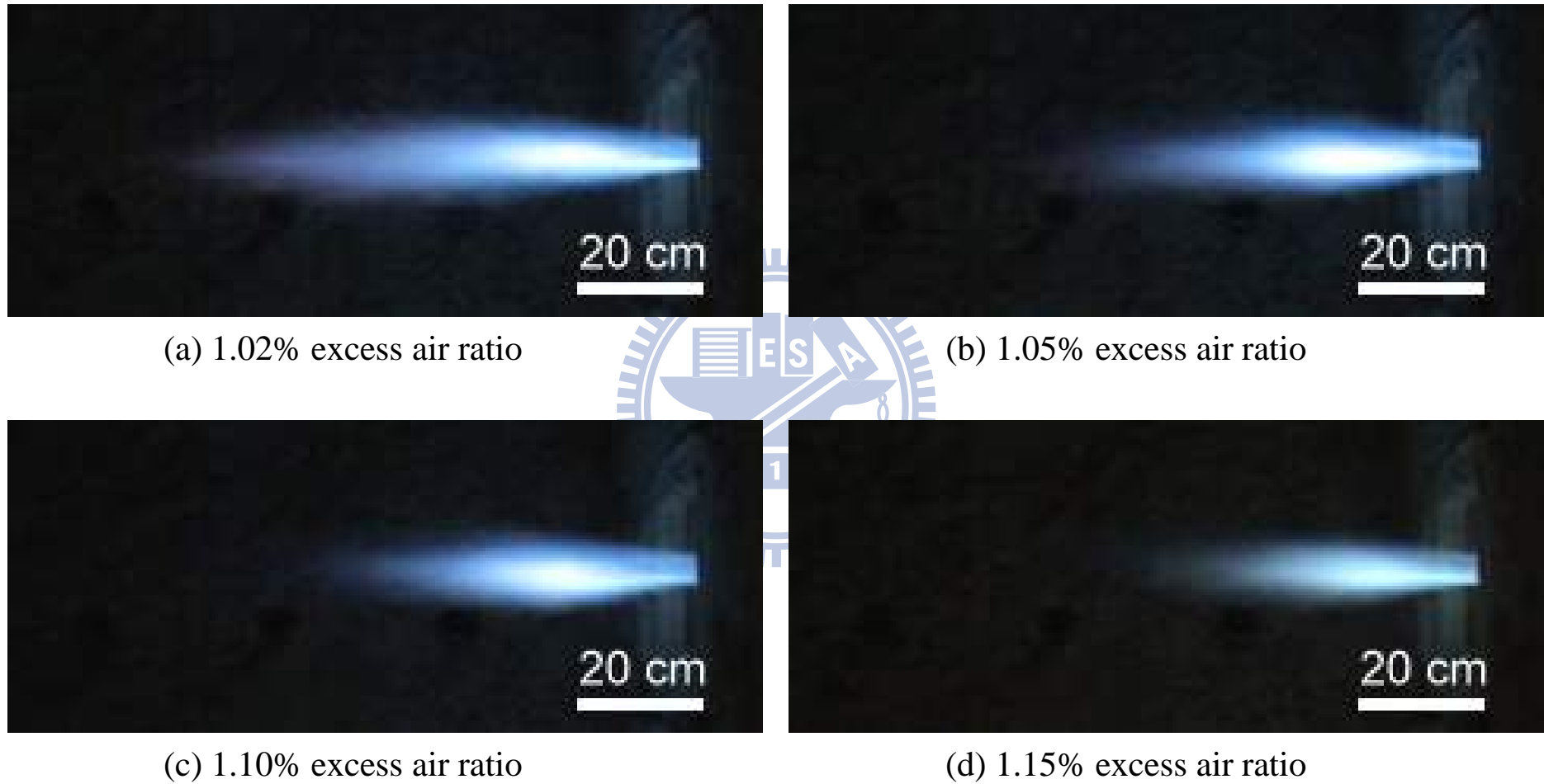(a) 1.02% excess air ratio

(b) 1.05% excess air ratio

(c) 1.10% excess air ratio

(d) 1.15% excess air ratio

Figure 4.13 Flame shapes at 21% O_2 (Pilot-Scale)

(a) 1.02% excess air ratio

(b) 1.05% excess air ratio

(c) 1.10% excess air ratio

(d) 1.15% excess air ratio
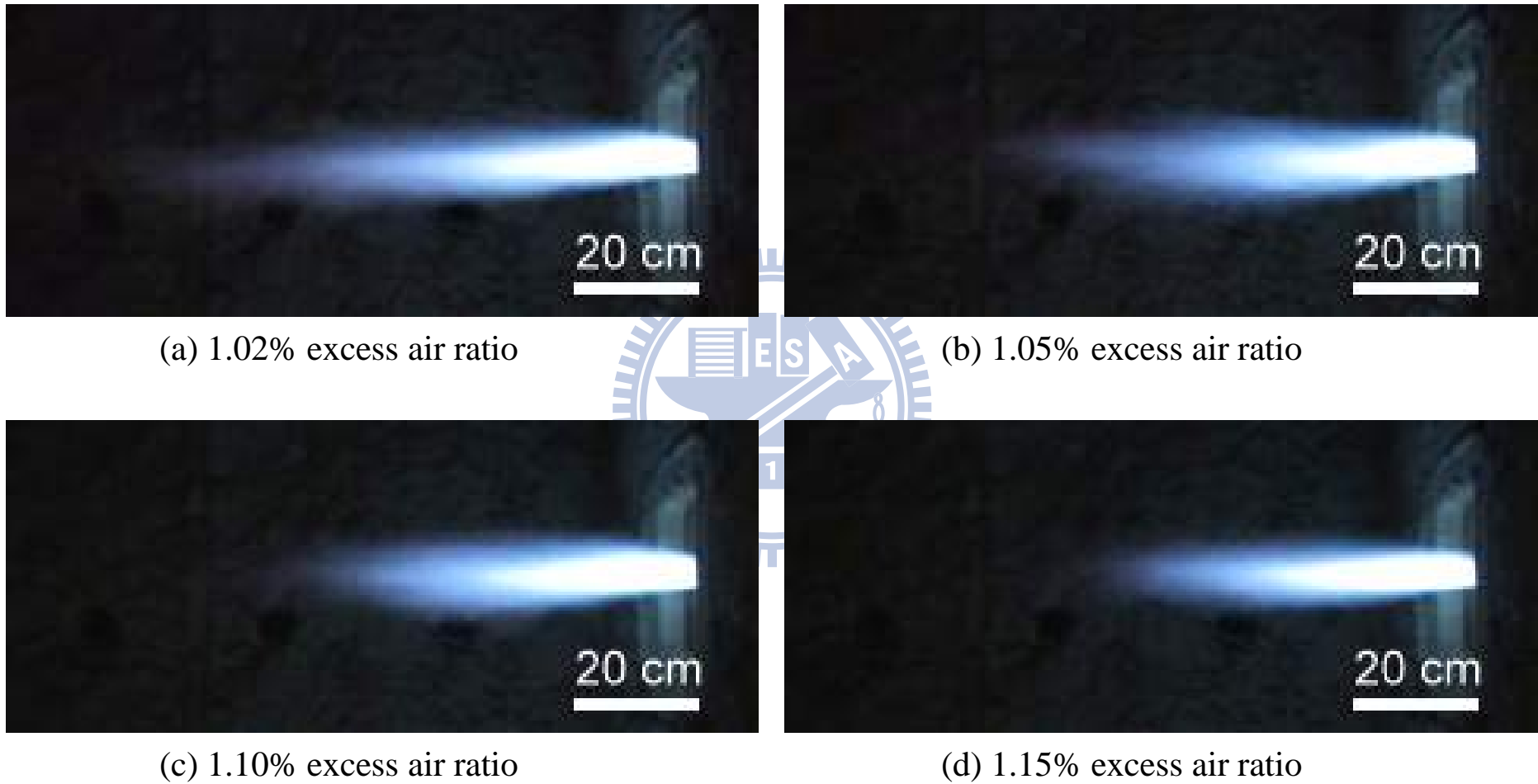
Figure 4.14 Flame shapes at 24% O_2 (Pilot-Scale)

(a) 1.02% excess air ratio

(b) 1.05% excess air ratio

(c) 1.10% excess air ratio

(d) 1.15% excess air ratio

Figure 4.15 Flame shapes at 26% O_2 (Pilot-Scale)

(a) 1.02% excess air ratio

(b) 1.05% excess air ratio

(c) 1.10% excess air ratio

(d) 1.15% excess air ratio
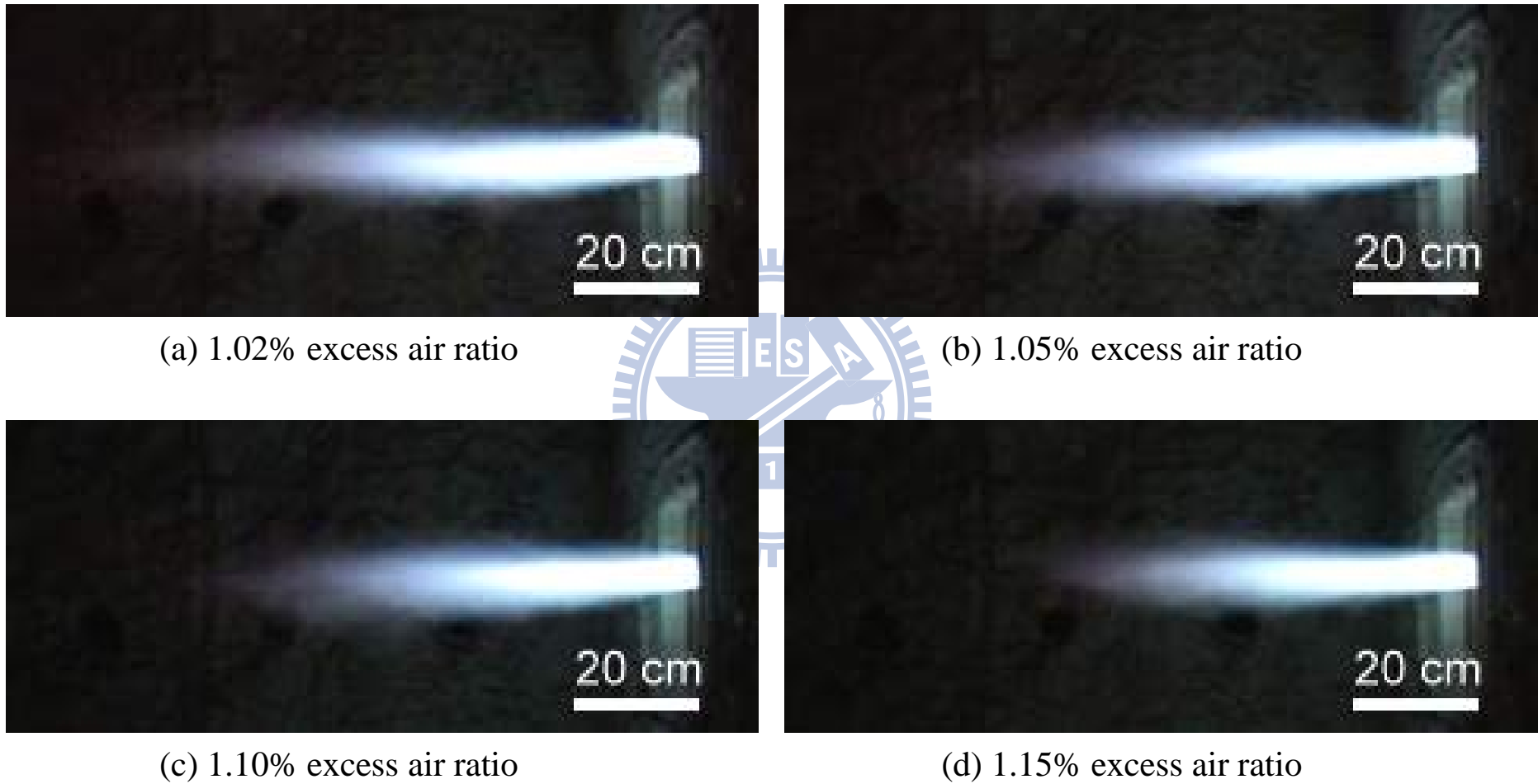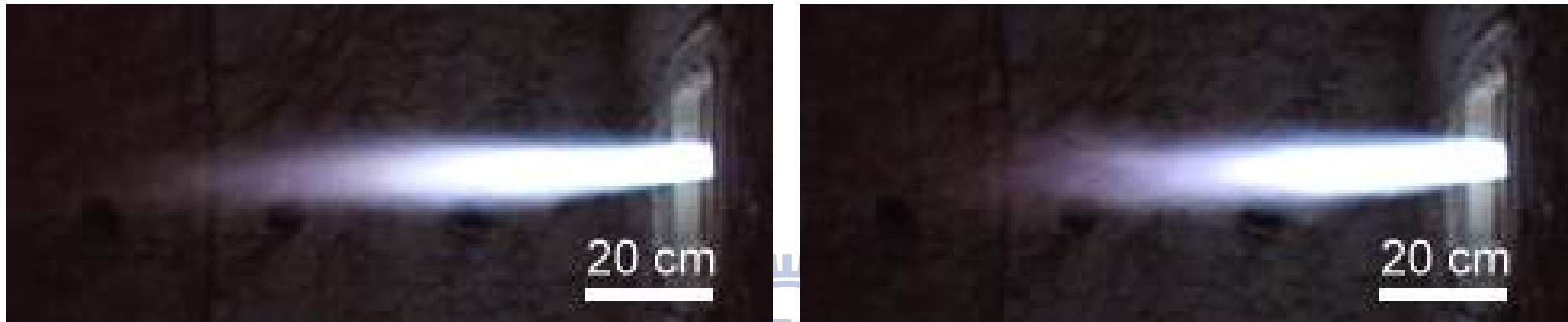
Figure 4.16 Flame shapes at 28% O_2 (Pilot-Scale)

(a) 1.02% excess air ratio

(b) 1.05% excess air ratio

(c) 1.10% excess air ratio
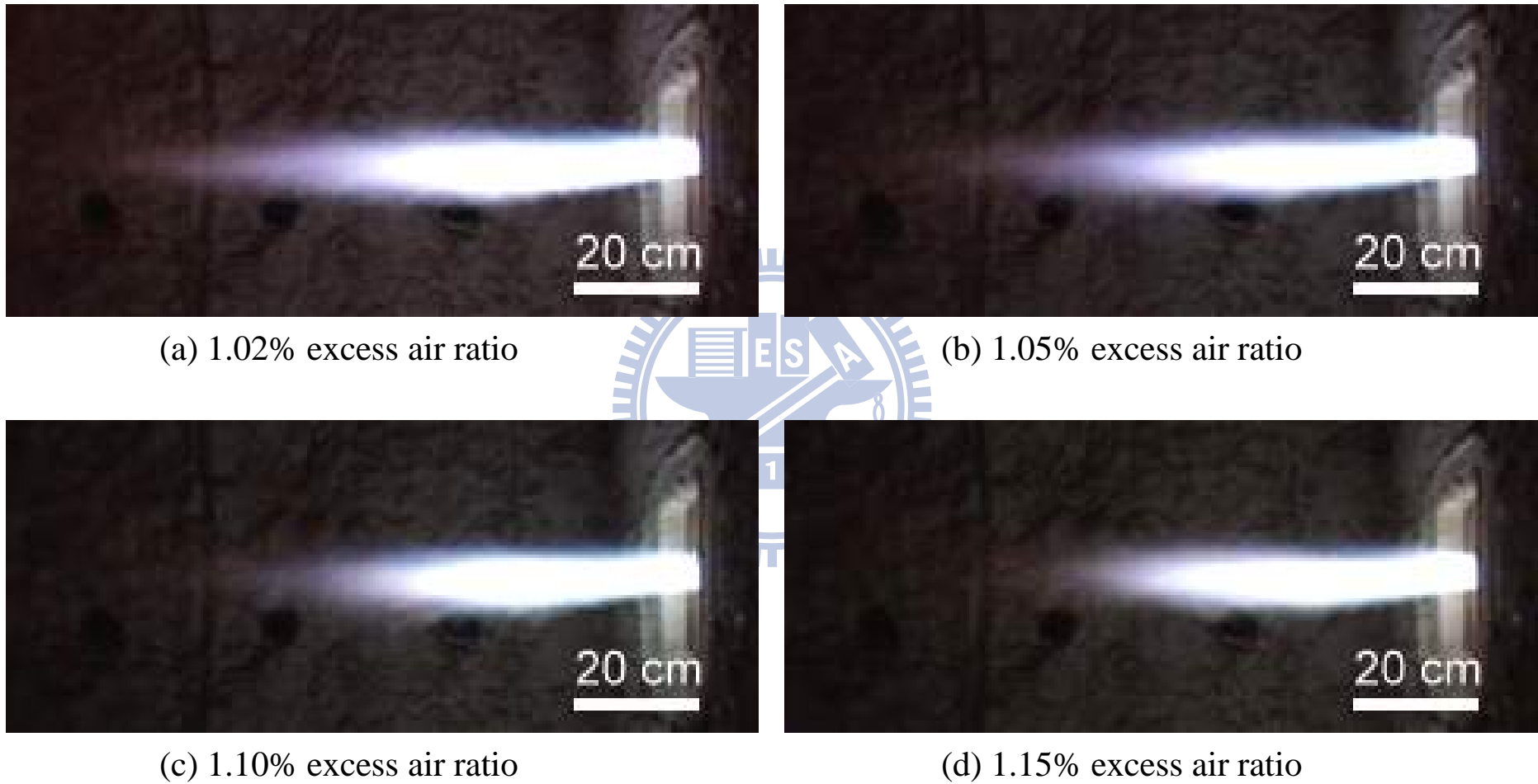
(d) 1.15% excess air ratio

Figure 4.17 Flame shapes at 30% O_2 (Pilot-Scale)
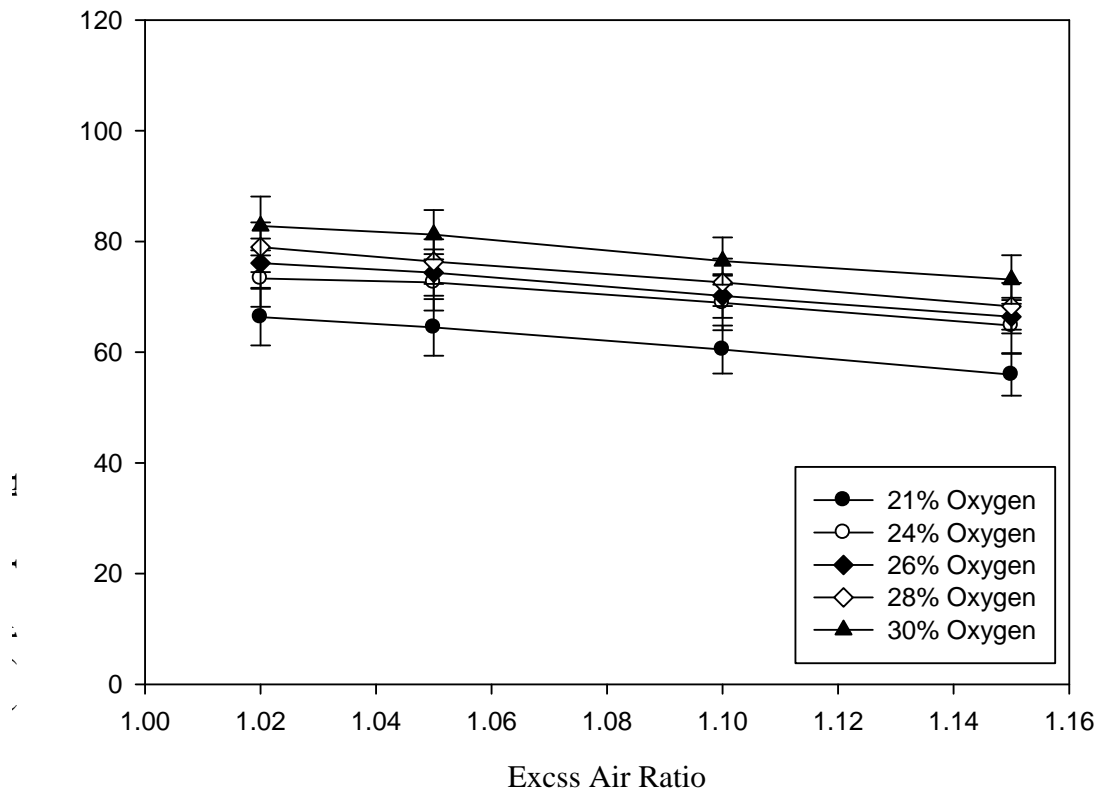
Figure 4.18 Variations of flame length at different oxygen

concentrations and excess air ratio (Pilot-Scale)
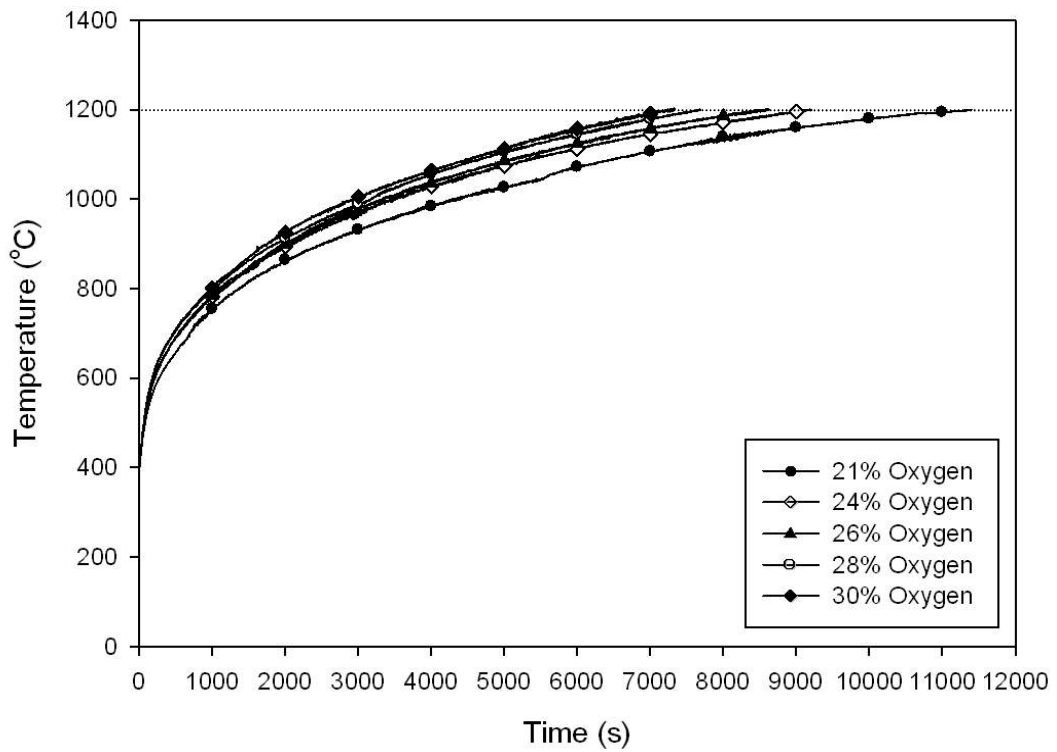
Figure 4.19 Heating times for different oxygen concentrations

(Pilot-Scale)

Figure 4.20 Variations of CO and CO_2 emission at different

oxygen concentration in the fixed furnace temperature test

(Pilot-Scale)

Figure 4.21 Variations of CO_2 emission per million joules at

different oxygen concentration in the fixed furnace

temperature test (Pilot-Scale)

Figure 4.22 Variations of fuel flow rate at different oxygen

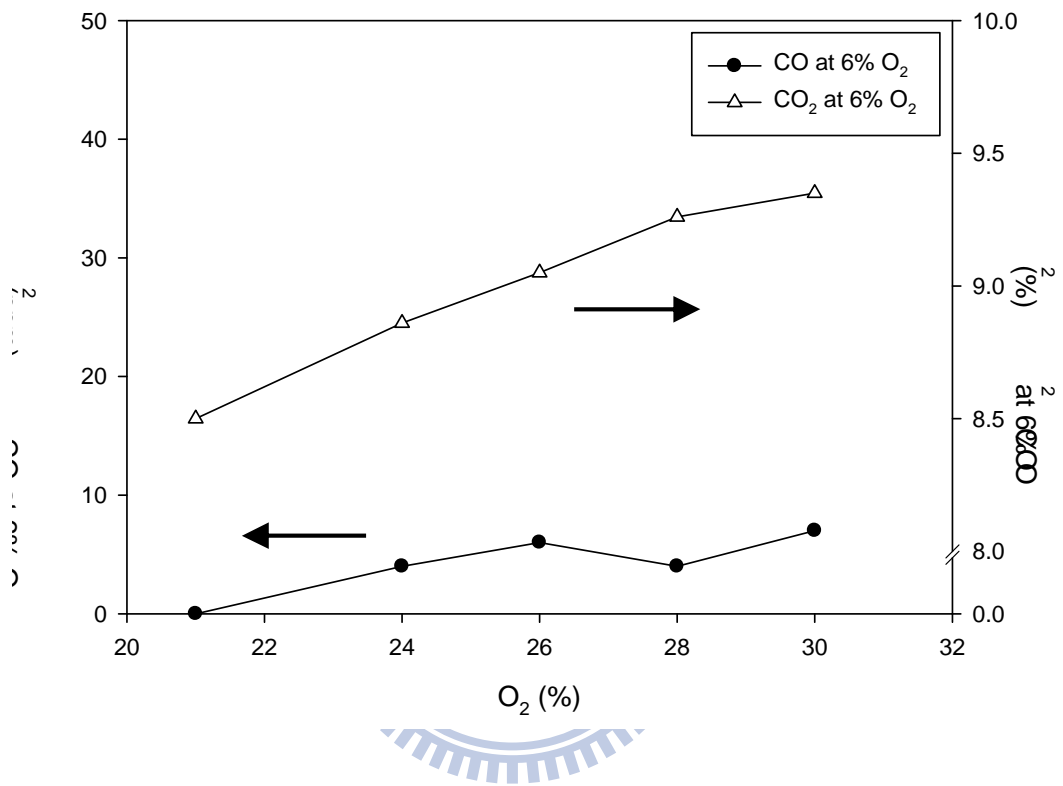concentration in the fixedg furnace temperature test (Pilot-Scale)

Figure 4.23 Variations of NO$_x$ emission at different oxygen

concentration in the fixed furnace temperature test (Pilot-Scale)

Figure 4.24 Variations of total NO_x emission per hour at different

oxygen concentration in the fixed furnace temperature test
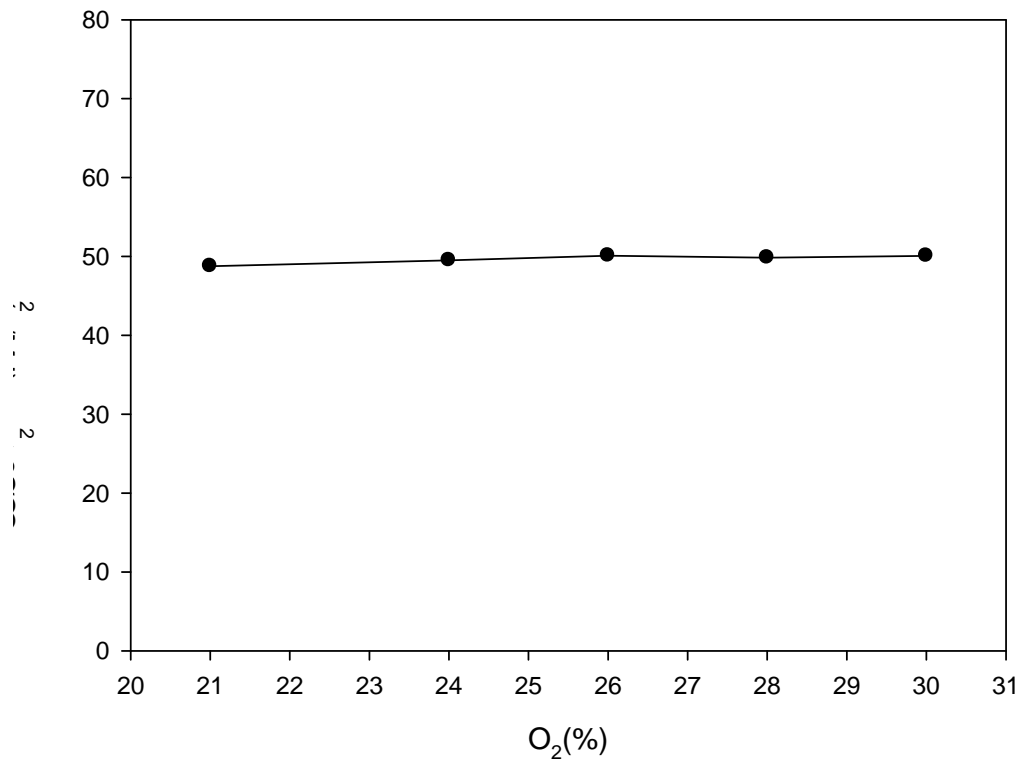
(Pilot-Scale)

Figure 4.25 Variations of NO_x emission per million joules at different oxygen concentration in the fixing furnace temperature test (Pilot-Scale)
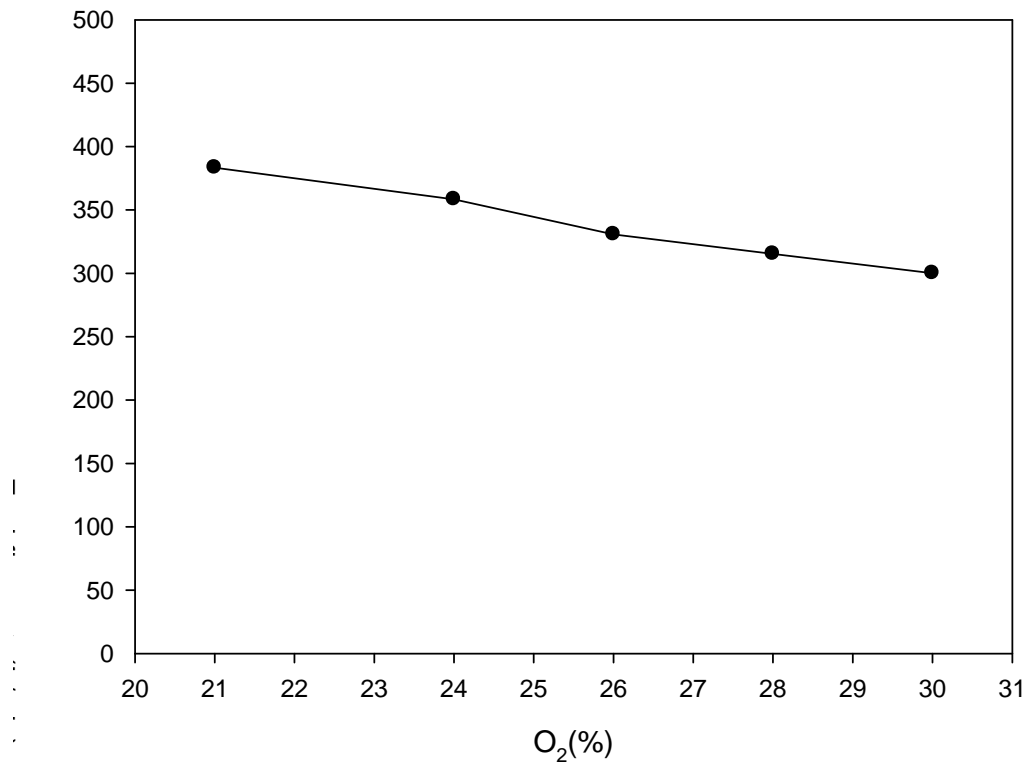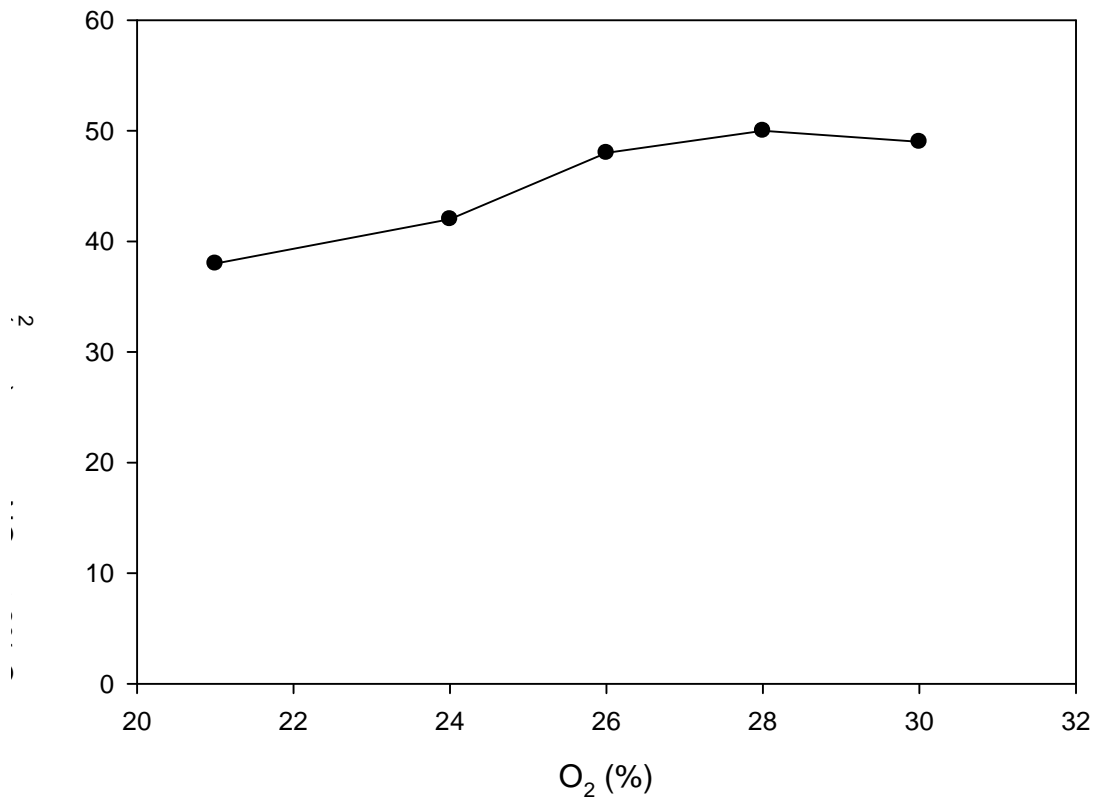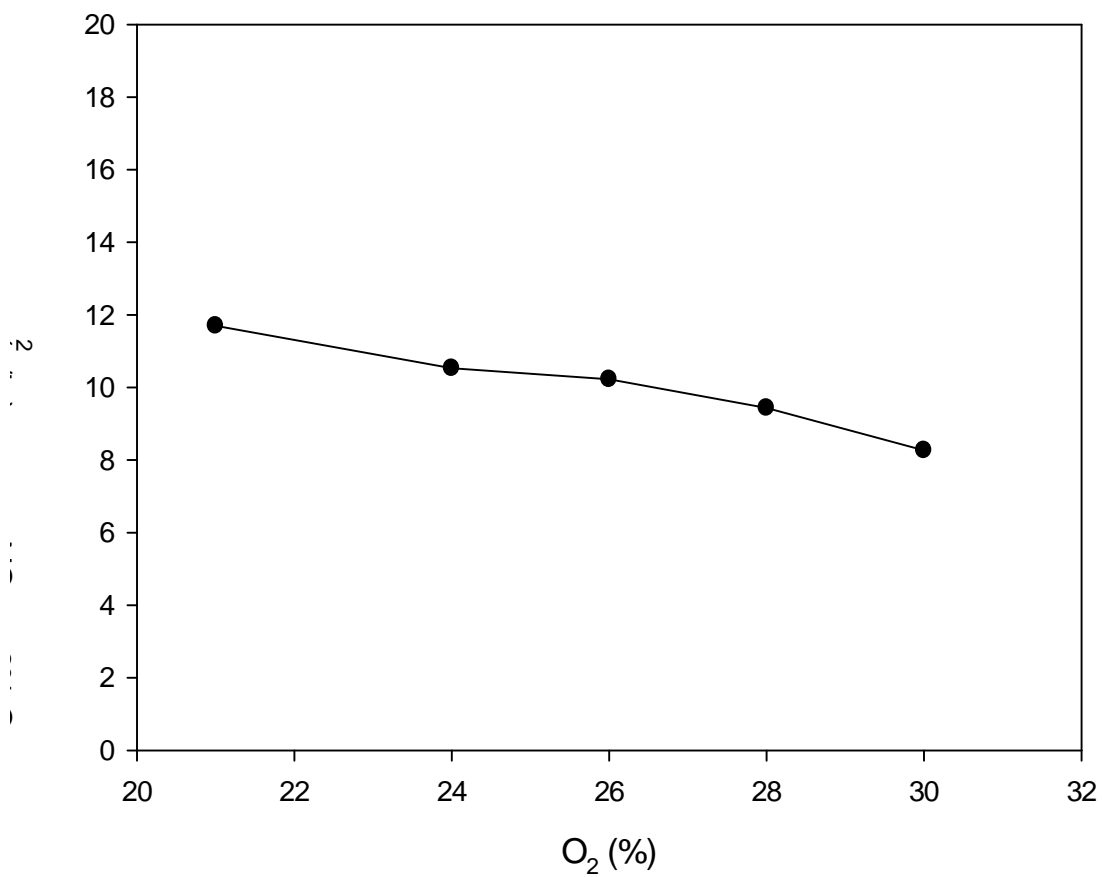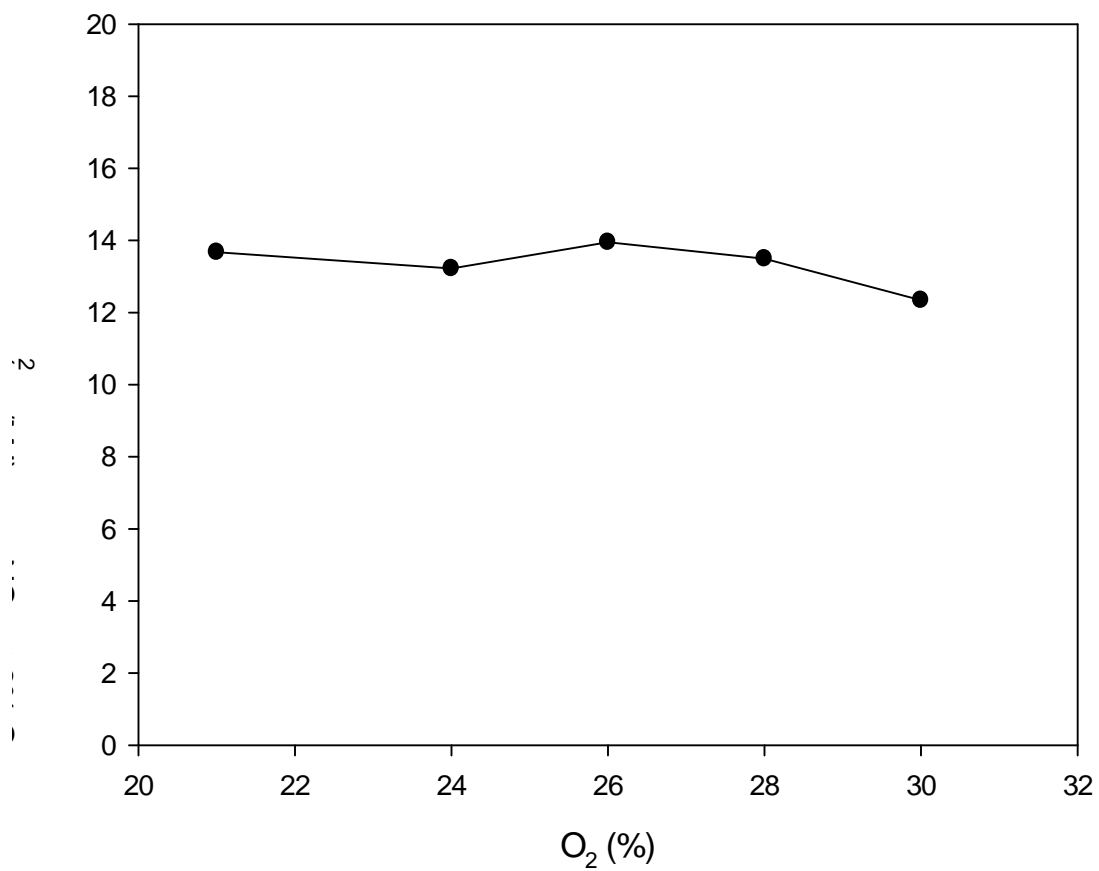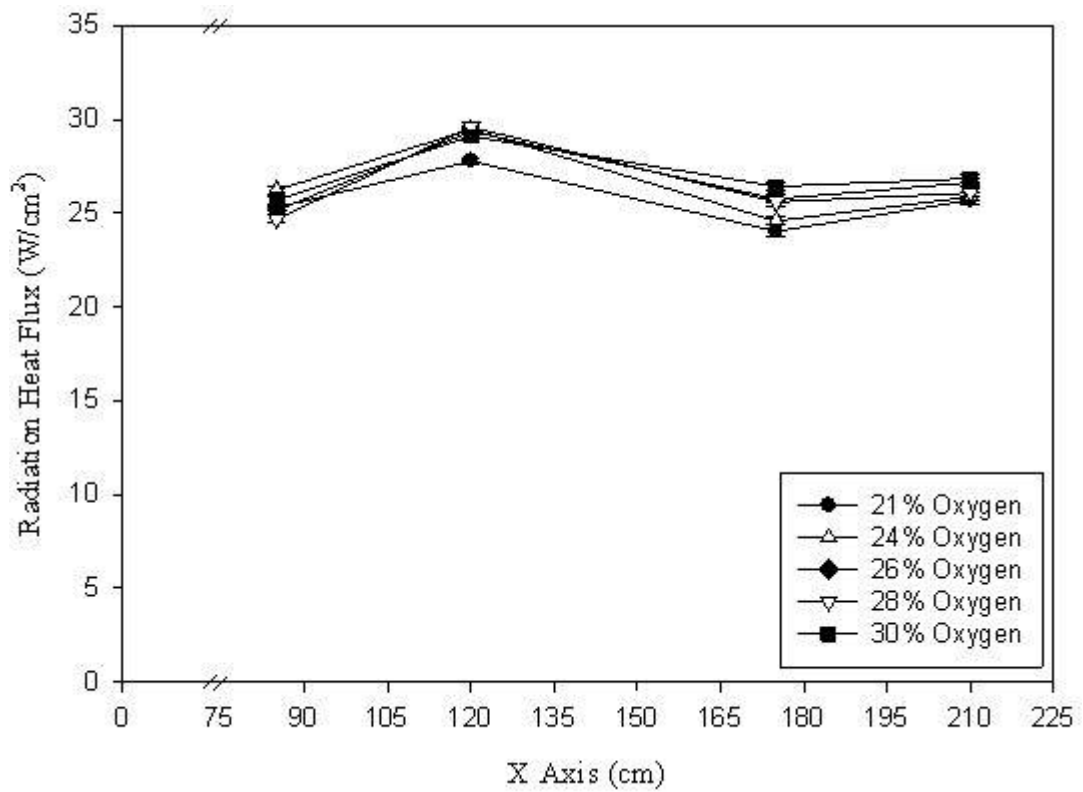
Figure 4.26 Radiate heat flux distributions at different oxygen

concentration in the fixing furnace temperature (Pilo-Scale)

Chapter 5

Conclusions

In the present study, the heating and fixed furnace temperature tests were adopted to investigate the effects of oxygen concentration in the range of 21-30% O_2. The influences of oxygen concentration on the heating speed, emissions, temperature distributions, flame shape, radiate heat flux and fuel consumption were examined. The general conclusions drawn from the results of this work were as follows:

Lab-Scale Experiments

1. The heating speed was fast due to the reduction of combustion air and increasing oxygen concentration. Compared with 21% O_2, the elapsed time of heating to 1200℃ was only needed 46.4% for 30% O_2. However, the difference of heating speed for all cases is unobvious when the furnace temperature is lower than 700℃. Oppositely, the advantage of heating speed for oxygen-enriched combustion is apparent for the high furnace temperature situation.

2. The NO_x emission increased sharply due to the higher furnace temperature as oxygen concentration increased in the heating test. The NO_x concentration increased 6.33 times above when oxygen concentration was increased from 21% to 30%.

3. The CO_2 concentration increased nearly linearly with oxygen concentration in spite of in the heating test or the fixed furnace temperature test. This phenomenon can reduce post-processing cost and improve CO_2 capture efficiency.

4. For maintaining furnace temperature, the fuel utility and radiation heat transfer were growth with increasing oxygen concentration so that the

fuel consumption decreased with increasing oxygen concentration. The fuel consumption of 30% O_2 reduced 26.1% compared with 21% O_2 when the furnace temperature was maintained at 1220±10℃.

5. The trend of NO_x emission in the fixing furnace temperature test was basically the same as one in the heating test; however, the NO_x concentration was much less than one in the heating tests at the same oxygen concentration owing to furnace temperature and excess oxygen.

6. Increasing the oxygen concentration led to non-uniform temperature distribution since convection heat transfer was changed.

Pilot-Scale Experiments

1. Under the fixed fuel supply rate, 508.4 L/min, the excess air ratio for the best combustion is chosen as 1.05, below which the concentration of carbon monoxide is skyrocketed and the combustion is incomplete.

2. The flame length decreases with increasing the excess air ratio. Furthermore, the flame length increases with the oxygen concentration at the constant excess air. The natural gas and air mixture becomes less uniform, as oxygen concentration is increased by using high-speed burner when using oxygen-enriched combustion.

3. The heating speed is fast due to the reduction of N_2 in combustion air as increasing the oxygen concentration. For 30% O_2, the elapsed time of heating to 1200℃ only needs 64.3% of that of 21% O_2. However, the difference of heating speed for all cases is not as obvious when the furnace temperature is lower than 700℃. Oppositely, the advantage of heating speed for oxygen-enriched combustion is apparent for the high furnace temperature situation.

4. The fuel consumption rate decreases from 383.4 L/min for 21% O_2 to 300.0 L/min for 30% O_2 at a constant furnace temperature of 1220 ±

10°C. This implies that 21.74% of fuel can be saved when the oxygen concentration is increased to 30%.

5. The total amount of NO_x emissions was almost invariant as the oxygen concentration increased. This is due to poor mixing of oxidant and fuel of burner.

6. The radiation heat flux increases with oxygen concentration. The reason is mainly resulted from dilution of N_2 concentration due to an increase of oxygen concentration in combustion air under the fixed air/fuel ratio. Furthermore, the CO_2 and H_2O are good radiation emitters, the total gas emissivity are increased when the oxygen-enrichment level is upgraded; in turn, causes the radiation intensity to become stronger.

Chapter 6

Future Works

The target of the future research will be the practical application that is extended from the results of present experimental study. Because the NO_x emission increased sharply as the experimental scale became greater, so how to reduce NO_x effectively in the future real scale test is a challenging task. The industrial applications of oxygen-enhanced combustion are major in the high temperature environments, such as aluminum remelting furnace, incinerator, glass melting furnace, ladle furnace and so on. The oxygen concentrations in these applications are often higher or pure oxygen. However, if the existent combustion system wants to use higher oxygen or pure oxygen combustion, the burner and furnace body have to be retrofit substantially due to potential problems, like heat transfer, flame structure, refractory damage and so on. It will limit the applications of oxygen-enhanced combustion. Some researches, Dalton A.I. et al. [3] and Joshi S.V. et al. [4], indicate that many conventional air/fuel burners can be adapted for low-level oxygen enrichment, but the characteristics of low-level oxygen enrichment using on air/fuel combustion system do not study detail yet. Therefore, this is a practical problem, on which the future extension of this work can focus.

References

[1] Baukal C.E. (1998): "Oxygen-Enhanced Combustion". *CRC Press*, Boca Raton, FL.

[2] Baukal C.E. and Gebhart B. (1997): "Oxygen-enhanced/natural gas flame radiation". *International Journal of Heat and Mass Transfe*r, Vol. 40(11), pp. 2539-2547.

[3] Dalton A.I. and Tyndall D.W. (1989): "Oxygen enriched air/natural gas burner system development". *NTIS report PB91-167510*, Springfield, VA.

[4] Joshi S.V., Becker J.S. and Lytle G.C. (1986): "Effects of oxygen enrichment on the performance of air-fuel burners". *Industrial Combustion Technologies,* Ed. by Lukasiewicz, M. A. American society of metals, Materials park, OH.

[5] Qiu K. and Hayden A.C.S. (2009): "Increasing the efficiency of radiant burners by using polymer membranes", *Applied Energy*, Vol. 86, pp. 349-354.

[6] Sekar R. R., Marr W. W., Assanis D. N., Cole R. L., Marciniak T. J. and Schaus J. E.(1991): "Oxygen-Enriched Diesel Engine Performance: A Comparison of Analytical and Experimental Results". *Journal of Engineering for Gas Turbines and Power*, Vol. 113, pp. 365-369.

[7] Assanis D.N., Karvounis E., Sekar R.R. and Marr W.W. (1993): "Heat Release Analysis of Oxygen-Enriched Diesel Combustion". *Journal of Engineering for Gas Turbines and Power*, Vol. 115, pp. 761-768.

[8] Iida N., Suzuki Y., Sato G.T. and Sawada T. (1986): "Effects of Intake Oxygen Concentration on the Characteristics of Particulate Emissions From D.I. Diesel Engine". *SAE Paper*, No. 861233.

[9] Chen R. and Axelbaum R.L. (2005): "Scalar dissipation rate at

extinction and the effects of oxygen-enriched combustion". *Combustion and Flame*, Vol. 142, pp. 62-71.

[10] Bejarano P.A. and Levendis Y.A. (2007): "Combustion of coal chars in oxygen-enriched atmospheres". *Combustion Science and Technology*, Vol. 179, pp. 1569-1587.

[11] Murphy J.J. and Shaddix C.R. (2006): "Combustion kinetics of coal chars in oxygen-enriched environments", *Combustion and Flame*, Vol. 144, pp. 710–729.

[12] Beltrame A., Porshnev P. and Merchan-Merchan W. (2001): "Soot and NO Formation in Methane-Oxygen Enriched Diffusion Flame". *Combustion and Flame*, Vol. 124, pp. 295-310.

[13] Kang K.T., Hwang J.Y., Chung S.H. and Lee W. (1997): "Soot zone structure and sooting limit in diffusion flames: Comparison of counterflow and co-flow flames". *Combustion and Flame*, Vol. 109(1-2), pp. 266-281.

[14] Ishizuka S. and Tsuji H. (1981): "An experimental study of effect of inert gases on extinction of laminar diffusion flames". *Proceedings of the Combustion Institute*, Vol. 18, pp. 695-703.

[15] Puri I.K. and Seshadri K. (1986): "Extinction of diffusion flames burning diluted methane and diluted propane in diluted air". *Combustion and Flame*, Vol. 65, pp. 137-150.

[16] Chen C.L. and Sohrab S.H. (1991): "Simultaneous effects of fuel/oxidizer concentrations on the extinction of counterflow diffusion flames". *Combustion and Flame*, Vol. 86, pp. 383-393.

[17] Zhao D. and Yamashita H. (2001): "A numerical study on flame structure and NO_x formation of qxygen-enriched air/methane counterflow diffusion flame". *Proceedings of 3rd International*

Symposium on Advanced Energy Conversion Systems and Related Technologies, pp. 300-308.

[18] Beltrame A., Porshnev P., Merchan W.M., Saveliev A., Fridman A., Kennedy L.A., Petrova O., Zhdanok S., Amouri F. and Charon O. (2001): "Formation of NO from combustion of volatiles from municipal solid wastes". *Combustion and Flame*, Vol. 124, pp. 295-310.

[19] Lee K.O., Megaridis C.M., Zelepouga S., Saveliev A.V., Kennedy L.A., Charon O. and Ammouri F. (2000): "Soot formation effects of oxygen concentration in the oxidizer stream of laminar coannular nonpremixed methane/air flames". *Combustion and Flame*, Vol. 121, pp. 323-333.

[20] Naik S.V. and Laurendeau N.M. (2002): "Quantitative laser-saturated fluorescence measurements of nitric oxide in counter-flow diffusion flames under sooting oxy-fuel conditions". *Combustion and Flame*, Vol. 129, pp. 112- 119.

[21] Naik S.V., Laurendeau N.M., Cooke J.A. and Smooke M.D. (2003): "Effect of radiation on nitric oxide concentration under sooting oxy-fuel conditions". *Combustion and Flame*, Vol. 134, pp. 425-431.

[22] Hedley J.T., Pourkashanian M. and Williams A. (1995): "NO_x Formation in Large-Scale Oxy-Fuel Flames". *Combustion Science and Technology*, Vol. 108, pp. 311-322.

[23] Ho K.K., Yongmo K., Sang M.L. and Kook Y.A. (2007): "Studies on Combustion Characteristics and Flame Length of Turbulent Oxy-Fuel Flames". *Energy and Fuels*, Vol. 21, pp. 1459-1467.

[24] Narayanan K., Wlodzimierz B. and Anders L. (2004): "Development of High Temperature Air and Oxy-Fuel combustion technologies for minimized CO_2 and NO_x emissions in Industrial Heating". *Sustainable*

Energy and Environment, 1-3 December, Hua Hin, Thailand.

[25] Buhre B.J.P., Elliott L.K., Sheng C.D., Gupta R.P. and Wall T.F. (2005): "Oxy-fuel combustion technology for coal-fired power generation". *Progress in Energy and Combustion Science*, Vol. 31, pp. 283–307.

[26] Czakiert T., Bis Z., Muskala W. and Nowak W. (2006): "Fuel conversion from oxy-fuel combustion in a circulating fluidized bed". *Fuel Processing Technology*, Vol. 87, pp. 531–538.

[27] Neff D.S., Mohr P.J. and Rue D. (1999): "OEAS offers an economical NOx reduction solution". *Glass*, Vol. 76(1), pp. 14-16.

[28] El-Salmawy H.A. (2001): "Control of NO_x emissions from a diffusion flame in an oxygen enriched combustion". *Journal of Engineering and Applied Science*, Vol. 48(3), pp. 565-581.

[29] Bool L., Kobayashi H. and Wu K.T. (2002): "Oxygen for NO_x control －a step change technology". *Nineteenth Annual Pittsburgh Coal Conference*, Pittsburgh, PA.

[30] Riley M.F., Kobayashi H. and Deneys A.C. (2001): "Praxair's dilute oxygen combustion technology for pyrometallurgical applications". *JOM*, Vol. 53(5), pp. 21-24.

[31] Nishimura M., Suyari M. and Suzuki T. (2001): "Recirculated gas entrainment and mixing for NO_x reduction in oxygen enriched air combustion". *Kobelco Technology Review*, Vol. 24, pp. 41-44.

[32] Poirier D., Grandmaison E.W. and Lawrence A.D. (2004): "Oxygen-Enriched combustion studies with the low NO_x CGRI burner". *International Flame Research Foundation Combustion Journal*, No. 200404.

[33] Kennedy L.A., Saveliev A.V., Bingue J.P. and Fridman A.A. (2002):

"Filtration combustion of a methane wave in air for oxygen-enriched and oxygen-depleted environments". *Proceedings of the combustion Institute*, Vol. 29, pp. 835–841.

[34] Molina A. and Shaddix C.R. (2007): "Ignition and devolatilization of pulverized bituminous coal particles during oxygen/carbon dioxide coal combustion", *Proceedings of the Combustion Institute*, Vol. 31, pp. 1905-1912.

[35] Liu H. and Okazaki K. (2003): "Simultaneous easy CO_2 recovery and drastic reduction of SOx and NOx in O_2/CO_2 coal combustion with heat recirculation". *Fuel*, Vol. 82, pp. 1427-1436.

[36] Huang I.T., Chang Y.C. and Wu K.K. (2008): "The development of key technology to improve thermal energy utilization". *ITRI technical report* No. 553971644.

[37] Fox R. W. and McDonald A. T. (1994): "Introduction to Fluid Mechanics". *John Wiley and Sons*, Canada.

[38] Kline S. J. and Mcclintock F. (1953): "Describing Uncertainties in Single-Sample Experiments". *Mechanical Engineering*, Vol. 75, pp. 3-8, 1953.

[39] Moffat R. J. (1982): "Contributions to the Theory of Single-Sample Uncertainty Analysis". *Journal of Fluid Engineering*, Vol. 104, pp. 250-260, 1982.

[40] Figliola R. S. and Beasley D. E. (1995): "Theory and Design for Mechanical Measurements". *John Wiley and Sons*, 2nd Ed. Canada.

[41] Holman J. P. (1989): "Experimental Methods for Engineers".

McGraw-Hill, 5th Ed., New York.

[42] Chen J.H. (2002): "Comparative Studies on Fire Suppression Performance of Water Mist and Conventional Sprinkler in Machinery Space". *MS thesis*, National Chiao Tung University, Taiwan
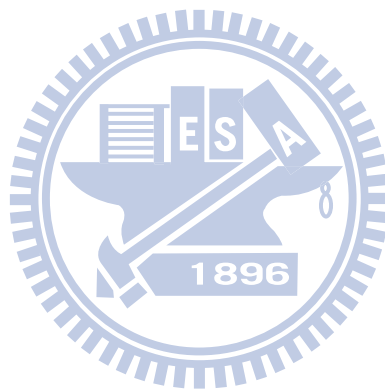
Publications List

Wu K. K., Chang Y. C., Chen C. H. and Chen Y. D. (2010): "High-efficiency Combustion of Natural Gas with 21-30% Oxygen-Enriched Air". *Fuel*, Vol. 89, pp. 2455–2462.

Chen Y. D., Chen D. D. and Chen C. H. (2008): "Transient Behaviors of a Flame Over a Tsuji Burner". *Acta Mechanica Sinica*, Vol. 24, Issue 6, pp. 645-659.

Wu K. K., Chang Y. C., Chen C. H. and Chen Y.D. (2009): "The effects of oxygen concentration for energy saving and emission with a gas-fired burner". *The 20th International Symposium on Transport Phenomena*, July 7-10, Victoria BC, CANADA.

Chen Y.D., Wu K. K. and Chen C. H. (2008): "Oxygen-Enriched combustion in the heating process". *The 19th International Symposium on Transport Phenomena*, 17-20 August, Reykjavik, ICELAND.